

NOTE TO USERS

This reproduction is the best copy available.

UMI

UNIVERSITY OF CALGARY

**Fiber Optic Current Sensor Network:
Innovations and Applications**

by

Andres E. Canalizo M.

A THESIS

SUBMITTED TO THE FACULTY OF GRADUATE STUDIES
IN PARTIAL FULFILLMENT OF THE REQUIREMENTS FOR THE
DEGREE OF MASTER OF SCIENCE

DEPARTMENT OF ELECTRICAL AND COMPUTER ENGINEERING

CALGARY, ALBERTA

MAY, 1999

© Andres E. Canalizo M. 1999



National Library
of Canada

Acquisitions and
Bibliographic Services

395 Wellington Street
Ottawa ON K1A 0N4
Canada

Bibliothèque nationale
du Canada

Acquisitions et
services bibliographiques

395, rue Wellington
Ottawa ON K1A 0N4
Canada

Your file *Votre référence*

Our file *Notre référence*

The author has granted a non-exclusive licence allowing the National Library of Canada to reproduce, loan, distribute or sell copies of this thesis in microform, paper or electronic formats.

The author retains ownership of the copyright in this thesis. Neither the thesis nor substantial extracts from it may be printed or otherwise reproduced without the author's permission.

L'auteur a accordé une licence non exclusive permettant à la Bibliothèque nationale du Canada de reproduire, prêter, distribuer ou vendre des copies de cette thèse sous la forme de microfiche/film, de reproduction sur papier ou sur format électronique.

L'auteur conserve la propriété du droit d'auteur qui protège cette thèse. Ni la thèse ni des extraits substantiels de celle-ci ne doivent être imprimés ou autrement reproduits sans son autorisation.

0-612-48057-7

Canada

ABSTRACT

Commercially optical current sensors are becoming a reality and a network of multiple sensors can be very beneficial especially if they have a single transceiver unit. Following the work of S. Goyal, an all-fiber optic current sensor network is developed which uses a single detection scheme for current sensing and is capable of measuring DC and AC line-currents.

The Time Division Multiplexed (TDM) network presented, details the implementation of a system which is capable of accurately measuring AC and DC simultaneously from more than one sensor. One of the main innovations is the ability of this system to measure AC and DC current flowing through a single sensor.

Since this is a sampled system, the information gathered can be used to plot the current being measured at each sensor and even trace transient conditions on the line current.

ACKNOWLEDGEMENTS

The author would like to express his sincere gratitude to Dr. Dave Irvine-Halliday, the author's thesis supervisor, for his valuable support, encouragement, suggestions and constructive criticism throughout this project.

Thanks to Mr. Rob Thomson, John Shelley and Warren Flaman for their invaluable help and technical support throughout the duration of this project. Their assistance and expertise has gone a long way in making this project a success.

Special thanks to Mr. Patrick Walsh for helping in the set-up of the power supply facilities for the large current experiments, and for his invaluable advice.

Sincere thanks to the Department of Electrical and Computer Engineering for all their support, to NSERC for their funding of this project and to 3M for donating the Fiber Optic Current Sensors and the Single Mode Fiber.

My heartfelt gratitude to my family and friends for their support and encouragement.

A MIS PADRES Y MIS HERMANOS

TABLE OF CONTENTS

APPROVAL PAGE	ii
ABSTRACT	iii
ACKNOWLEDGEMENTS	iv
DEDICATION	v
TABLE OF CONTENTS	vi
LIST OF TABLES	xi
LIST OF FIGURES	xii
LIST OF SYMBOLS	xv
LIST OF ACRONYMS	xvii
I. INTRODUCTION	
1.1 BACKGROUND	1
1.2 OPTICAL CURRENT SENSORS	2
1.3 FIBER OPTIC CURRENT SENSOR NETWORK (FOCSNET)	3
1.4 SCOPE OF THE THESIS	5
II. OPTICAL THEORIES	
2.1 OVERVIEW	7
2.2 FARADAY MAGNETO-OPTIC EFFECT	7
2.3 POLARIZATION	9
2.4 JONES CALCULUS	10
2.5 POLARIZATION AND FIBER OPTICS	13
2.6 SENSING FIBER COIL	16
III. NETWORK	
3.1 OVERVIEW	17
3.2 NETWORK	17
3.2.1 Time Division Multiplexing (TDM)	18

3.2.2 Star Network	18
3.3 BASIC NETWORK DESIGN	19
3.4 FIBER NETWORK COMPONENTS.	21
3.4.1 Transmitter	22
3.4.2 Fiber Optic Network	23
3.4.2.1 Single Mode Star Couplers	24
3.4.2.2 Single Mode Fiber	24
3.4.2.3 Polarization Controllers	25
3.4.2.4 Current Sensing Head	26
3.4.3 Total System Optical Loss	27
 IV. DIGITAL RECEIVER	
4.1 OVERVIEW	29
4.2 RECEIVER COMPONENTS	30
4.2.1 Photodetector/Amplifier	30
4.2.2.1 Bandwidth requirements	31
4.2.2.2 Noise Requirement	31
4.2.2.3 Receiver Front End	32
4.2.2.4 Amplifier	33
4.2.3 Differential Amplifier	34
4.2.4 Analog to Digital Converter (ADC)	35
4.2.5 Field Programmable Gate Array (FPGA)	37
4.2.5.1 ADC Clock.	39
4.2.5.2 Sample Window	39
4.2.5.3 Data Acquisition-Data Process Block (DA/DP)	40
4.2.5.4 RAM Addressing:	42
4.2.5.5 FPGA – DSP Handshaking	44
4.2.5.6 Time Simulation	45
4.2.6 RAM Unit	47
4.2.7 Digital Signal Processor (DSP)	48

4.2.8 Personal Computer	50
4.3 FUNCTIONAL DIAGRAM	52
V. PARAMETERS AND PERFORMANCE	
5.1 OVERVIEW	54
5.2 PREDICTED PERFORMANCE	54
5.2.1 Faraday Rotation	54
5.2.2 Signal To Noise Ratio (SNR)	55
5.2.2.1 Thermal noise	55
5.2.2.2 Shot noise	56
5.2.2.3 Op-amp noise	56
5.2.2.4 Signal to Noise Ratio	57
5.2.3 System Resolution	58
5.3 SYSTEM PARAMETERS	59
VI. EXPERIMENTAL INVESTIGATION AND RESULTS	
6.1 OVERVIEW	64
6.2 OPTICAL NETWORKED DC CURRENT SENSING EXPERIMENT	64
6.3 OPTICAL NETWORKED AC CURRENT SENSING EXPERIMENT	67
6.4 LIGHT SOURCE DEPENDENCY	69
6.4.1 Laser Characteristics	70
6.4.2 Different Light Intensity Readings	71
6.5 RATIO TECHNIQUES THEORY	74
6.5.1 AC Ratio	74
6.5.2 DC Ratio	76
6.5.2.1 Reference ZCL	77
6.5.3 Simultaneous AC and DC	78
6.5.3.1 AC calculation	80
6.5.3.1 DC Calculation	80
6.6 EXPERIMENTAL RESULTS	81

6.6.1 SNR	81
6.6.1.1 AC Reading Error	82
6.6.1.2 DC Reading Error	84
6.6.2 DC Ratio Experimental Readings	85
6.6.2.1 Set UP	85
6.6.2.2 Results	85
6.6.2.3 Measurements	85
6.6.2.4 Test	86
6.6.3 AC Ratio Experimental Readings	88
6.6.3.1 Set UP	88
6.6.3.2 Results	88
6.6.3.3 Measurements	88
6.6.3.4 Test	88
6.6.4 Simultaneous DC & AC Experimental Readings	91
6.6.4.1 Set Up	91
6.6.4.2 Results	92
6.6.4.3 Measurements	92
6.6.4.4 Tests	92
i. Varying AC while DC is constant.	93
ii Varying DC, while AC constant.	96
6.6.5 Current Calculations	97
6.6.5.1 AC Experimental Example	100
6.6.5.2 DC Experimental Example	102

VII. CURRENT TRACES AND TRANSIENTS

7.1 OVERVIEW	105
7.2 LINE CURRENT TRACES	105
7.2.1 AC Traces	106
7.2.2 DC Traces	107
7.2.3 Simultaneous AC & DC	108

7.3 TRANSIENTS	109
7.3.1 Hall Effect Traces	111
7.3.2 FOCSNET Transient Traces	112
VIII. CONCLUSIONS AND FUTURE WORK	115
REFERENCES	118

LIST OF TABLES

4.1	Objective Specifications	30
6.1	Perceptual Light Intensity change for different Laser Power levels for Sensor II	72
6.2	Table 6.2 Types of Networks	77
6.3	Table 6.3 SNR under different MF conditions	82
6.4	SNR for AC current under different Laser Power conditions	82
6.5	AC Ratio Error under different Laser Power conditions	83
6.6	AC varying with DC constant	93
6.7	DC varying with AC constant	95
6.8	AC Current Calculations using Slope	99
6.9	DC Current calculations using slope	103
7.1	Figs. 7.8-7.10 Characteristics	113

LIST OF FIGURES

2.1	Faraday Effect Concept	8
2.2	Relationship between orthogonal components and type of polarization	11
2.3	Polarization Maintaining Fiber Core Structures	15
3.1	Pulse gap at Receiver	20
3.2	Two sensor Star Network	21
3.3	Laser Output Power vs. Drive Current	23
3.4	Operation of the Current sensor. Faraday Rotation of θ	28
4.1	Photodiode/Amplifier Schematic	32
4.2	LDP (upper) and the output from the Photodetector/amplifier (lower)	33
4.3	Differential Amplifier	35
4.4	ADC output bus, as seen from a 10-bit DAC	36
4.5	Optical pulse time difference ADC output (upper), Ph/Amp output (lower)	37
4.6	Time difference between LDP (lower) and ADC (upper) output.	37
4.7	Sample window pulses and ADC.	40
4.8	RAM WRITE pulse (upper) Vs. Sample Windows (lower)	41
4.9	FPGA time simulation	46
4.10	Receiver Functional Diagram	53
5.1	The Current Sensor	58
5.2	Minimum LDP period for a two sensor network With 400ns LDP and a 400ns time gap	60
5.3	The Receiver (a) ADC, FPGA, DSP and RAM Unit. (b) Complete Receiver with Photodetector/Amplifier and Differential Amplifier	62
5.4	Fiber Optic Current Sensor Network	63
6.1	Output Increase with 80A DC flowing through both sensors Sensor I: 20mV displacement, Sensor II: 35mV displacement	65
6.2	System Response with different DC currents passing through the two sensors	66

6.3	AC Effect on Receivers output	68
6.4	System Response with different AC currents passing through the two Sensors	69
6.5	Laser Stability Characteristics	70
6.6	Sensor II readings at different light intensity levels	72
6.7	Percentage increments of two AC current readings under different Laser driving current conditions.	73
6.8.	AC Oscillation with offset of ZCL	75
6.9	AC and DC simultaneous response	79
6.10	DC Ratio Experiment. Readings on Sensor II with Sensor I as Reference	86
6.11	DC Ratio Experiments with Different laser drive current. Current set at: 50mA and 40mA	87
6.12	AC Ratio on Sensor I	89
6.13	AC Ratio on Sensor II Laser Driving Current Values set at: 70mA, 52mA and 35mA	89
6.14	AC Ratio Resolution. Sensor II. Steps of 1.55Arms	90
6.15	AC and DC simultaneous Through Sensor II. DC set at 100A. AC varying 20-100Arms	93
6.16	AC and DC simultaneous Through Sensor II. DC set at 0A. AC varying 20-100Arms	94
6.17	Caparison of Figs. 6.15 and 6.16	95
6.18	AC and DC simultaneous Through Sensor II. AC set at 100Arms. DC varying 20-100A	97
7.1	Plot of a 100Arms AC	106
7.2	85Arms on Sensor I & 60Arms on Sensor II	107
7.3	DC Current on Sensor II	108
7.4	110A & 100A DC (upper). 110 Arms & 0A DC (lower).	109
7.5	Capacitive load schematic	110
7.6	Hall Effect trace of a Capacitive transient on line current. Time scale is set at 5ms/div	111

7.7	Hall Effect trace of a Capacitive transient on line current. Time scale is set at 2ms/div	111
7.8	Capacitive Transient. FOCSNET Trace I	113
7.9	Capacitive Transient. FOCSNET Trace II	114
7.10	Capacitive Transient. FOCSNET Trace III	114

LIST OF SYMBOLS

A_x	amplitude of x-axis orthogonal component
A_y	amplitude of y-axis orthogonal component
α	attenuation factor of the system
α_s	splice loss
C_{p1}	couplers between the transmitter and the sensors
C_{p2}	couplers between the sensors and the receiver
c	velocity of light in free space
$dn/d\lambda$	dispersion of the medium
Δf	noise equivalent bandwidth
\vec{E}	electric field vector of polarized wave
E_x	electric field vector of x-axis orthogonal component
E_y	electric field vector of y-axis orthogonal component
e	charge on electron
e/m_0	specific charge of the electrons
γ	magneto-optical constant
H	magnetic field intensity
h	hexadecimal numeral
I	current present in the conductor
I_{amp}	op-amp noise current
I_d	dark current
I_{in}	op-amp input noise current
I_p	photo current
I_s	shot noise current
I_t	thermal noise current
J	intensity of light at input of first polarizing fiber
J_{in}	intensity of light at output of first polarizing fiber
J_{out}	intensity of light at output of second polarizing fiber
k	Boltzmann's constant

L	length of the optical path
L_1	length of the first fiber
L_2	length of the second fiber
L_{CI}	excess loss of the coupler
L_{TI}	tap ratio loss of coupler to sensor (90:10)
L_{SC}	excess loss of the Star coupler
L_{T1}	tap ratio loss of coupler on the transmitting fiber (10:90)
L_{T2}	tap ratio loss of the couplers on the receiving fiber (50:50)
L_{TS}	tap ratio loss of the Star coupler
λ	optical wavelength
m	slope
m_e	mass of electron
N	number of turns of optical path around the conductor
n	refractive index of the medium
θ	faraday rotation angle
ω	angular frequency
ϕ_x	phase angle of x-axis orthogonal component
ϕ_y	phase angle of y-axis orthogonal component
R_f	feedback resistance
T	temperature
t_{L1}	time taken by leading edge of the first pulse to reach the receiver
t_{L2}	time taken by leading edge of the second pulse to reach the receiver
t_p	pulse duration
t_{sep}	separation between the two pulses
V	Verdet constant
V_{amp}	op-amp noise voltage
V_{in}	op-amp input noise voltage
V_{noise}	total system noise voltage
V_s	shot noise voltage
V_t	thermal noise voltage

LIST OF ACRONYMS

AC	Alternate Current
ADC	Analog to Digital Converter
CT	Current Transformer
DC	Direct Current
DSP	Digital Signal Processor
EMI	Electro Magnetic Interference
FDM	Frequency Division Multiplexing
FOCSNET	Fiber Optic Current Sensor Network
FPGA	Field Programmable Gate Array
IC	Integrated Circuit
LDP	Laser Driving Pulse
LPF	Low Pass Filter
MF	Multiplication Factor
MSPS	Mega-Samples per Second
Op-Amp	Operational Amplifier
OTDR	Optical Time Domain Reflectometry
PC	Personal Computer
PCB	Printed Circuit Board
Ph/Amp	Photodetector Amplifier
PM	Polarization Maintaining
PZ	Polarization Fiber
RAM	Random Access Memory
SAP	Stress Applying Parts
SNR	Signal to Noise Ratio
SOP	State of Polarization
TDM	Time Division Multiplexing
WDM	Wavelength Division Multiplexing
ZCL	Zero Current Level

I. INTRODUCTION

1.1 BACKGROUND

Electrical current measurements are fundamental in power networks, particularly where they are used for metering, tracing, tracking, control and monitoring. Since the 1800's conventional Current Transformers (CTs) have performed these tasks.

CTs have increased in size due to the demand for high voltage electric power systems. Porcelain insulators and oil-impregnated materials have to be used to provide insulation between the primary bus and the secondary windings. Insulation prevents field stresses that can cause insulation breakdown [1]. The saturation of the iron core under fault current and the low frequency response of the conventional CTs reduce the dynamic range and do not allow them to respond well under transient conditions. This is true especially for those currents with transient DC components which aid a remnant flux condition pre-existing in the core, and may cause inappropriate function of the relays [1]. In power systems the line current is much smaller under normal conditions than under fault conditions (e.g. 10:1 ratio). Because of the small dynamic range of magnetic coupling between the primary and secondary winding in a CT, more than one set of coils is needed to cover the requirements for metering and relaying [2].

New computer-based digital control systems have been implemented onto power systems but power systems have trouble interfacing with conventional CTs because of induction of Electro-Magnetic Interference (EMI) through the ground loop. An opto-insulator auxiliary CT is required to avoid this problem.

Performance limitation and various failures have led the power industry to question the reliability of conventional CTs, thus the need for new technologies to take on this task. The newly emerged Optical CT provides a solution for many of the mentioned problems [2].

1.2 OPTICAL CURRENT SENSORS

Optical CTs or Optical Current Sensors have been recognized as having significant advantages in many different applications where current measurement is required. Optical CTs small size, immunity to EMI, extended dynamic range and wide frequency response and the provision of an insulated optical link from the CT to any relaying system provides an appealing solution to the conventional CTs limitations. Optical Current Sensing techniques are breaking their way into the power industry and as they are developed further they will no doubt satisfy the needs for the vast potential market.

The optical current measurements are typically done by means of the Faraday Magneto-Optic Effect [3], which was first observed by Michael Faraday in the 1800's. The Faraday Effect is the phenomenon by which the orientation of polarized light rotates under the influence of the magnetic field and the angle of the rotation is proportional to the strength of the magnetic field component flowing in the direction of light propagation in the optical path [4,5].

In an optical CT system a sensor element is placed near a current carrying conductor. A light source is injected into it either through an optical fiber or free space. The incident light is modulated by the sensor and returned to a receiver where the modulation is detected, quantified and translated into an equivalent current value.

The Faraday Effect alters the State of Polarization (SOP) of the light and this is measured by a one-detector or two-detector method. In the two-detector system the change in Polarization State is detected using a Wollaston prism and a pair of photo-detectors arranged to measure the two orthogonal polarization components emerging from the prism [4]. A single-detector system detects the change in the intensity of light caused by the change of Polarization State [6].

The majority of optical CT systems have adopted the two-detector approach, which improves Signal to Noise Ratio (SNR) though this approach is harder and more costly to implement especially in an all-fiber system.

The design of optical CTs has fallen into two categories, Bulk Glass and Fiber Optic. The Bulk Glass design [2,4,7,8] consists of an optical glass prism used as the sensing unit and an optical fiber is used to transmit the signal. The prism is formed around a conductor enabling the light beam to travel around the conductor to pick up the Faraday rotation. The bulk glass approach requires lenses, polarizers, free space optics and highly stable assemblies to connect the sensing element to the rest of the optical system. Fiber optic sensors [3,9,10,11] consist of a series of turns of the fiber around the conductor in order to pick up the Faraday rotation. The optical fiber is used both to sense the magnetic field produced by the line current and to transmit the optical signal as well.

Devices to-date have used the easily misaligned Bulk Glass system but, because of the potential cost, size and reliability advantages, the industry is moving to systems where all the optics, including polarizing elements, are made from optical fiber technology.

1.3 FIBER OPTIC CURRENT SENSOR NETWORK (FOCSNET)

Optic CTs have been used and installed since 1986 [12]. All of these systems, most being the Bulk-Glass-based, use a single point sensor system, i.e. there is one light source and one receiver per installed sensor.

Using an all-fiber optic approach it is much simpler to design a sensor network having a single transmitter and receiver with multiple sensors placed at different locations networked together [13]. With bulk glass sensors, it is extremely complex to build such a network.

The sensor technology has reached the point where the fiber optic current sensors are commercially available. This enables the build-up of not only the single point sensor system, but also a whole network of sensors driven by a single optical source. A key advantage of sensor multiplexing is the reduction of the cost per sensor, because of the use of a single transceiver unit.

Different techniques can be used to build such a network [14,15], like Frequency Division Multiplexing (FDM), Time Division Multiplexing (TDM) and Wavelength Division Multiplexing (WDM). The multiplexing method may be said to be passive, if only passive sensors and interconnection elements are used (i.e., there is no external electrical power required). Fiber optic sensors are intrinsically suited to such passive multiplexing schemes.

The TDM approach consists of launching a series of equidistant fixed length light pulses into the system and detecting the differentially delayed returning pulses caused by the difference in fiber lengths to each sensor [14,15]. In FDM, every sensor is assigned a frequency channel within which the signal can be modulated in amplitude or frequency. WDM, similar to FDM, takes advantage of the enormous bandwidth of optic fibers. Here a separate wavelength is assigned to each sensor of the network. Although highly accurate, FDM requires complex electronics and WDM requires very sensitive and selective optical components.

Distributed sensing schemes like Optical Time Domain Reflectometry (OTDR) where the fiber itself acts as the sensor have also been investigated [14,16]. OTDR utilizes an optical radar concept to measure the backscatter power versus time characteristics when a light pulse is launched into the fiber. Work has also been done on coherence multiplexing of sensors where a short coherence length continuous optical source is used [17]. The main principle behind this technique is that the delay in the sensor array is arranged so that the returning optical signals are mutually incoherent and therefore do not interfere

with one another. The signal from each sensor can be retrieved separately by matching the delay in the receiving interferometer.

The TDM approach appears to be the more pragmatic choice over the other methods mentioned due to its overall simplicity.

1.4 SCOPE OF THE THESIS

Optical CTs are now commercially available and a significant amount of research continues to be done on them every day, especially in regards to the all-fiber CTs. The development of systems where these types of CTs are used is also growing. The implementation of an all-fiber current sensor network (TDM) has been recorded showing promising results [13].

The aim of this thesis is to investigate the possible improvements of the all-optical fiber current sensor network. Improvements include the study and development of a technique that enables a TDM-based network to detect AC and DC current accurately and reliably. It also investigates the feasibility of capturing current transients.

In the following chapters the optical theories, engineering design, fabrication and testing of a TDM Fiber Optic Current Sensor Network (FOCSNET) are described.

Chapter II deals with the optical theories developed and used to make magneto-optic current sensing possible and the ones used to create a fiber optic sensor. Chapter III details the design and components of the fiber network used in this project. This structure dictates how information is going to be gathered and in which format it is presented so it can be adequately processed to obtain the final results of line current information. Chapter IV describes the design of the Digital Receiver which, is the brain of the whole

system. With it the display of line current values flowing through the sensors are possible, as well as the capability to capture and display specific segments of the current signal.

In Chapter V system characteristics and parameters are presented. Chapter VI presents the experimental results of the system. The development of the two ratio techniques are detailed here since these are the basis for reliable AC and DC measurements. Data in this chapter was gathered from tests and experiments done on the system. These results include: DC current measuring experiments, AC current measuring experiments, these last two tested under networked conditions. Test results are also shown in regards to measurements of networked DC and AC line currents simultaneously flowing on different sensors. An experiment showing how DC and AC currents flowing through the same sensor can be measured simultaneously is also detailed in this chapter. Chapter VII focuses on the capability of the receiver to capture transient on the line current. Plots of line currents measured are traced. This chapter also deals with the ability of the system to record and plot transient conditions on line currents.

II. OPTICAL THEORIES

2.1 OVERVIEW

The basic element in the system described in this thesis is the Sensor or Transducer and the theories behind the Fiber Optic Current Sensor are detailed in this chapter. The two main concepts, the Faraday Magneto-Optic Effect and Polarization, are first explained and how these concepts work within Fiber Optics is then described.

2.2 FARADAY MAGNETO-OPTIC EFFECT

When linearly polarized light propagates through an optically active material its plane of polarization rotates under the influence of a magnetic field flowing parallel to the direction of the propagating light. The rotation angle is proportional to the intensity of the magnetic field [18]. This phenomenon was first seen by Michael Faraday in 1845 and thus is known as the Faraday Effect. The rotation is generally given by the empirical law,

$$\theta = V \int_0^L \vec{H} \cdot d\vec{l} \quad \text{Eq. 2.2.1}$$

Where θ is the angle of rotation, V is the Verdet constant of the material (rad/ampere-turn), H is the magnetic field intensity and, L is the optical path length. The above expression can be simplified when the magnetic field is uniform and is flowing parallel to the optical path.

$$\theta = VHL \quad \text{Eq. 2.2.2}$$

When the light propagation direction differs from the magnetic field direction by an angle ϕ , the rotation is given by,

$$\theta = VHL \cos \phi \quad \text{Eq. 2.2.3}$$

When polarized light through a magneto-optical material encircles a current carrying conductor, then using Ampere's Law [4] the rotation is given by,

$$\theta = VNI \quad \text{Eq. 2.2.4}$$

Where N is the number of turns of the optical path around the conductor and I is the current carried by the conductor.

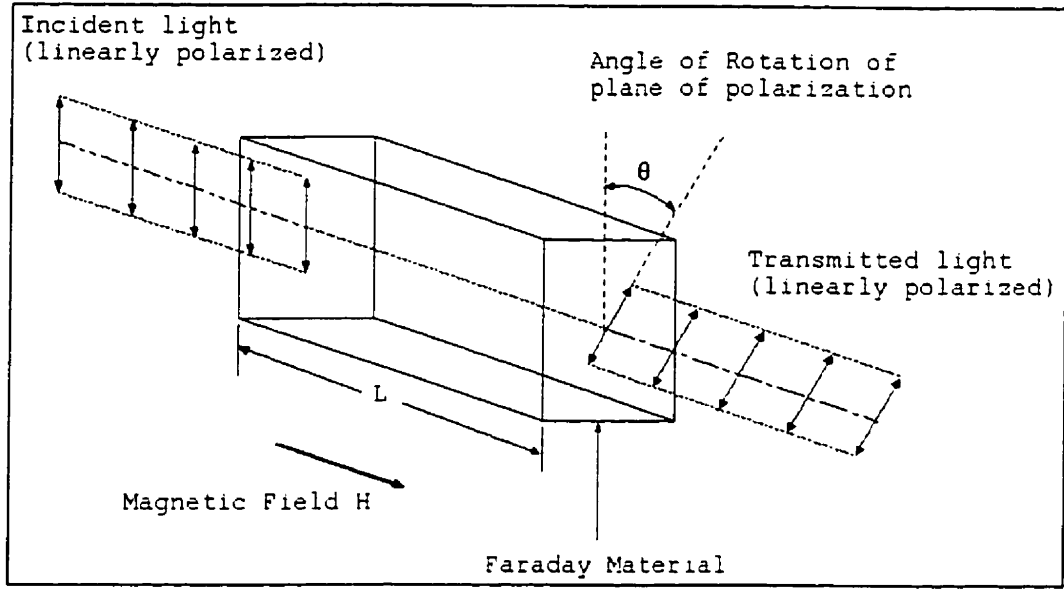


Fig. 2.1 Faraday Effect Concept

The dependence of the Verdet constant on wavelength and refractive index is expressed as follows [1,2],

$$V = \gamma \frac{e_0}{m_0} \frac{\lambda}{2c} \frac{dn}{d\lambda} \quad \text{Eq. 2.2.5}$$

Where γ is the magneto-optical constant, c is the velocity of light in free space, e_0/m_0 is the specific charge of the electrons and $dn/d\lambda$ is the dispersion. The higher the dispersion of the material the larger Verdet constant it has. The Verdet constant is also temperature and some times field dependent, and it varies for different materials.

The Faraday effect is a dispersion effect and can be understood in terms of the space anisotropy introduced by the magnetic field [4]. All dielectric materials exhibit, to some extent, this effect. In particular it is found in glasses and silica, the materials from which optic fibers are made; these materials have a measurable Verdet constant. As silica has a relatively small Verdet constant it is necessary to have a strong magnetic field or a large amount of current in the conductor in order to measure the Faraday Effect. This makes a fiber optic sensor suitable for the power industry where currents of 1000 Amperes + flow through their transmission lines.

2.3 POLARIZATION

A beam of light consists of many waves each having its own electrical field component. Normally the orientation of these electric field components are randomly distributed, such light is known as unpolarized light. Polarized light is one in which the electric field components of the beam have similar orientations. Light polarization was first observed by Erasmus Bartolinus in 1669, and was later developed by Hugen, Malus, Brewster and Young amongst others [19].

The orientation characteristics of the electric vector representing the polarized light determine the state of polarization (SOP) of the wave [20]. If the incoming wave is seen from the direction of propagation (e.g. z-axis), the locus of the tip of the electric vector is a measure of the polarization. If the locus is a straight line the wave is said to be linearly polarized. When the locus is a circle the polarization is circular and it may be divided into right or left circularly polarized light [13]. Polarized light beams can be resolved into a pair of mutually orthogonal components of the electric field traveling along the direction of light propagation [2,13]. Intensity, orientation and polarization-type depend on these orthogonal components. The orthogonal components lie along the x and y-axes when light is propagating in the z direction. When the two components are in phase linear

polarization is the result. The orientation also depends on the relative amplitudes of the two components (e.g. $\tan^{-1} (A_y/A_x)$). If amplitudes are matched the wave will have a 45° orientation.

If the components are equal in amplitude and 90° out of phase the resultant wave is said to be circularly polarized. If the resultant vector rotates clockwise in reference to the source, it is known as right circularly polarized light and visa-versa. Circularly polarized light does not have any orientation as such thus its amplitude and sense of rotation describe it. Elliptical polarization is generated when the components have unequal amplitudes and a phase difference, or have matched amplitudes but a phase difference other than 90° . Fig 2.2 shows the effect that amplitudes and phase differences of the two orthogonal components have on the overall state of polarization of the light wave [13].

2.4 JONES CALCULUS

In 1941, R.C. Jones determined that a 2×1 -column vector, known as the Jones vector [21], could represent polarized light. Each element of the Jones vector describes a component of the electric vibration at a given location. The first element indicates the amplitude and phase of the x -component and the second element of the y -component.

A beam of polarized light traveling at the speed of light along the z -axis can be considered as a plane wave. Its electric field vector \vec{E} can be specified in terms of its orthogonal components E_x and E_y , with amplitude and initial phase A_x , ϕ_x and A_y , ϕ_y respectively, so then,


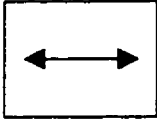

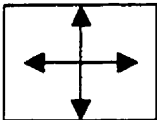
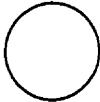
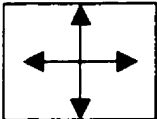

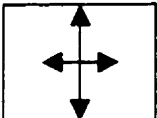
Spectral Pattern of Polarized Wave	Sectional Patterns of Orthogonal Components	Orientation (in degrees)	Phase Difference Between Components	Type of Polarized Light
		0	0	Linear
		45	0	Linear
		-	90	Right Circular
		90	90	Left Elliptical

Fig. 2.2 Relationship between orthogonal components and type of polarization

$$E_x = A_x \cos\left[w(t - \frac{z}{c}) + \phi_x\right] = \Re[A_x e^{i\{w(t - \frac{z}{c}) + \phi_x\}}] \quad \text{Eq. 2.4.1}$$

$$E_y = A_y \cos\left[w(t - \frac{z}{c}) + \phi_y\right] = \Re[A_y e^{i\{w(t - \frac{z}{c}) + \phi_y\}}] \quad \text{Eq 2.4.2}$$

When $|\phi_x - \phi_y| = 90^\circ$, and $A_x = A_y$, then \vec{E} is circularly polarized. When $|\phi_x - \phi_y| = 0^\circ$, \vec{E} is linearly polarized. In the general case \vec{E} is elliptically polarized. In a Matrix form the above equations can be rewritten as,

$$\begin{bmatrix} E_x \\ E_y \end{bmatrix} = \begin{bmatrix} A_x e^{i\phi_x} \\ A_y e^{i\phi_y} \end{bmatrix} e^{i[w(t - \frac{z}{c})]} \quad \text{Eq. 2.4.3}$$

The Jones vector is an alternative way to represent \vec{E} as a column vector,

$$\begin{bmatrix} E_x \\ E_y \end{bmatrix} = \begin{bmatrix} A_x e^{i\phi_x} \\ A_y e^{i\phi_y} \end{bmatrix} \quad \text{Eq. 2.4.4}$$

For example, $\begin{bmatrix} 1 \\ 0 \end{bmatrix}$ is a linearly polarized light with the orientation of the x-axis, $\begin{bmatrix} 0 \\ 1 \end{bmatrix}$ is a linearly polarized light with the orientation of the y-axis, $\begin{bmatrix} 1 \\ i \end{bmatrix}$ is a right circularly polarized light, and $\frac{1}{\sqrt{2}} \begin{bmatrix} 1 \\ 1 \end{bmatrix}$ is a linearly polarized light with 45° orientation.

The main use of the Jones vector is in computing the effect of inserting polarizers in a given polarized beam. The effect is computed by multiplying the Jones vector of the incident beam by the matrices that represent the polarizers [22].

When polarized light is passed through a polarization device, the output light can be represented as another column vector which is the product of the Jones matrix of the device and the Jones vector of the input light. The Jones Matrix is a 2x2 matrix that represents a polarization device [13].

$$\begin{bmatrix} E_{2x} \\ E_{2y} \end{bmatrix} = \begin{bmatrix} J_{11} & J_{12} \\ J_{21} & J_{22} \end{bmatrix} \begin{bmatrix} E_{1x} \\ E_{1y} \end{bmatrix} \quad \text{Eq. 2.4.5}$$

The four elements of the Jones Matrix are complex and depend on the device itself [2]. For example a quarter wave plate, which is an important optical component, can provide

a 90°-phase difference between the two orthogonal components of the polarized light. If the orientation of the quarter wave plate is 45°, then the Jones matrix is,

$$J = \frac{1}{\sqrt{2}} \begin{bmatrix} 1 & i \\ -i & 1 \end{bmatrix} \quad \text{Eq. 2.4.6}$$

And if the Jones Vector for the input light is $E_{in} = \begin{bmatrix} 0 \\ 1 \end{bmatrix}$; the output light will be the product,

$$E_{out} = \frac{1}{\sqrt{2}} \begin{bmatrix} 1 & i \\ -i & 1 \end{bmatrix} \begin{bmatrix} 0 \\ 1 \end{bmatrix} = \frac{1}{\sqrt{2}} \begin{bmatrix} 1 \\ i \end{bmatrix} \quad \text{Eq. 2.4.7}$$

Which is a right-circular polarized light.

The Jones matrix for any material that rotates the polarized light by an angle of θ is given by,

$$R = \begin{bmatrix} \cos \theta & \sin \theta \\ -\sin \theta & \cos \theta \end{bmatrix} \quad \text{Eq. 2.4.8}$$

Using Jones Matrices the effects of a train of polarizers on a given beam is calculated by multiplying the vector of the incident beam by the matrices of the polarizers. Since matrices do not commute, they must be written in the correct order [22]. The order must be the same as how the polarizers are physically arranged.

2.5 POLARIZATION AND FIBER OPTICS

The presence of stresses such as bends or twists can alter the SOP of light traveling through a single mode fiber [23,24,25]. If the fiber is subjected to external perturbations, for instance temperature changes, then the final output polarization will vary with time.

This is true even for short lengths of fiber and it is undesirable in many applications which require a constant output polarization from the fiber [13].

Polarization Maintaining fibers (PM fibers), also known as High Birefringent (Hi-Bi) fibers, have been developed to deal with this problem. Birefringence refers to the difference in the propagation constant of the two orthogonal polarizations traveling through the fiber [20,26,27]. Birefringence breaks the circular symmetry in an optic fiber creating two principal transmission axes within the fiber known as the fast and slow axes of the fiber. The high birefringence of these fibers prevents power coupling between the orthogonal components. This results in very low noise and cross talk with a consistent SOP of the light traveling through the fiber. When linearly polarized light is injected into a PM fiber, and it is orientated along one of the two axes, the output light will remain linearly polarized and aligned with the principal axis even under conditions where external stresses are present.

Birefringence is created by a non-circular fiber core, or by inducing constant stresses within the fiber with stress applying parts (SAP) [26,27,28]. The elliptical core fiber is a good example of the shape-induced birefringence. The optical losses in these types of fibers are generally high due to the large refractive index difference and imperfection of the core shape. Stress induced birefringent fibers, such as Bow Tie and PANDA fibers, have low optical losses and low cross talk by setting a buffer layer between the core and the SAP's [27].

Several polarizing core/cladding structures are shown in Fig 2.3, the dashed lines in the drawings show the slow axis of each structure.

In Polarizing fiber (PZ), a special type of PM fiber, one mode is driven to cut-off [29,30]. At cut-off the mode ceases to be guided within the fiber core and its energy is lost through the cladding. The light launched into the slow axis is guided inside the fiber and

it emerges as linearly polarized light having the same orientation as that of the slow axis. No light emerges from the fast axis for any light launched into it is driven to cut-off. Thus, a PZ fiber outputs linearly polarized light in the orientation of the slow axis regardless of the nature or SOP of the input light. The amplitude of the output light is proportional to the relative difference between the orientation of the input light and the slow axis of the PZ fiber. If the light is totally depolarized the amplitude of the output light will be half that of the input.

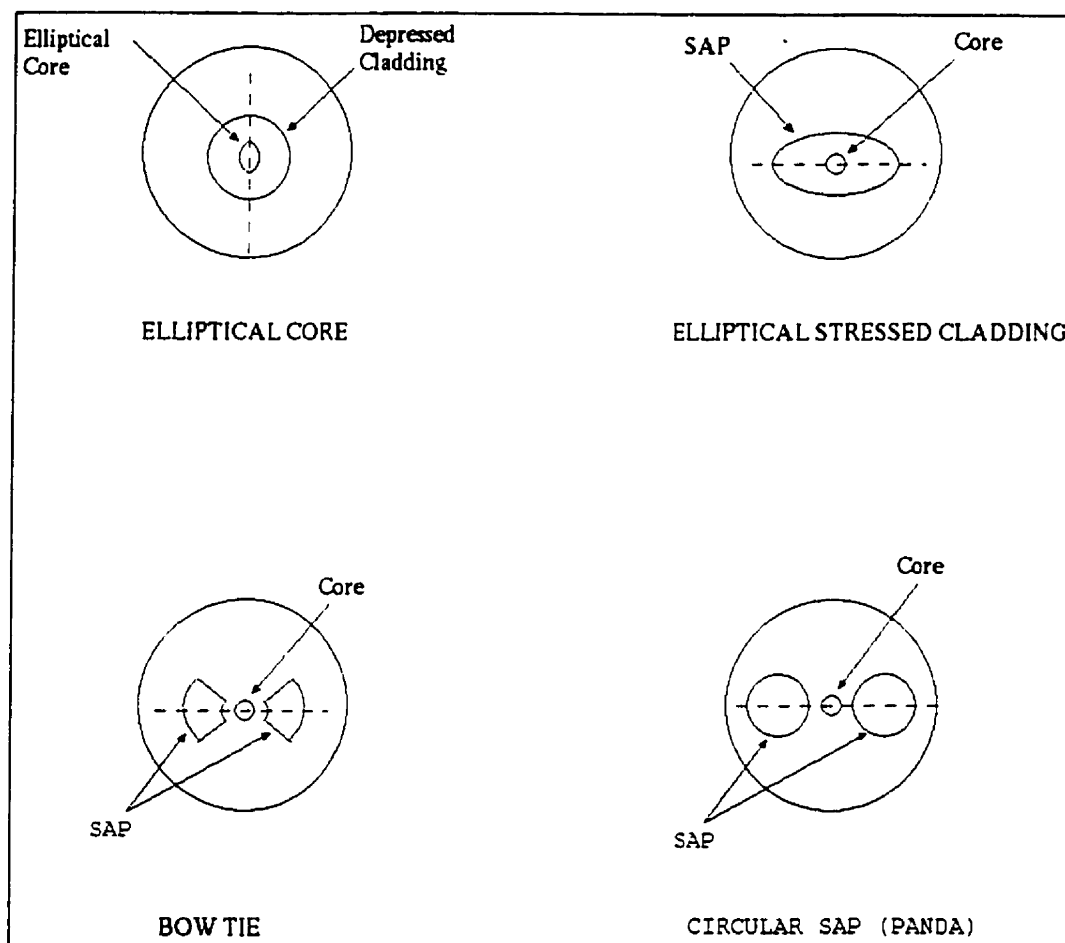


Fig.2.3 Polarization Maintaining Fiber Core Structures

2.6 SENSING FIBER COIL

The plane of polarization of the polarized light inside a current sensing fiber is rotated when it experiences the Faraday Effect [13]. The sensing fiber must have very low birefringence for this rotation to take place. A high birefringent fiber may resist the magnetically induced circular birefringence of the Faraday Effect. The presence of even small amounts of linear birefringence interferes with the Faraday Effect, making it nearly unmeasurable [31]. A considerable amount of research has been done to reduce and try to eliminate linear birefringence in sensing fibers and one approach is to introduce circular birefringence into the fiber. Circular birefringence causes a rotation of the plane of polarization that merely adds to that caused by the Faraday Effect. If the circular birefringence is sufficiently large then the linear birefringence arising from bending or other effects has little effect.

Circular Birefringence is introduced to a fiber by torsional stress caused by twisting [32,33]. This method is only effective for large fiber coils and a few turns. For small coils the twist necessary to achieve the effect exceeds the breaking strength of the fiber. With this method there is still the dependency on temperature and therefore a stability problem. It has been shown that both the inherent and bend-induced linear birefringence can be reduced substantially by annealing the fiber [32]. Current sensors based on annealed fiber have better temperature stability. Another advantage of the annealing process is that with it a sensing coil can be produced from ordinary telecommunications fiber [33].

In order to minimize a coil's sensitivity to vibration, it must be carefully packaged. A ceramic mold encased in an identically shaped plastic holder is how some commercial sensors are presently encased [9].

III. NETWORK

3.1 OVERVIEW

The aim of this thesis is to further investigate the behavior and applications of a Fiber Optic Current Sensor Network.

Optic current sensing is based on the Faraday Effect which is detailed in the previous chapter. This chapter depicts how the Faraday sensors are arranged into a network, how this network is designed and what components it consists of.

The project is based on the Network implementation presented in S. Goyal's 1997 thesis, *"Fiber Optic Current Sensor Network"* [13] where it was determined that a TDM approach provided the optimum solution for a Multiplexing Technique. As far as Network topology goes S. Goyal determined that a Star network offers the best performance in terms of total system loss and it shows better results when additional sensors are added to the network [13].

In the following sections of this chapter the Sensor Network design is described, as well as a detailed summary of all the components that make up the system. The system receiver is merely mentioned in this chapter. Chapter IV describes in great detail the receiver, its design, components and functionality.

3.2 NETWORK

The FOCSNET, as for most other networks, is based on a pre-established topology. The chosen topology of a Fiber Optic Current Sensor Network is determined by the desired method of sensor modulation and interrogation. As mentioned in the introductory chapter

there are several multiplexing techniques (e.g. TDM, FDM, and WDM), which can be implemented into topologies such as Ladder or Star.

3.2.1 Time Division Multiplexing (TDM)

TDM consists of launching short equally spaced light pulses into a multiple point network. The sensors are spatially distributed in order to delay the returning pulses by a time interval given by,

$$t_i = \frac{nL_i}{c} \text{ [s]} \quad \text{Eq. 3.2.1}$$

Where L_i is the fiber link length of the i th sensor and n is the core refractive index of the fiber. At the receiver, the pulses arrive separated in time due to the different path lengths traveled to and from each sensor [14,15] and they are then converted to electrical signals and the original signal is decoded. The number of sensors that can be successfully multiplexed is governed by factors such as Laser pulse power, pulse width, repetition rate of the Laser, optical fiber loss, coupler split ratios and insertion loss [13].

3.2.2 Star Network

In this system one passive star coupler is connected at the transmitter and a second one at the receiver. Each sensor is independently connected to the transmitter and receiver through these couplers. This is very robust since each sensor is connected individually. There is no interference between sensor signals, and if a fiber is damaged, it only disables one sensor and not the entire system. Topographically it is very flexible thus there are minimal complications when adding or removing a sensor [13].

The following is an expression for Total System Loss (TLS) for a star network,

$$TSL = 2(L_{SC} + L_{TS}) + 4\alpha_s \text{ [dB]} \quad \text{Eq.3.2.2}$$

Where L_{SC} is the Excess loss of the star coupler, L_{TS} is the tap ratio loss for the star coupler and α_s is the loss for a single splice. Using conventional values for these losses the expression in turn looks like,

$$TSL = [2(2 + 10\log_{10}N) + 4(0.1)] \text{ [dB]} \quad \text{Eq. 3.2.3}$$

The TSL is a logarithmic function of the number of sensors (N) in the network, rather than a linear function [13]. Because of this, losses increase only slightly when the number of sensors is increased.

The star network promises low system loss and other advantages such as a high level of security, great flexibility and affordability. It was concluded that it is the optimum topology for this project. Several sensors can then be connected onto a single transceiver unit.

Description and comparison of other applicable multiplexing techniques and network topologies are described in detail by S. Goyal's [13].

3.3 BASIC NETWORK DESIGN

As mentioned previously the fiber network used in this project is based on the network designed by S.Goyal, with which he showed that two or more fiber optic current sensors can be successfully networked together using a single transceiver unit [6].

A very important factor in the design of the network is the lengths of the optical paths between the transmitter and receiver, especially the difference of lengths between sensors, since the time delay or separation of the optical pulses reaching the receiver depends on this difference [13]. Fig. 3.1 shows two optical pulses in the time domain.

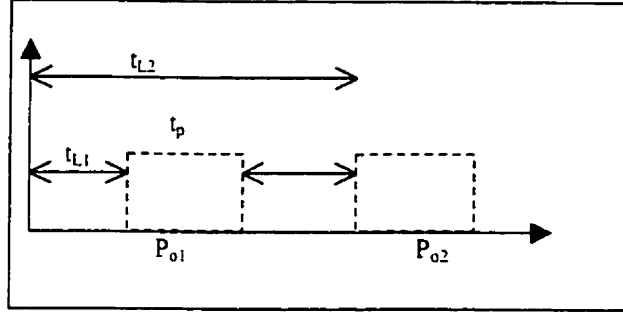


Fig.3.1 Pulse gap at Receiver

The time separation of the two pulses at the receiver is,

$$t_{sep} = t_{L2} - (t_{L1} + t_p) \quad \text{Eq. 3.3.1}$$

Where t_{L1} and t_{L2} are the times taken to reach the receiver by the leading edges of the P_{o1} and P_{o2} pulses respectively and t_p is the pulse width. The optimal value for the Laser Driving Pulse (t_p) and t_{sep} were found to be 400ns, so

$$\begin{aligned} (t_{L2} - t_{L1}) &= t_p + t_{sep} \\ 400\text{ns} + 400\text{ns} &= 800\text{ns} \end{aligned} \quad \text{Eq. 3.3.2}$$

Thus the difference in the optical path lengths to the receiver must be equivalent to 800ns.

The time taken by a light pulse to travel a distance of L in a medium of n refractive index is given by,

$$t_L = \frac{nL}{c} \quad \text{Eq. 3.3.3}$$

To generate a time gap of 800ns between pulse leading edges the difference between fiber lengths to the receiver should be,

$$L2 - L1 = \frac{\delta t_L c}{n} = \frac{(800 \times 10^{-9})(3 \times 10^8)}{1.5} = 160m$$

The values for the two fiber paths in this project were set at 10m and 170m for the first and second sensor respectively.

The design of a two sensor star network is shown in Fig. 3.2.

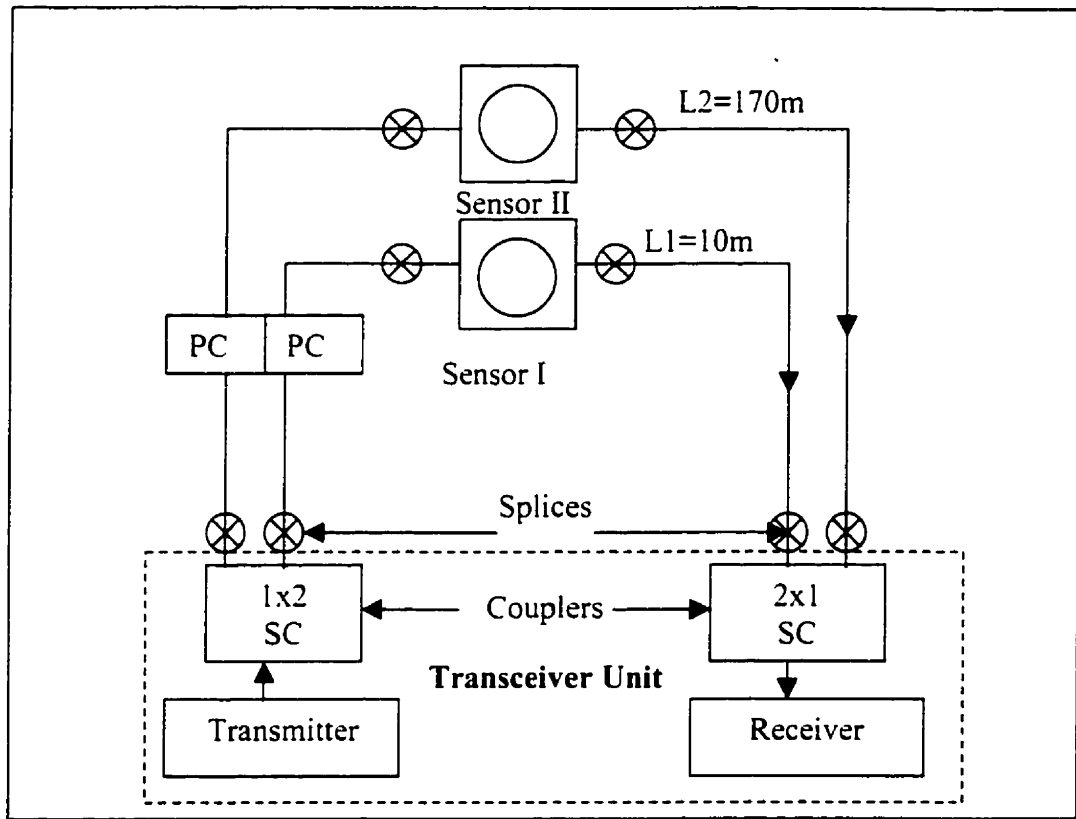


Fig. 3.2 Two sensor Star Network

3.4 FIBER NETWORK COMPONENTS.

The all-fiber FOCSNET has several optical and electronic components that are detailed in this section. Each pulse generated by the Laser light source is split into two identical pulses through a star coupler. Before reaching the two sensors, each fiber is connected to

a polarization controller in order to maximize the light input to the sensors. At the sensor the level each pulse is modulated in amplitude due to the Faraday rotation. The two pulses from the two sensors travel different fiber lengths to be combined by another coupler at the receiver.

The FOCSNET can be divided into three parts,

- Transmitter
- Fiber Network and sensors
- Receiver

The transmitter consists of the pulsed light source. The receiver consists of a photodetector and the following components: Amplifier, differential amplifier, Analog to Digital Converter (ADC), Field Programmable Gate Array (FPGA), Digital Signal Processor (DSP) and RAM Unit. The description of each component as well as the overall functionality of the receiver is described in chapter IV.

The following is a list of the fiber network components and their descriptions.

3.4.1 Transmitter

The transmitter consists of a pulsed Laser Diode (LD) operating at a wavelength of 820nm. The LD is modulated by a signal generated by a very precise pulse generator. The LD transmits 400ns wide pulses at 25 μ s intervals as per system specifications. The stability of the Laser light source is very important since any change in the value of the light intensity will or could be taken as a change in the current being measured by the sensor. The laser built for this project was designed, with the help of TR Labs, Edmonton, to be as stable as possible. The Laser was constructed with provision for internal thermal compensation to resist changes in temperature. The Laser diode is a SHARP LT017; the

units' output is a pigtail single mode fiber terminated with a FCAPC angled fiber connector. This results in a high coupling efficiency from laser to the fiber.

Varying the drive current, the Lasers' output is smoothly adjusted. Measurements were made to quantify the effect of the drive current on the output power and Fig.3.3 shows that relationship.

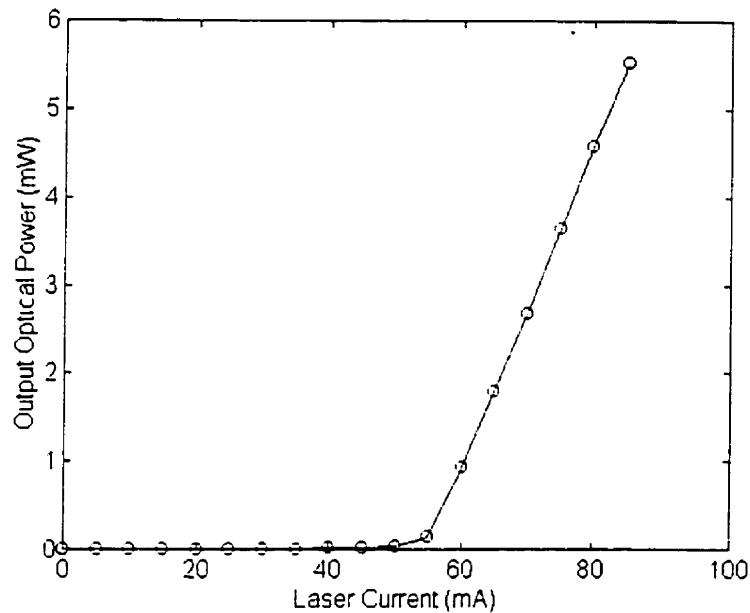


Fig. 3.3 Laser Output Power vs. Drive Current

3.4.2 Fiber Optic Network

Once in the fiber, the light pulse from the LD is split into two identical pulses, by the 1x2 star coupler, which then proceed to each of the sensors where they are modulated in intensity by the line current flowing around them. The intensity-modulated signals then carry on to the receiver for signal processing. The fiber optic network consists of the following components: single mode star couplers, single mode fiber, polarization controllers, fusion splices and fiber current sensors.

3.4.2.1 Single Mode Star Couplers

The two single mode star couplers are found at the beginning and at the end of the fiber network. One is used to split the Laser Pulse into two pulses. Later the second coupler rejoins the pulses onto the same path and on to the receiver. For this network a 1x2, 50:50 split ratio single mode coupler was used on the front end. (A 1x2 optical fiber coupler is essentially the same as a 2x2 coupler except that only one leg is activated at the input. On a 2x2, 50:50 split ratio coupler; light on either input will be split equally in half at the two output fibers.)

In the input coupler a 50% optical loss is generated due to the fact that the signal is split equally in power. At the output coupler due to tap losses only 50% of the light of each input channel is transmitted to the receiver, the reason being, since its a 2x2 star coupler there are two output channels but only one is used. The insertion loss (IL) for each of the two couplers is given by,

$$\begin{aligned}
 IL &= \textit{Splitting Loss} + \textit{Excess Loss} && \text{Eq. 3.4.1} \\
 &= 10\log_{10}(2) + 0.5 \\
 &= 3 + 0.5 \\
 &= 3.5 \text{ dB}
 \end{aligned}$$

3.4.2.2 Single Mode Fiber

Single mode fiber is used to transmit the input light pulses to the sensor. Single mode fiber is used since the sensor head's fiber is also single mode and in order to obtain efficient splicing it is essential that the core and cladding of both fibers are the same in diameter.

The purpose for these fibers is to position the current sensor geographically and to provide the required time delay between the two pulses at the receiver, and this time separation depends on the relative lengths of the two fibers. For this project, the two fibers running from the sensors to the receiver have 10m and 170m lengths respectably.

This difference in path lengths provides an 800ns separation between the leading edges of the two pulses at the receiver. Since the light pulse is 400ns wide, a 400ns gap makes up the idle time between pulses at the receiver.

The fiber used in this project is a 3M single mode fiber with an attenuation of 2.1dB/km. The longest path in the presented network is 170m and, thus it has an attenuation of 0.36 dB.

3.4.2.3 Polarization Controllers

The State of Polarization of the Laser Output through the coupler and into the sensor is very important. The Laser light is not completely un-polarized in nature. The Laser output is a mixture of polarized and un-polarized light and the orientation of the polarized light is at 20° [13]. With the aid of the polarization controller, the polarization alignment is controlled and the losses at the first polarizing fiber of the sensor head are kept to a minimum.

The polarization controllers in this project work on the basis of the birefringence caused by twisting the fiber. By twisting a single mode fiber, its slow axis is aligned in the direction of the twist applied [34]. Having control of the twisting mechanism of the fiber makes precise polarization alignment possible.

3.4.2.4 Current Sensing Head

The 3M current sensing head contains the coiled sensing fiber and within this fiber the light rotates its polarization plane in the presence of the magnetic field that accompanies the line current. This Faraday rotation has to be opto-electronically measured at the receiver. In the absence of detectors allowing the direct measurement of the polarization orientation of light, the relation signal must first be converted into an amplitude signal. This conversion is done optically by the sensing head. It consists of two polarizing fibers (PZ) with an annealed sensing fiber (AF) between them. The annealed sensing fiber is

enclosed in a ceramic frame that has a circular hole in the middle in order for the current conductor to pass through and the AF is coiled around this hole. The polarization axes of the two PZ fibers are 45° apart [35].

As discussed in the previous chapter the PZ fiber acts as a very effective polarizer. The light coming from the Laser source to the first PZ fiber through the input coupler arrives at the input of the first PZ fiber with intensity J . Let the intensity of the light coming out of the first polarizing fiber be J_{in} , which is in fact the light intensity entering the AF, and let J_{out} be the intensity of the light coming out of the second polarizing fiber. Light intensity is reduced by half after passing through a polarizer set at any angle [25] therefore,

$$J_{in} = \frac{J}{2} \quad \text{Eq. 3.4.2}$$

As discussed in the previous chapter, the intensity of a polarized beam of light passing through a second polarizer follows a \cos^2 relation of the differences between their polarization axes. If the orientation of the first PZ fiber is assumed to be α , then the orientation of the second PZ fiber will be $(\alpha + 45^\circ)$. When there is no current flowing through the sensor, thus no rotation of the plane of polarization, the output light intensity is given by,

$$J_{out} = J_{in} \cdot \cos^2[(\alpha + 45^\circ) - \alpha] \quad \text{Eq. 3.4.3}$$

$$\begin{aligned} &= J_{in} \cdot \cos^2(45^\circ) \\ &= \frac{J_{in}}{2} \\ &= \frac{J}{4} \end{aligned} \quad \text{Eq. 3.4.4}$$

When line current is present and the plane of polarization is rotated by an angle θ , the difference between the orientation of the polarized light and the orientation of the second polarization fiber is no longer 45° and it becomes $(45^\circ - \theta)$,

$$\begin{aligned}
J_{out} &= J_{in} \cdot \cos^2(45^\circ - \theta) \\
&= \frac{J_{in}}{2} [1 + \cos(90^\circ - 2\theta)] \\
&= \frac{J_{in}}{2} (1 + \sin 2\theta)
\end{aligned}
\tag{Eq.3.4.5}$$

So the change of intensity can be given as,

$$\begin{aligned}
\Delta J_{out} &= \frac{J_{in}}{2} (1 + \sin 2\theta) - \frac{J_{in}}{2} \\
&= \frac{J_{in}}{2} \sin 2\theta \\
&= \frac{J}{4} \sin 2\theta
\end{aligned}
\tag{Eq.3.4.6}$$

Eq.3.4.7

Thus a polarization change is converted to an intensity change, which can now be detected by the receiver as a variation in the amplitude and the corresponding value of the line current is calculated based on that intensity change. Fig.3.4 details the operation of the current sensor head. In terms of loss all light traversing the sensor will have 75% or 6 dB loss at the output of the second PZ fiber. The PZ fibers are responsible for the bulk of the loss, each one with a characteristic 3-dB loss.

3.4.3 Total System Optical Loss

The total optical loss is the sum of all the losses mentioned in each of the components' description. Other losses need also be taken into consideration. The three fusion splices per sensor line (0.4dB/splice) and the two end connectors (0.2 dB/connector) have a combined loss of 1.6dB. Losses of 2dB are estimated for the attenuation due to bends, imperfect cleaves and backscatter. The Total System Optical Loss comes out to be 16.96dB. The attenuation factor is then,

$$\alpha = 10^{(-16.96 \text{ dB} / 10)} = 0.020
\tag{Eq. 3.4.8}$$

This means that only 2% of the light transmitted by the Laser to a particular sensor reaches the receiver's photodiode. It is important to note that the fiber itself is responsible for a minimal portion of the loss, thus larger distances between the sensors and transmitter or receiver can be implemented without much influence in Total System Optical Loss.

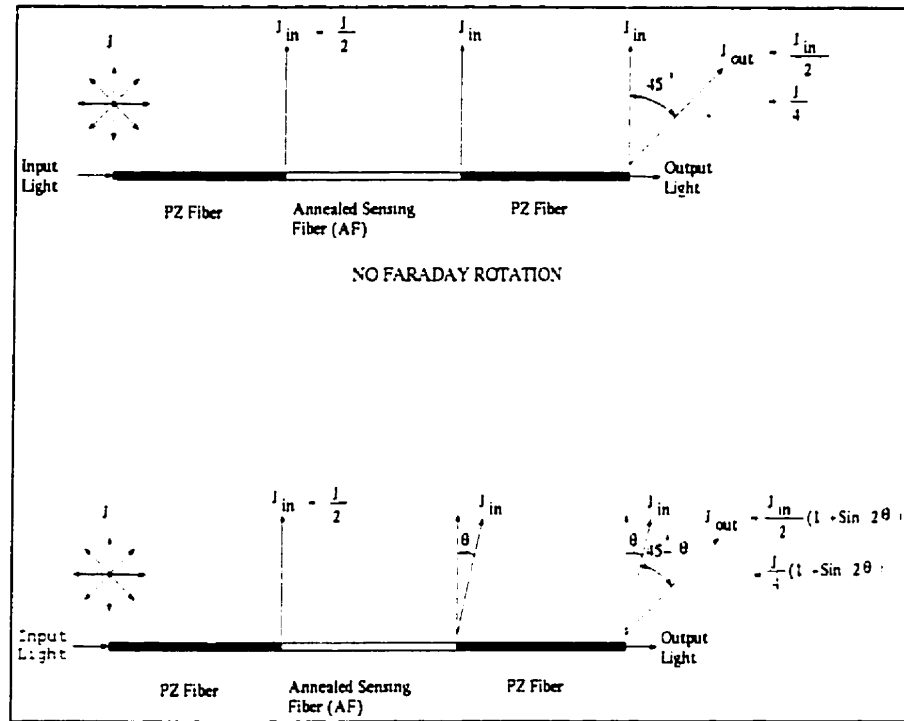


Fig.3.4 Operation of the Current sensor: Faraday Rotation of θ

IV. DIGITAL RECEIVER

4.1 OVERVIEW

The FOCSNET is a wide-ranging high-current measuring system based on Faraday Sensors. How the Faraday Effect transducers work and how the network is set up dictate how the information is going to be processed. The previous chapters dealt with the optical theories behind Optical Current Transformers and with the design and components of an all-fiber network. In this chapter the system's receiver is presented.

Although the network concept of this system is based on S. Goyals' [13] work, the receiver design and the way the information is handled is completely different in this thesis. In this new design, considerations for reliable AC and DC measurements are taken into account.

The receiver for this project is specifically designed to interface with a Personal Computer where the line current information AC and/or DC is displayed either in numerical form or as a trace of the line current signal. For any computer process the receiver must be digital in nature and there are several digital components that enable the signal to be processed at high speeds (e.g. FPGA, DSP). The front end of the receiver consists of amplifiers to deal with the analog signal from the fiber network and an ADC to convert the signal into the digital domain.

The receiver presented in this chapter is designed for the proof of concept of this thesis with all the parameters being set for a TDM two- sensor Optical Fiber Network.

The components of the receiver are detailed in the following sections of this chapter and several oscilloscope traces are used to depict how the signal is being processed within these components.

4.2 RECEIVER COMPONENTS

The light pulse signal emerging from the fiber network is first converted into the electric domain via a Photodetector. Two amplification stages increase the signal so that the ADC can read it properly. The ADC output bus delivers the digitized information to the brain of the receiver, the FPGA. The FPGA and DSP do all the signal processing and eventually the results are sent to a PC to be displayed.

Following is a detailed list of all the receiver components, their functionality and interconnections.

4.2.1 Photodetector/Amplifier

A photodetector is an optical component that converts optical energy into an electric signal. It is based on a photosensitive component, typically a photodiode.

To be compatible with other existing system elements such as transmitter and optical fiber the photodetector must meet the following specifications.

Operating Wave Length	820nm
Minimum 3 dB Bandwidth	20 MHz.
Maximum Rise and Fall times	40ns
Minimum Noise Voltage	0.59mV rms.
Minimum Optical power level	0.5 μ W
Minimum Responsivity	10mV/ μ W

Table 4.1 Objective Specifications

4.2.2.1 Bandwidth requirements

Since the transmitter is capable of generating 400ns pulses, with equal time intervals then a 400ns square pulse is the minimum the receiver should normally detect. However it should be able to detect higher speeds and shorter period between pulses for system upgradability. To detect 400ns pulses with a reasonable square shape and minimal distortion a 20MHz 3-dB bandwidth is required.

Theoretically, a square pulse in the time domain (with pulse width T) will be a " $\text{Sinc}(f.T)$ " wave form in the frequency domain. Thus to get the exact replica of a square pulse infinite bandwidth is required since the tails of the " Sinc " function would go to infinity. However in practice we need to have only a few significant side lobes.

Since $T = 400\text{ns}$, $1/T = 2.5\text{ MHz}$, the main lobe will have 5 MHz Bandwidth. Thus to get a reasonably good pulse we need at least 20 MHz Bandwidth, with a flat response from DC to 20 MHz.

4.2.2.2 Noise Requirement

As mentioned before, we particularly need a low noise signal because we are measuring minute changes in the amplitude of the signal.

The system, so far, has no long distances to travel so not much dispersion or attenuation is caused to the signal. The sensing mechanism of the Faraday-coils alters light polarization, which lowers the signal power level through the system. Added losses will be caused by the couplers needed to network the system and the various splices required to connect the various elements. The noise performance of the receiver is critical.

A good photon-electron transfer (responsivity) is essential so the output signal has a high enough level to be well above the noise interference.

The HP HFBR-24X6 photodetector was selected since it met all requirements, it is relatively inexpensive and readily available. The HP photodetector along with an Op-Amp are the basis for the design of the complete linear, low noise, high bandwidth fiber-optic receiver. The complete schematic of the receiver is shown Fig.4.1. The bandwidth of the photodetector/amplifier is limited by the bandwidth of the Op-Amp (Maxims MAX-4106). This Op-Amp was selected since it has excellent noise characteristics.

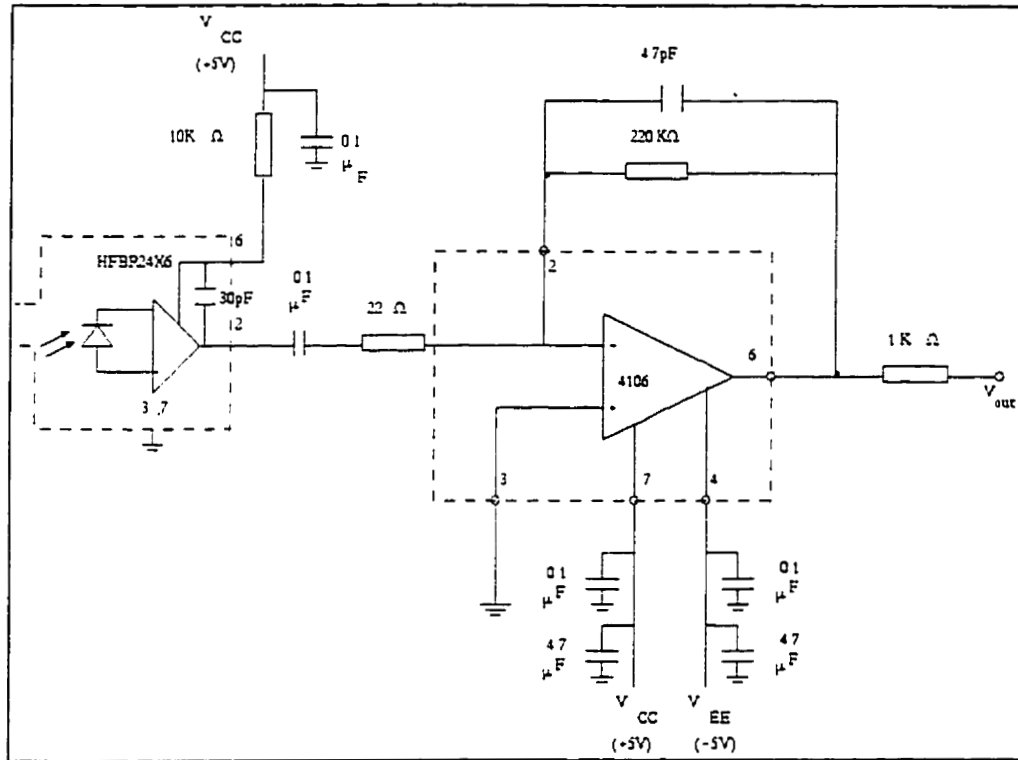


Fig. 4.1 Photodiode/Amplifier Schematic

4.2.2.3 Receiver Front End

The HFBR-24X6 receiver contains a PIN photodiode and low noise transimpedance pre-amplifier. The HFBR-24X6 receives an optical signal and converts it to an analog voltage. The output is a buffered Emitter-Follower, which increases the speed of the detector [36]. Due to the built-in transimpedance amplifier the output signal amplitude from the HFBR-24X6 is much larger than from a simple PIN photodiode and it is less susceptible to Electro-Magnetic Interference (EMI), especially at high signaling rates.

The photodetector has a dynamic range of 23dB and a frequency response from DC to 125 MHz.

4.2.2.4 Amplifier

The Max4106 Op-Amp combines high speed performance with ultra low noise response. Since the output of HFBR-24X6 has a small peak-to-peak voltage (e.g. 0.1Vpp) it requires adequate amplification thus the Op-Amp is designed for a gain factor of 10. A 4.7pF capacitor in the feedback loop eliminates high frequency noise. The cut off frequency was chosen to be 154 MHz. This ensures very low noise and avoids signal distortion. If the cut off frequency is too low then the rise and fall time of the pulse will increase, while if the cut off frequency is too high then the high frequency noise would not be removed.

The Op-Amp has a gain-bandwidth product of 350MHz thus the receivers bandwidth is limited to 35MHz, since a gain of 10 is required for an output of 1Vpp. The Op-Amp has very small voltage noise (i.e. 0.75nV/√Hz) which means the Op-Amp adds virtually no noise to the Photodetector's output. Fig. 4.2 shows the output of the photodetector/Amplifier (ph/amp) resulting from a 400ns Laser Driving Pulse (LDP).

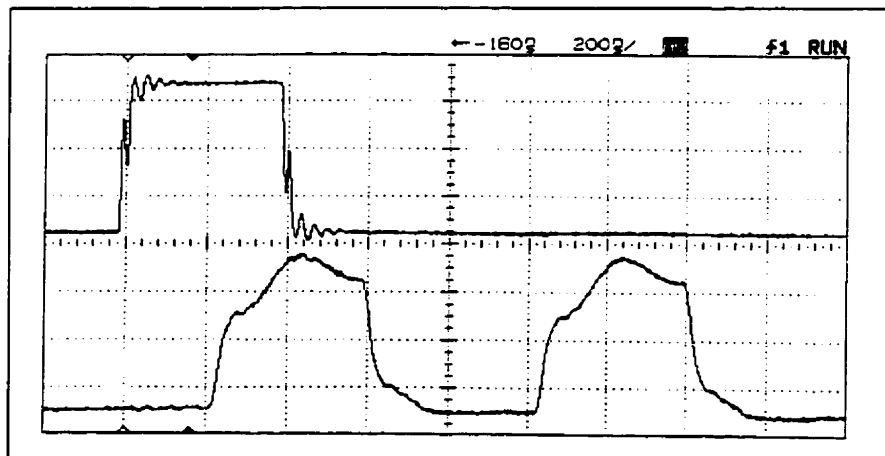


Fig.4.2 Shows LDP (upper) and the output from the Photodetector/amplifier (lower)

The shape of the pulses at the receiver is “square-like”. Their irregular shape is a product of the modulation circuitry of the transmitter and it is this shape that travels along the fibers of the network. Each pulse is well defined within its 400ns width. Its irregular shape is taken into consideration for amplitude calculation in later sections, for it is in the amplitude of each pulse where the information of the Faraday rotation lies.

To obtain optical pulses closer in shape to the LDP the design of the modulation circuitry for the Laser source has to be significantly modified. This is not a trivial task since communication Laser diodes, such as this network's light source, are not regularly driven by square pulses but by bell shaped pulses. With this shape the harmonic components of square pulse are not present.

4.2.3 Differential Amplifier

The output voltage signal from the ph/amp is fed to a differential amplifier and the use of the latter serves two purposes. First, it brings the voltage level of the signal into the optimal operating range of the ADC that is -1V to +1V. It increases the sensitivity of the system by amplifying just the change in the intensity, which is the crucial parameter needed in order to calculate the line-current.

The difference signal V_{ref} is provided by a Universal Power Source, as it provides highly accurate and very low noise voltage levels. The value of V_{ref} is chosen such that when there is no line current the output of the differential amplifier is 0V. Thus the value of V_{ref} is the same as the value of input voltage signal from the photodiode V_{in} when there is no current flowing through the sensors. When line-current is present and the Faraday rotation takes effect, the rotation is translated as a change of the light intensity and this change is converted to a voltage signal by the photodiode. Due to the differential amplifiers' set up only this change is amplified and fed to the ADC. Fig. 4.3 is the schematic for the differential amplifier.

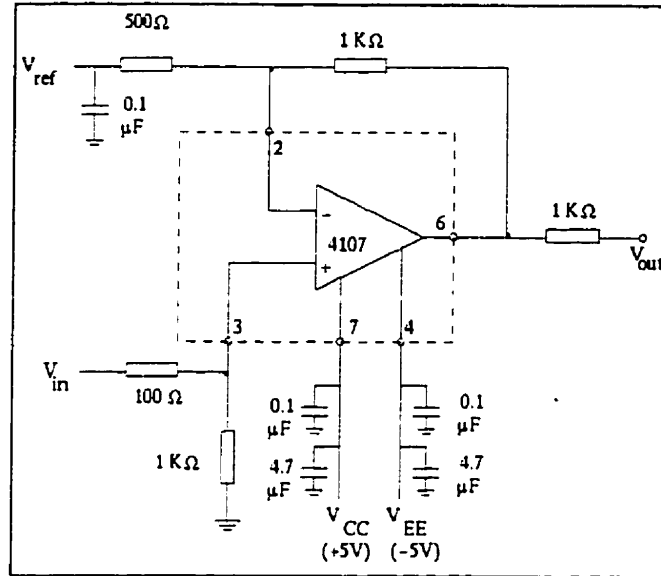


Fig.4.3 Differential Amplifier

As with the first amplification stage the differential amplifier is implemented with a very fast, high bandwidth and low noise performance Op-Amp, the MAX4107. The input resistor values used were 100Ω and 500Ω respectively for V_{in} and V_{ref} , as they were determined to be the optimum values.

4.2.4 Analog to Digital Converter (ADC)

The ADC digitizes the analog voltage signals from the differential amplifier. There are two main characteristics in the selection of the ADC. Resolution and Samples per Second (SPS). The ADC runs at a rate of 25MSPS, which is clocked by a 40ns (25MHz) pulse generated by the FPGA. The Analog Devices AD9040A ADC has a Maximum sample rate of 40MSPS though a rate of 25MSPS is optimum for synchronization with the FPGA, as is later described.

At the set rate of 25MSPS each 400ns optical pulse is sampled 10 times but only 4 of these samples will be used to determine the average magnitude of that pulse. Fig. 4.4 shows how the pulse is sampled. The first 4 and the last 2 samples are disregarded due to

the irregular shape of the incoming pulse as well as the uncertainty of the rising and falling edges. Since each pulse has a slight variation in the time of its rising and falling edges then to avoid calculation errors the samples close to the edges are disregarded. The ADC is sampling continuously and the decision as to which samples are to be used and averaged is done by the FPGA.

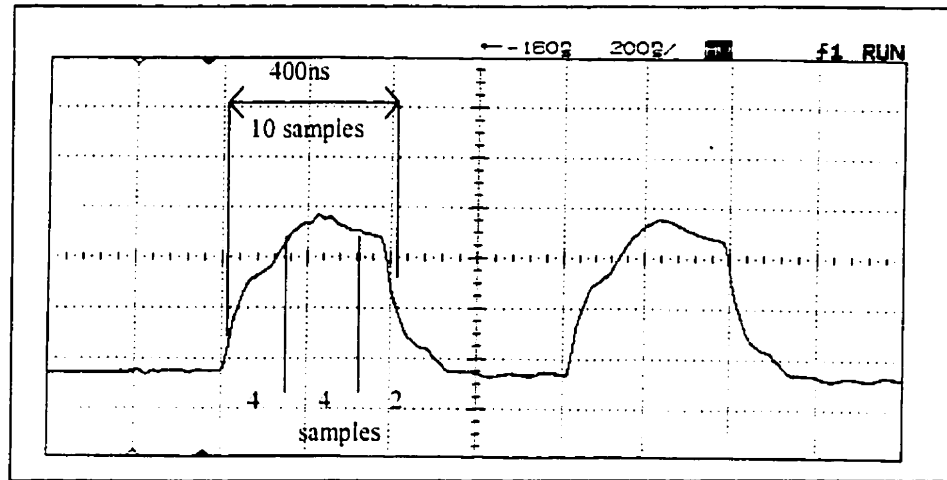


Fig.4.4 ADC output bus, as seen from a 10-bit DAC

The ADC has a 10-bit resolution and a 2V operating range which means it can detect 1,023 levels of 2mV each. As mentioned before the differential amplifier takes care of adapting the signal to the -1V to 1V range of the ADC.

It is important to note that as the ADC has a 3 cycle output delay, this means that data sampled will be available for reading at the output bus 3 clock cycles after being sampled. It is of great importance for the FPGA to know when and which samples to process. Fig.4.5 shows the time difference between of the optical signal i.e. the ph/amp output vs the ADC output after digitization. Fig 4.6 shows the LDP vs. the output of the ADC. Again it is 3 ADC clock cycles after it is present at the output of the ph/amp, shown in fig 4.2.

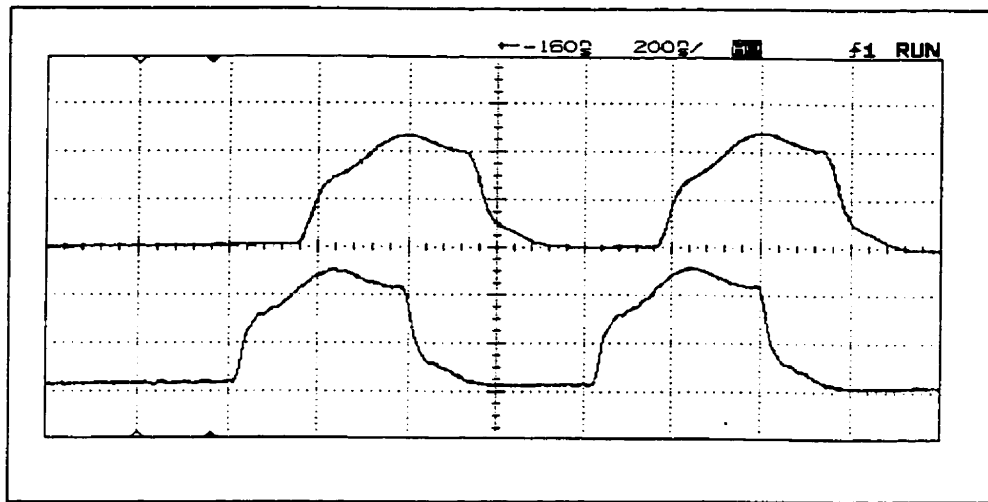


Fig.4.5 Optical pulse time difference. ADC output (upper), Ph/Amp output (lower)

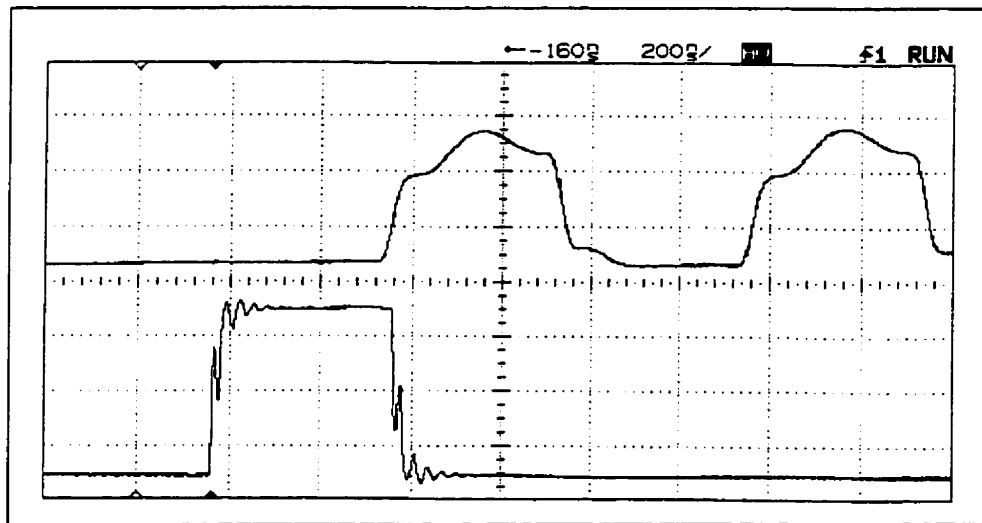


Fig.4.6 Time difference between LDP(lower) and ADC(upper) output.

4.2.5 Field Programmable Gate Array (FPGA)

Running at 50MHz the Field Programmable Gate Array (FPGA) is the fastest electrical component of the FOCSNET. An FPGA is a digital cell based IC made up of thousands of simple digital logic components (e.g. logic gates, flip-flops). These components are the basis of more complex digital instrumentation (i.e. counters, multiplexers, adders) thus an FPGA has great flexibility to generate complex digital logic.

Within the FPGA resides the control of the FOCSNET's digital receiver. Its functions are divided into I/O buses, data processing, and control buses. It has a 10-bit input bus connected to the output bus of the ADC to collect the digitized information of the sampled pulses. The information from each pulse is accumulated to generate a single value for the amplitude of that pulse. That information is then stored in the RAM via a 12-bit data bus. The address bus for the RAM is also controlled by the FPGA. All the pulse information from each sensor in the system is stored in specific RAM locations handled by the FPGA. Other control mechanisms implemented on the FPGA are: the generation of the ADC clock and the handshaking with the DSP that enables both of these components to access the RAM. For complete system synchronization all processes done by the FPGA are matched up against the Laser Driving Pulse (LDP).

To accomplish all of the above, several Blocks were designed and implemented on a Xilinx 4005E FPGA. The Xilinx Foundation Series software was used to implement, simulate and test the FPGA's logic on a host computer. A Demonstration Board along with a logic analyzer was used to test the implementation directly on the IC.

For the design of these blocks several system parameters such as LDP width and period and oscillator frequencies were taken into account. The design of each block is aimed to be as flexible as possible to accommodate changes in the system or the network. The receiver for this thesis is designed for a two-sensor network. Changes such as addition of sensors and different LDP widths or periods, may require simple changes in FPGA implementation. There will be no need for any other external ICs since changes to the system can be dealt within the FPGA itself. This also means no changes in PCB design.

The following is a description of the blocks that constitute the full implementation of the FPGA. A time simulation details the most important signals, internal and external, of the FPGA.

4.2.5.1 ADC Clock.

In order to synchronize the FPGA and the ADC a 25MHz clock is generated by the FPGA and fed to the ADC. A single flip-flop (FF) is used to divide the FPGA's clock in half. The FF is a basic logic component in FPGA implementation and thus has the smallest time delay from T to Q (e.g. 3ns) [37]. Synchronization of the two components on the same edge of the clock pulse is very precise.

4.2.5.2 Sample Window

As mentioned previously the ADC is sampling continuously. This means it samples not only the incoming pulse signal, but also the signal between pulses that contains no useful information. It is the duty of this block to select a specific number of continuous samples containing useful pulse information.

The parameters taken into consideration are: the LDP Width (i.e. 400ns) and the ADC sample frequency (i.e. 25MHz). As mentioned before each 400ns pulse, at a rate of 25MSPS, is sampled 10 times. As per the system specifications only 4 (i.e. 160ns) of these 10 samples will be added and averaged.

A 200ns window is generated to capture the desired samples and it has to match the desired portion of the 400ns pulse to be processed. This window is 40ns (1clock cycle) larger than the system specification (160ns) to avoid any loss of data. Counters are implemented for this purpose. The counters are triggered by the LDP and this block generates a 200ns window per system sensor. For the network where the signals from the two sensors are 800ns apart, these windows are generated at 550ns and 1350ns from the rising edge of the LDP. At these times respectively the desired digitized portions of the pulses from the optical system are present at the output bus of the ADC. Fig. 4.7 shows the output signal from the ADC and the window pulses generated by the FPGA's. The pulse windows shown in this figure are 160ns in width and it can be seen they match the part of the sampled signal to be processed.

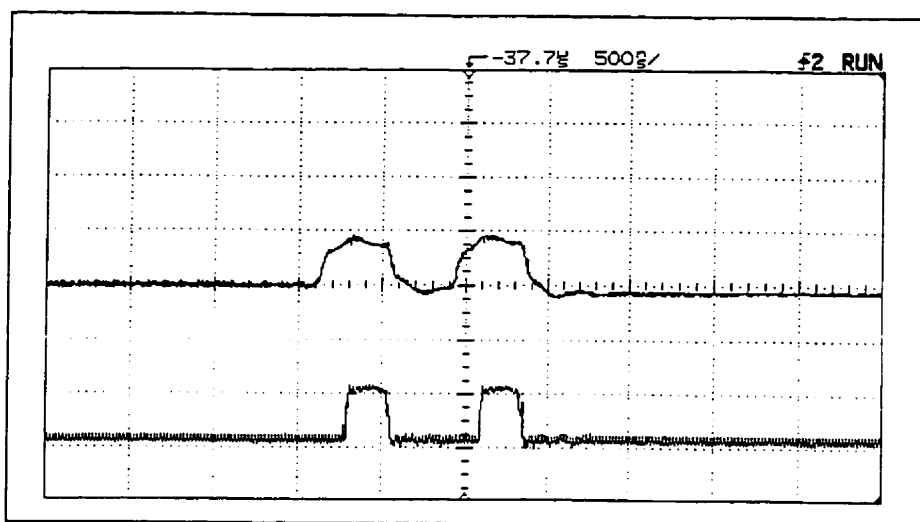


Fig.4.7 Sample window pulses(lower) and ADC output.

Using counters and adders this block generates precise length window pulses for each sensor in the system. These pulses are used to enable other working blocks implemented in the FPGA. It has a pin output in order to monitor its activity and to make sure it is always aligned with the digitized pulse from the output bus of the ADC.

4.2.5.3 Data Acquisition-Data Process Block (DA/DP)

This block handles all the I/O data buses and it is in charge of all the FPGA's data processing. It is divided into three stages. In the data input section it interfaces with the ADC via a 10-bit bus. In the same manner it interfaces with the RAM-Unit via a 12-bit output bus. In between these two buses data is processed, using a simple accumulator, the four samples chosen to depict each digitized pulse are accumulated to generate a single value equivalent to the amplitude of that pulse.

This block is enabled only during the 200ns window described previously. When enabled, the desired pulse information is present at the ADC output bus. By means of synchronization already described, this information is admitted through the FPGA's input bus and fed to an accumulator that will add the four samples. A counter clocked with the

same clock as the ADC (i.e. 25MHz), for precise synchronization, generates the four-count.

This block also consists of several control signals both internal and external and the RAM Unit's WRITE and ENABLE pins are controlled from this block. Internally it controls RAM addressing and also DSP-FPGA handshaking. These latter functions are described in subsequent sections.

Once the four samples are accumulated, a pulse is generated by this block for indication of the proper RAM address to the addressing block and WRITE and ENABLE signals are generated for the RAM-Unit. The WRITE signal is shown in Fig. 4.8 along with the 200ns window pulses generated by the previous block.

The WRITE/ENABLE pulse is generated 160ns from the rising edge of the window pulse. 160ns matches system specification for accumulation of 4 samples (i.e. 40ns per sample @ 25MSPS).

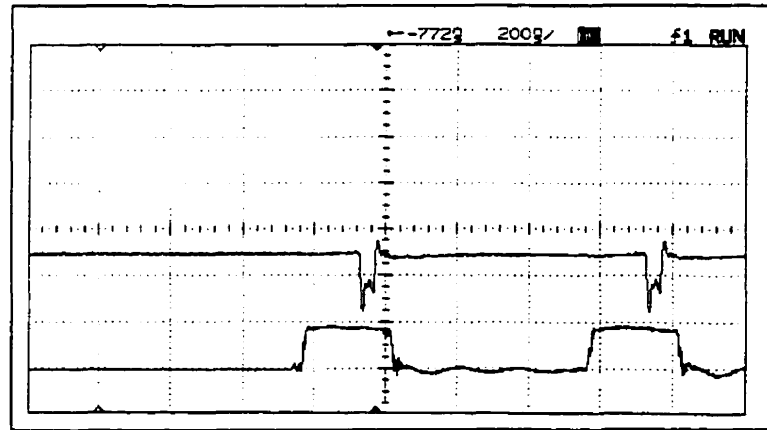


Fig.4.8 RAM WRITE pulse (upper) Vs. Sample Windows (lower)

When the RAM's WRITE is enabled, the sum of the 4 samples is input as a 12-bit word into a predetermined location on the RAM. This process is repeated every time this block is enabled, that is to say every time there is digitized information of an optical pulse

present at the ADC. In a two-sensor network, this operation will be performed twice per LDP. In general the operation will be performed as many times per LDP as there are number of sensors in the system.

A 12-bit output data bus is used because the accumulated sampled data will not exceed this value. The maximum value for a 10-bit word is $3FFh$ and this would be a saturation state for the ADC (i.e. +1v). If 4 counts of this maximum value are accumulated,

$$3FFh \times 4 = FFCh$$

The added value of $FFCh$ does not exceed a 12 bit ($FFFh$ max.) word.

For this project the Sample Window block is set up to enable the DA/DP for a system consisting of a 400ns LDP and two sensors. In the presence of a greater number of sensors only the Sample Window configuration would have to be adjusted. The DA/DP would remain the same as long as the LDP remains set at a minimum of 400ns and the ADC sample rate remains at 25MSPS no matter how many sensors the system has or what the fiber difference is between them.

4.2.5.4 RAM Addressing:

The addressing of the RAM is very simple. The FPGA stores pulse information in continuous RAM locations. The number of sensors in the system governs the number of continuous locations on the RAM per LDP. In the specific case of two sensors, information from the first sensor (e.g. the one with the shortest fiber length between the sensor and the receiver) is stored in location $00001h$ and information from the second sensor is stored in location $00002h$. This will terminate the storage for that specific LDP. For the next LDP the process continues starting at location $00003h$ for the first sensor, and so on and so forth.

The DSP, which also interfaces with the RAM, takes this information for further processing. The DSP's software is designed to know how many sensors there are in the system, thus it knows which RAM locations correspond to each sensor. DSP functions are discussed in a later section.

This block generates the 18 bit (3FFFFh) addresses required for a 256k RAM, and it is incremented by a control pulse from the DA/DP block. This block is also implemented as an 18 bit counter formed by a 16-bit and a 2-bit counter. As per system specification, a 60Hz cycle is sampled 666 times, thus 666 locations per cycle.

$$666 \times 2 \text{ sensors} = 1,332 \text{ RAM_locations}$$

Given the size of the RAM, the number of 60Hz cycles that can be stored is:

$$\frac{\text{RAM locations Available}}{1,332} = \frac{256k}{1,332}$$

$$\approx 192 \text{ cycles}$$

This means:

$$\frac{192 \text{ cycles}}{60 \text{ Hz}} = 3.2$$

3.2 second of Data

For 3 seconds of Data:

$$3 \text{ sec} \times 60 \text{ Hz} = 180 \text{ cycles}$$

$$180 \times 1,332 = 239,760 \text{ locations}$$

239,760 location of RAM are used to store 3 Seconds of data coming from the two sensors for a LDP period of 25 μ s. When these locations are filled the RAM starts rewriting itself with new pulse information. With this capacity on the RAM there will always be 3 seconds of information stored for a 2-sensor system,

4.2.5.5 FPGA – DSP Handshaking

The entire RAM unit's output pins (i.e. Control pins, Address and Data buses) are accessed by both the FPGA and the DSP. When either of these components are accessing the RAM the other component's outputs must be in a High Impedance state in order not to interfere.

HOLD is feature on the DSP that can be asserted at any time during a clock cycle it prevents the DSP from accessing the Data and Address buses (i.e. High Impedance), thus it also prevents program execution. When set, the instruction in progress is completed and then a HOLDA (acknowledgment) pulse is generated. Bus access and program execution is restored when HOLD is released.

The FPGA generates a HOLD pulse for the DSP and waits for the HOLDA from the latter. With this state the FPGA has complete access to the RAM and the DSP in this period of time is halted. When this HOLD is released (by the FPGA) the DSP acknowledges this and regains access to the RAM. The FPGA pin-outs are then set to High Z.

The FPGA has access to the RAM starting with the rising edge of the LDP and ending when the DA/DP has written all pulse values to the RAM for the corresponding LDP. When the FPGA detects the LDP it sends a HOLD to the DSP and the FPGA then waits for the DSP's HOLDA to enable all I/O pins. At this point the FPGA does all operations previously described and on the falling edge of the last sample window pulse the HOLD is released and the FPGA losses access to the RAM. The DSP regains RAM access one

instruction cycle later, for this is the time it takes the DSP to acknowledge the release of the HOLD (e.g. HOLDA).

The FPGA has access to the RAM for approximately $1.620\mu\text{s}$ thus the time between LDP's that the DSP has Access to the Data stored with the LDP Period set at $25\mu\text{s}$, is,

$$25\mu\text{s} - 1.620\mu\text{s} = 23.38\mu\text{s}$$

Since the DSP has over $23\mu\text{s}$ to work with, this is more than enough time to do its tasks, as it is described in subsequent sections. These calculations are for a two-sensor network and the system has sufficient flexibility to expand far beyond the two sensors. The FPGA implementation is designed for such expansions, but it should be noted that for every sensor that is added to the network, the time the DSP has to accomplish its work is reduced, since the FPGA will have a greater access time to the RAM.

4.2.5.6 Time Simulation

The time simulation feature on the Xilinx software permits the verification of FPGA implementation and it is a very useful tool for trouble shooting. The following is a time graph (Fig. 4.9) showing the most important signals of the FPGA and their relationships with each other.

This graph shows the following: the FPGA 50MHz system clock generated by a crystal; the 25MHz clock generated by the FPGA for the ADC; the LDP input by the pulse generator into the FPGA; the HOLD for the DSP which is active-low; the input bus from the ADC (ACC_ADC); the sample window-pulses (SAMPLE); the output Data bus that will be written to the RAM (RAMDATA); the WRITE pulse for the RAM which is also active low and, finally, the active address bus for the RAM (ADD).

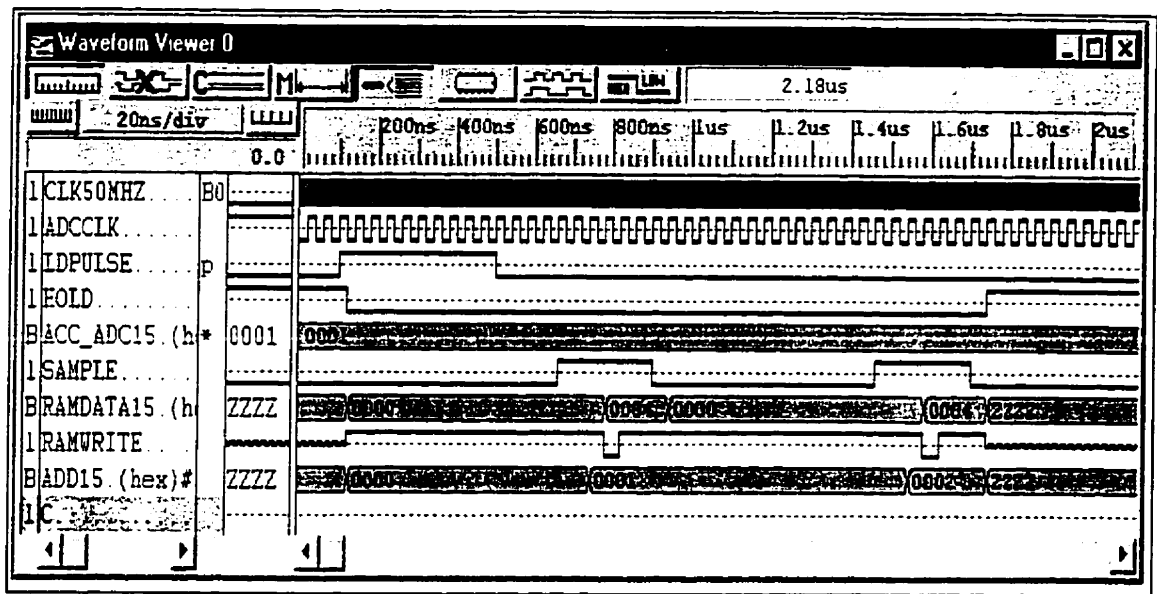


Fig.4.9 FPGA time simulation

The operation of the FPGA can be described as follows. The FPGA is idle until the LDP comes, on Fig. 4.9 it is shown as the first 100ns of the graph. At this point the 400ns LDP is input to the FPGA, the sample window block starts its count, the HOLD for the DSP is generated and the FPGA comes off its idle state. It can be seen on the address and data buses, as they come off a high Z state (ZZZZ) to a digital value, that they are both *0000h* since the simulation shown is for the first data input to the RAM.

For this simulation the input bus from the ADC has a constant *0001h* value to simplify explanation of the process. When the first sample window is generated at 650ns on the time graph (550ns from the LDP), four continuous samples from the ADC are accumulated. In this simulation the end result in the accumulator will be *0004h* (*0001hx4*) which is the value stored in the RAM and this can be seen in the Data bus line. The accumulator value is present at the time when the FPGA enables the WRITE pulse for the RAM. The Data value stays active until the accumulator is reset by the falling edge of the sample window. The control pulse for the RAM address comes from the DA/DP block in the middle of the sample window (not on simulation), thus the address is ready before the

Data and WRITE pulse. This is per RAM specification. The first location on the RAM (*0000h*) is never filled and all valid information starts with location *0001h*.

When the second window pulse arrives, the process described above takes place for the *0002h* RAM location. On the falling edge of the second window pulse the DSP HOLD is released and all pins on the FPGA that are connected to the RAM turn to a High Z state.

The whole process is repeated for the next LDP. The addresses keep incrementing until they reach the reset value of 239,760.

4.2.6 RAM Unit

The RAM unit is where the pulse information is temporarily stored and each location stores information for one specific pulse from each sensor on the network. The Motorola MCM6729D 256x4-bit fast static RAM (8ns-access time) was chosen for this receiver. Three ICs make up the RAM-Unit, the Address and control buses of the three are connected in parallel, and the Data buses are connected in such a way to result in a 12-bit word per location. The DSP and the FPGA, as described in the preceding section, share all RAM buses.

Specifications for the RAM requires for its Read or Write cycle that the Address be present at least 8ns prior to the Data or the WRITE. This is the minimum address set up time and the address bus has to be active for at least 8ns. WRITE enable must be active for at least 8ns and the Data must be valid for the duration of the WRITE enable pulse, with a 4ns-error margin. These considerations had to be taken into account for FPGA and DSP design.

4.2.7 Digital Signal Processor (DSP)

The Digital Signal Processor (DSP) takes care of most of the calculations required to obtain the value of the current flowing through each sensor in the Network. The arithmetic for the AC Ratio techniques described in chapter VI is implemented on the DSP. The DSP gathers the pulse information from the RAM and for each sensor determines its DC level value and its AC Ratio Value. These values are then transmitted to the PC where they are used to calculate AC and/or DC current values for each sensor in the system. The DSP also sends streams of sensor specific optical pulse information to the PC in order for the latter to generate a trace of the signal. This is of great importance in the study of transients, where a trace of the transient state of the signal is essential to record its behavior.

The following is a summary of the DSP operation:

- The DSP takes from the RAM the data from as many continuous locations as there are sensors in the system. Data from the RAM is divided by four on acquisition and placed in an accumulator corresponding to a specific sensor in the system. The information on each RAM location is the sum of 4 samples of a single pulse of a single sensor; the division by 4 generates the average value of amplitude for that pulse. This division is accomplished by a simple logical shift of the value. The simplicity of this operation is the reason why out of the 10 samples per pulse generated by the ADC it was chosen only to process 4. A logical shift can only be done on powers of 2 (i.e. 2,4,8...). For a division to make sense the number accumulated must match the number to be shifted, in this case 4.
- Each accumulator adds 666 pulses per sensor. As per system specification a 60Hz cycle is sampled 666 times. The average value for this sum is calculated per sensor. This average value is the DC value for each sensor. When there is no line-current present the value is the Zero Current Value (ZCL).

- Within the 666 values for each sensor, the maximum and minimum values are determined. Once determined the differential value of *Max-Min* for each sensor gives as a result the equivalent peak to peak value for each specific current (*Ipp*). This calculation is done to obtain a value for AC.
- Once this information is determined the DSP calculates the AC ratio for each sensor.

$$ACratio_{[n]} = \frac{V_{PP[n]}}{DClevel_{[n]}} \quad \text{Eq. 4.2.1}$$

- The following information is transmitted to the PC via a parallel port.
 1. AC Ratio values for every sensor in the system
 2. DC values for every sensor
- When the PC requests it, the DSP through a parallel port sends a stream of a specific sensor's pulse information. The PC uses this information to plot a trace of the signal.

The DSP used in this project is the TMS320C31 from Texas Instruments, which has a 40ns instruction cycle time, 50 MFLOPS and 25 MIPS speed. This DSP was used along with an application development board, which was very helpful as it provided the freedom to create custom software on a host computer, download, run, test and debug it as well.

The DSP and the FPGA run asynchronously since each of them have their own 50MHz crystal clock source. The only interaction these two components have is through the handshaking mechanism implemented on the FPGA which control's the access to the RAM.

The DSP is capable of parallel processing. The software designed for this project allows for parallel processing when the PC requires sensor specific optical pulse information, but since this is a user-specific request it is not always enabled. When the streams of

pulse information are being sent to the PC the running averages and ratio calculations are not interrupted.

4.2.8 Personal Computer

The above mentioned values from the DSP are sent to the PC for final current calculations and display. The PC also generates traces of specific segments of the current.

One of the main characteristics of this system, as will be shown in chapter VI, is the linearity of the sensor response for a range of different line current values. Each sensor has a characteristic linear response, depending on the sensors own sensitivity and the number of turns of conductor wrapped around the sensor. From this linearity a characteristic slope is obtained per sensor. This slope, along with the AC and/or DC ratios, is used for line current determination. This slope can change if the numbers of conductor turns are altered. Sensor linearity is discussed in detail in chapter VI.

The PC software, built on a C++ platform, is where the slope information is kept for each sensor, and if this changes it is simpler to re-calibrate using the C++ program without altering any other components on the receiver.

The PC takes the unique AC ratio values for each sensor and computes each line current using a liner equation,

$$I_n = \frac{ACratio_n}{m_n} \quad \text{Eq. 4.2.2}$$

Where m_n is the slope for the n_{th} sensor's response. This result is displayed on the PC monitor and it is continuously updated since the main objective of the system is to monitor constantly the line current activity.

The PC generates and displays a value for the DC currents in the same manner as for the AC current. The DC ratio has to be calculated first and the PC does this. As detailed in chapter VI for DC ratio calculations one of the sensors of the system has to serve as reference. For major system flexibility the PC can chose, or can be told which sensor to reference the others sensors to, and since this reference sensor might change depending on the application it is best to have the PC take care of this decision for it is the easiest way to modify it if need be. The reference sensor serves as the Zero Current Level (ZCL) for the system, thus no DC current can flow through it. There are no restrictions on AC current flowing through the reference sensor.

The DC ratio for each sensor is calculated by,

$$DCratio_n = \frac{DClevel_n}{DCref} = \frac{DClevel_n}{ZCL} \quad \text{Eq. 4.2.3}$$

In this project, where there are only two sensors, one is taken as the reference and the second one can be used to measure DC current. Both can measure AC current.

The following are the values displayed on the PC monitor.

1. AC current; Reference Sensor
2. AC current; Second Sensor of the system
3. DC current; Second Sensor of the system
4. ZCL value.

The ZCL value displayed is simply the DC level of the reference sensor and this is displayed in order to monitor the Laser power level at the receiver.

The PC can generate a trace of the line current flowing through a specific sensor. Streams of sensor specific pulse information are transmitted from the DSP on the PC's request. This is a user specific request.

The C++ software developed does not include any graphical interface. The software generates a file that can be loaded on a number of programs with plotting capabilities (i.e. Matlab, Excel). Traces are generated and examined using these alternative programs.

4.3 FUNCTIONAL DIAGRAM

A functional diagram of the entire receiver is shown in Fig 4.10

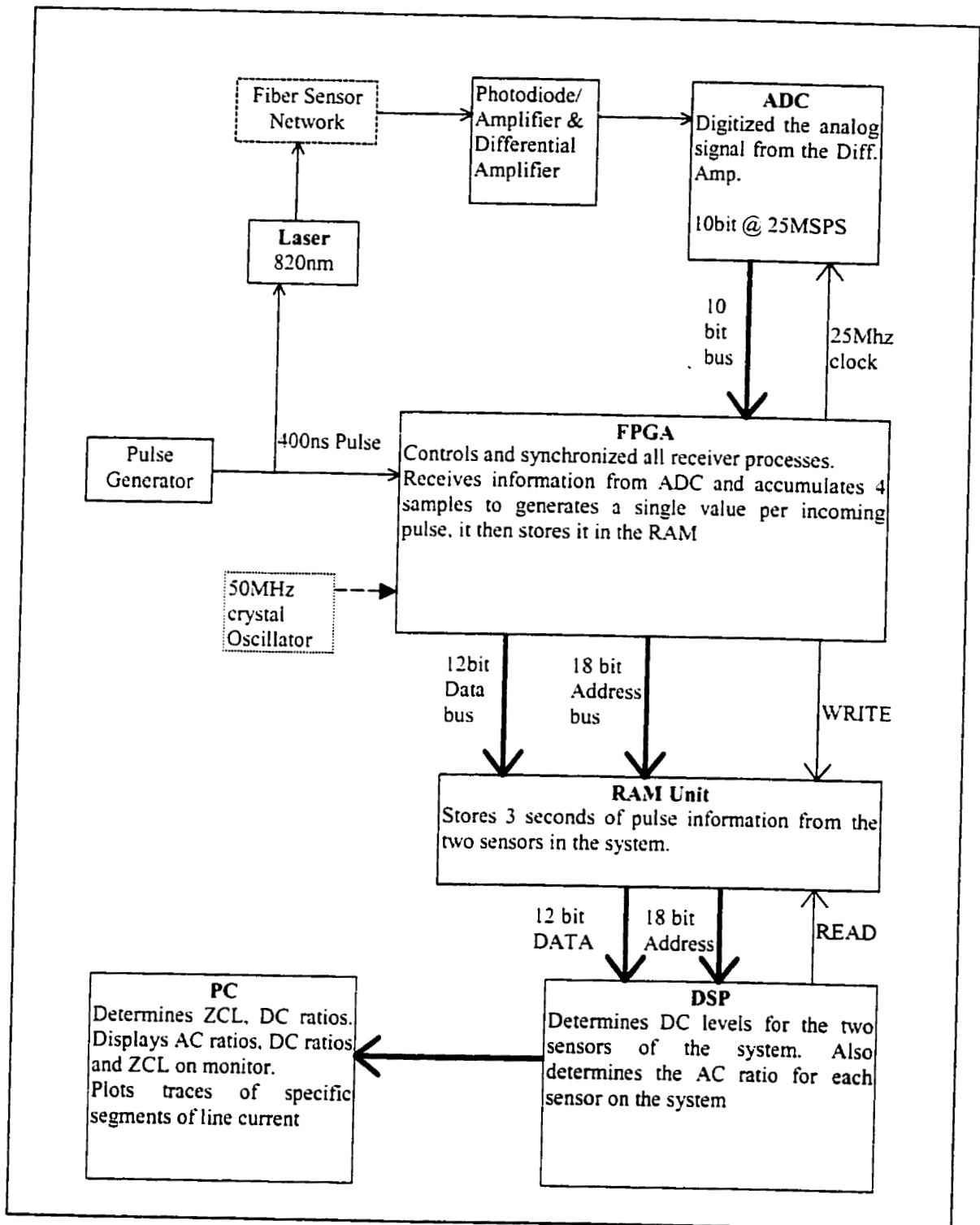


Fig.4.10 Receiver Functional Diagram

V. PARAMETERS AND PERFORMANCE

5.1 OVERVIEW

This chapter describes the parameters of the FOCSNET that will enable it to measure Line Current. In a measuring device the resolution is a very important factor and the resolution is essentially limited by the nature of the Faraday rotation and the system's noise. The Network topology and its parameters dictate how the line current is going to be sampled and therefore measured.

5.2 PREDICTED PERFORMANCE

5.2.1 Faraday Rotation

The angle of the Faraday Rotation is highly dependent upon the Verdet constant of the sensing fiber [6]. The larger the Verdet constant the larger the rotation and the larger the light intensity change.

The Verdet constant of the annealed sensing fiber is around 0.01 min/A at a wavelength of 820nm. This value is approximate as the annealing of the fiber may have resulted in some variations and it may also differ for different annealed fibers even if they are from the same manufacturer [13].

In the 3M-sensor head used in this project, the annealed fiber is wound four times around the conductor therefore the Faraday rotation angle is given by,

$$\begin{aligned} \theta &= VNI \\ \theta &= \left(\frac{0.01}{60} \right) \cdot 4 \cdot 1 = 0.00066^\circ / A \end{aligned} \tag{Eq. 5.2.1}$$

For this project the maximum currents used were of 100 A DC and of 100 Arms AC (i.e. 144Apeak AC) which delivers a maximum rotation of $0.066^\circ/\text{A}$ for 100A DC. The rotation angle is calculated for one turn of the conductor around the sensor and for every extra turn of the conductor the rotation angle increases by approximately the same amount. This is defined as the multiplication factor.

As the Verdet constant of the sensing coil is not large the Faraday rotation angle can be incremented effectively by increasing the number of turns of the current carrying conductor around the current sensor. In this project it is referred to as multiplication factor (MF) of the magnetic field, and each turn increments this factor by one approximately.

5.2.2 Signal To Noise Ratio (SNR)

The SNR is an important parameter in the evaluation of the measurement quality. An electric current is the contribution of many individual electron movements and each electron moves in a stochastic manner [2]. Each electronic component is a source of noise due to the quantum nature of electric current.

In the FOCSNET the receiver is responsible for the bulk of the systems noise and the shot noise from the photodetector and the thermal noise of the resistors in the amplification stages are the main noise contributors.

5.2.2.1 Thermal noise

The thermal noise is caused by the three dimensional random thermal movement of free electrons in the resistor [2]. The noise voltage is given by,

$$V_t = \sqrt{4kT\Delta f/R_f} [V] \quad \text{Eq. 5.2.2}$$

Where k is the Boltzmann's constant, T is the absolute temperature in °K, Δf is the Noise equivalent bandwidth in Hz and R_f is the feedback resistance in Ohms.

5.2.2.2 Shot noise

Current flowing through the photodetector generates shot noise. This current consists of a dark current (I_d) and a photocurrent (I_p). The shot noise voltage is given by,

$$V_s = R_f \sqrt{2e(I_d + I_p)\Delta f} [V] \quad \text{Eq. 5.2.3}$$

As per manufacturer specifications the HP HFBR-24 photodetector has an output noise of 0.4mV [36].

5.2.2.3 Op-amp noise

The manufacturer of a device generally specifies the op-amp noise. The voltage noise can given by,

$$V_{amp} = R_f \sqrt{\left[I_n^2 + \left(\frac{V_n}{R_{in}} \right)^2 \right] \Delta f} [V] \quad \text{Eq. 5.2.4}$$

Where, I_n and V_n are the input noise current and voltage respectively and R_{in} is the input resistance.

The amplifiers chosen for this project have the characteristic to be ultra-low-noise components. The manufacturer specifies that these amplifiers have an integrated voltage noise of 9.5µVrms

The total system noise can be given by,

$$V_{noise} = \sqrt{V_s^2 + V_t^2 + V_{amp}^2} [V_{rms}] \quad \text{Eq. 5.2.5}$$

$$V_{noise} \cong 0.4mV_{rms}$$

Thus the total noise is due predominantly to the photodetector.

5.2.2.4 Signal to Noise Ratio

The signal from the photodetector/amplifier is expected to be 1V. Therefore the intensity change due to Faraday rotation is,

$$V_{signal} = 1 \sin 2\theta \quad \text{Eq. 5.2.6}$$

For 100A DC the rotation angle is 0.066° thus the signal voltage for this current is,

$$V_{signal} = 1 \times \sin (2 \times 0.066^\circ) = 0.0023V \quad \text{Eq. 5.2.7}$$

Therefore the SNR for the system is

$$SNR = 20 \log_{10} \left(\frac{V_{signal}}{V_{noise}} \right) [dB] \quad \text{Eq. 5.2.8}$$

$$SNR = 20 \log_{10} \left(\frac{0.0023}{0.0004} \right) [dB] = 15.19 [dB] \quad \text{Eq. 5.2.9}$$

As can be seen from equation 5.2.7 the displacement of the plane of polarization due to 100A of current is very small in terms of voltage which is why several turns of the conductor are wrapped around the sensors. The turns increase the intensity of the magnetic field.

5.2.3 System Resolution

The resolution is the minimum detectable current and this occurs when the SNR = 1 [13]. The minimum Faraday rotation is then,

$$\begin{aligned} 0.4mV &= I \sin 2\theta_{min} \\ \theta_{min} &= 0.011^\circ \end{aligned} \quad \text{Eq. 5.2.10}$$

Thus the minimum detectable current, for MF = 1, is,

$$I_{min} = \frac{6 \text{ min}}{0.00066} = 16.6A \quad \text{Eq. 5.2.11}$$

Again the effective minimum detectable current will be enhanced by the Multiplication Factor provided by the multiple conductor turns around the sensor. The current sensor with multiple conductor turns is shown in Fig. 5.1

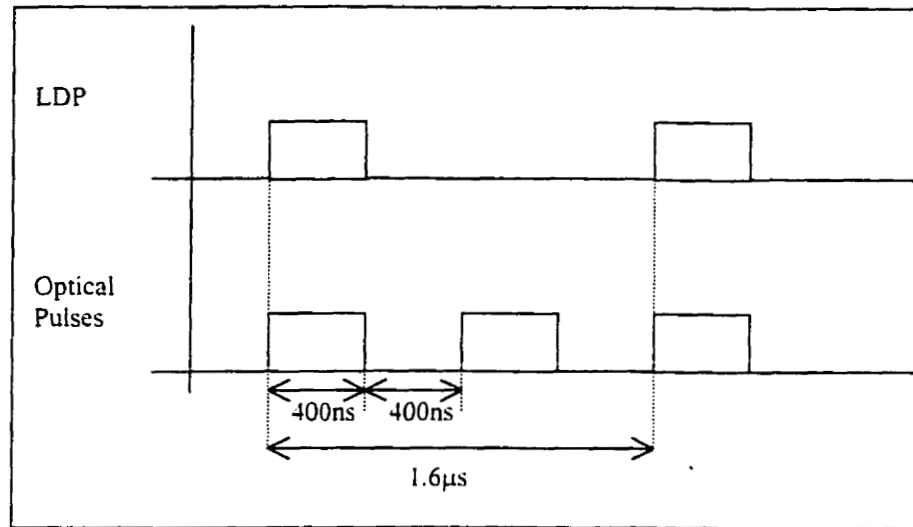


Fig. 5.1 The Current Sensor

5.3 SYSTEM PARAMETERS

This section presents the characteristics and parameters of the FOCSNET. The FOCSNET is a complex system made up of optical, analog and digital components. All of these components work together to determine the functional parameters of the systems and in a lot of instances the parameters are bound by the limitations of one component (e.g. the laser pulse used is 400ns wide since any pulse smaller than this gets distorted too much by the lasers' modulation circuitry). The following list of parameters determines the system's resolution and possible upgradability.

- The Laser Driving Pulse (LDP) chosen for this project was 400ns in width. Any pulse smaller than this was difficult to process at the receiver because of the distortion it suffers from the lasers' own circuitry. With improvements to the Laser smaller pulses could easily be used and the fiber lengths between sensors can be shortened.
- The fiber length difference between sensors, as described in chapter II, is what provides the time delay needed for a TDM system. The length difference of 160m for this project's two sensors generates an 800ns time gap between continuous rising edges of optical pulses. If any sensors were to be added to the network the fiber length difference should remain consistent. The fiber length difference is a parameter that would require a great effort to modify since the fibers would have to be physically changed.
- The LDP Period is the repetition rate of the Laser and it is set at 25 μ s for this project. The period can be adjusted to a value as low as 1.6 μ s and the smaller the period the more samples per second thus the higher the resolution. The larger the period the more sensors that can be added to the network. In the particular set up of this project the minimum period value is 1.6 μ s since at this rate the optical pulses will not overlap and the difference of 400ns between incoming pulses remains consistent.



*Fig.5.2 Minimum LDP period for a two sensor network
with 400ns LDP and a 400ns time gap*

The FOCSNET system is designed to measure DC and 60Hz AC line-currents. A $25\mu\text{s}$ period will sample a 60Hz signal close to 666 times per cycle, this being well over the Nyquist rate necessary for complete signal reconstruction. Nyquist has shown that in order that the original signal may be reconstructed from the samples the signal must be sampled at least twice per highest frequency in the signal [38]. In the case of a 60Hz signal the minimum Nyquist sample frequency is 120Hz.

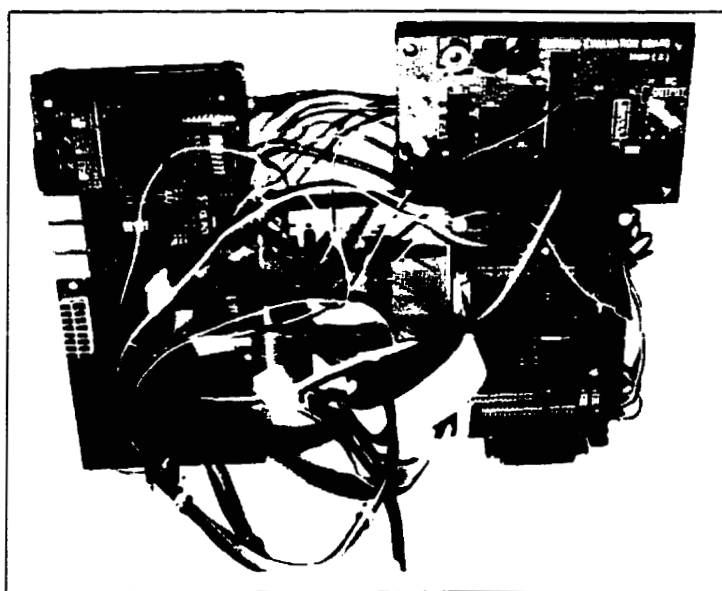
To be consistent any additional sensor must take up an 800ns time slot as seen in Fig.5.2 (i.e. 400ns pulse + 400ns time gap). With the set $25\mu\text{s}$ period up to 31 sensors could be networked together without altering any systems parameters.

It is important to note that for any number of sensors added to the network the input and output couplers' lines must match the number of sensors and the Laser power must be adjusted accordingly so that the receiver detects enough light intensity per sensor.

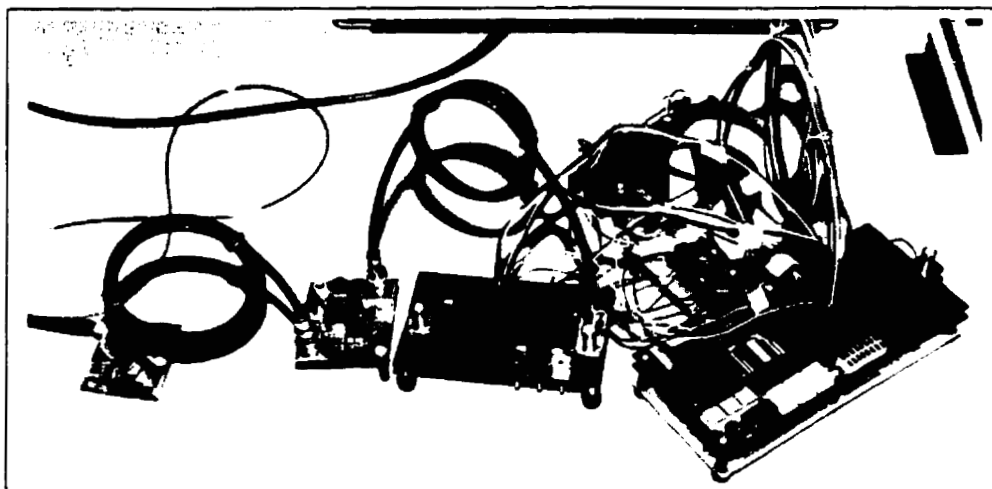
The parameters and characteristics of the Receiver are detailed in Chapter IV and these include the digital sampling of the pulses, the amount of information the RAM can store and the speed the FPGA and DSP.

A good example of how more than one component on the system affects parameters criterion is the averaging of only four samples per pulse. The Optical pulse is sampled 10 times due to the 25MSPS of the ADC. The ADCs' sample rate was set to be half the operating clock of the FPGA. The distortion suffered by the pulse due to the Lasers circuitry makes it impossible for all the samples to be used and only four are chosen, averaged and stored in a RAM location. Four samples are chosen since it is a power of 2 and is needed for the averaging in the DSP because this is done based on a Logical Shift.

Figs. 5.3 shows the receiver and its major components and Fig 5.4 shows the complete FOCSNET system.



(a)



(b)

Fig. 5.3 The Receiver (a) ADC, FPGA, DSP and RAM Unit. (b) Complete Receiver with Photodetector/Amplifier and Differential Amplifier

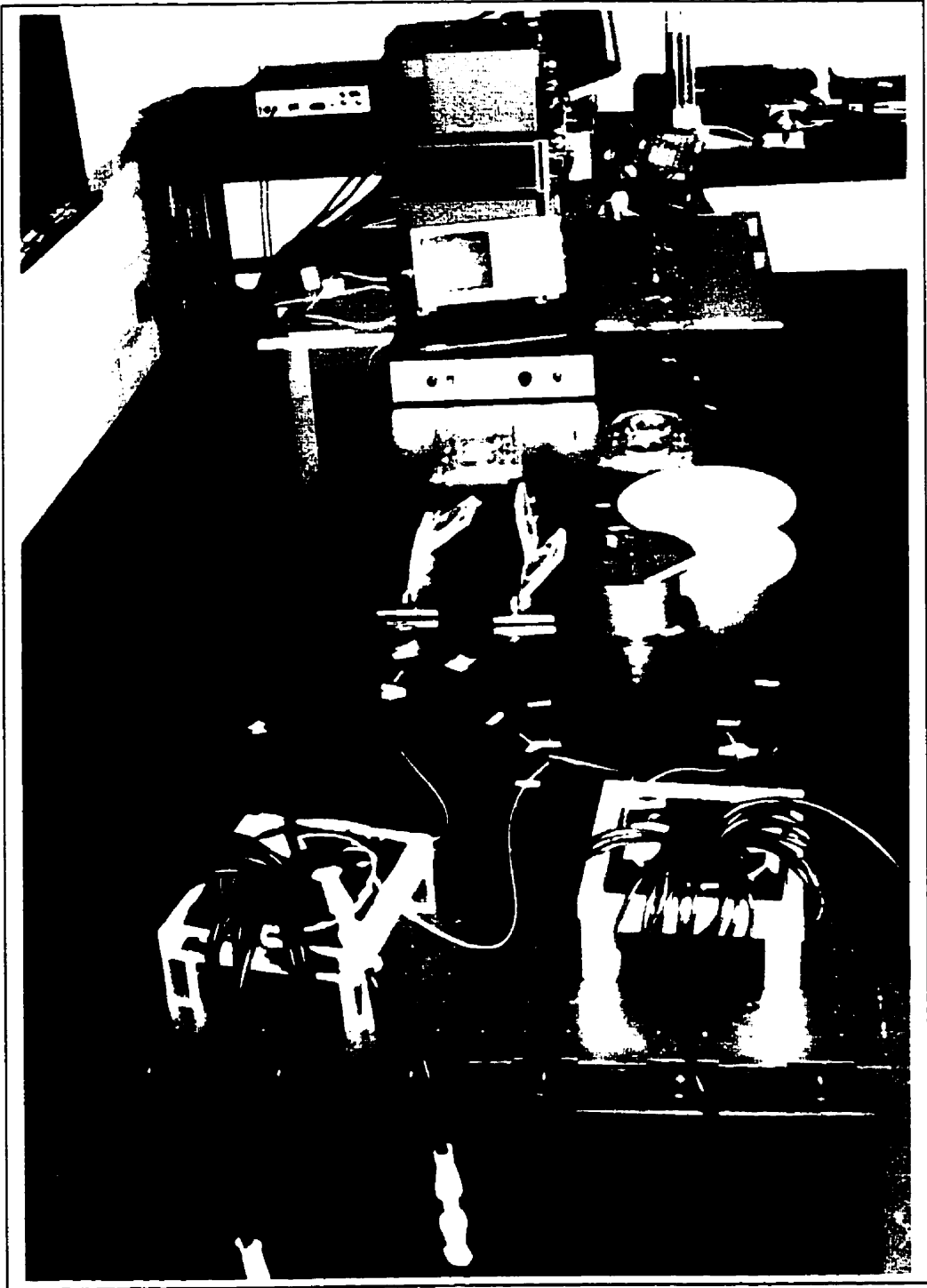


Fig 5.4 Fiber Optic Current Sensor Network

VI. EXPERIMENTAL INVESTIGATION AND RESULTS

6.1 OVERVIEW

This chapter shows the results of the Line-Current measurement investigation. In previous chapters the theoretical background that the system is based on was described. The network and receiver designs were discussed as well as the parameters and limitations that were taken into account for current measurements.

The FOCSNET is a system designed to measure DC and AC line currents and this chapter describes how these measurements are accomplished. After the current detection has been dealt with a theory is put forth as to how the system response becomes immune to external perturbances such as Laser output power variations.

Several considerations have been made in regards to the experiments and these are worth mentioning. Even when there is no current flowing through the system there is always a pulse value at the receiver. The amplitude of this pulse is defined as the Zero Current Value (ZCL). For experimental purposes Sensor-I is defined as the one with the least fiber distance between it and the receiver (i.e. 10m). Sensor-II has the longer fiber length to the receiver (170m). All the experiments and results described in the subsequent sections are for a pulsed optical network. No results are shown where the laser is operating in steady state.

6.2 OPTICAL NETWORK DC CURRENT SENSING EXPERIMENT

This section is a review of the DC experiments done by S. Goyal. The networked-DC-current experiments described in S. Goyals' Thesis [13] were repeated for this thesis. The following is a list of differences between the present experimental set-up and the former one recorded by S. Goyal.

- Although the Optical Network topology is exactly the same the photodetector is very different. The photodetector used has significantly better bandwidth characteristics than the one previously used. The two incoming pulses from the optical network are also virtually identical as shown in Fig. 4.2.
- The receiver for this project is completely different from the one implemented previously. Although several components are the same the signal-processing concept is completely different, which is why the results for this specific section are obtained using the aid of a digital oscilloscope.

The purpose of these experiments is to show the linear response of the sensors over a 100A DC range. More importantly the experiments show conclusively that two different DC currents can be measured simultaneously. Results from these experiments also show the difference in sensitivity of each sensor.

The FOCSNET is a time-division amplitude-modulated system where DC Current is calculated by means of amplitude difference. Fig 6.1 shows how the amplitude of the signal changes in the presence of line-current.

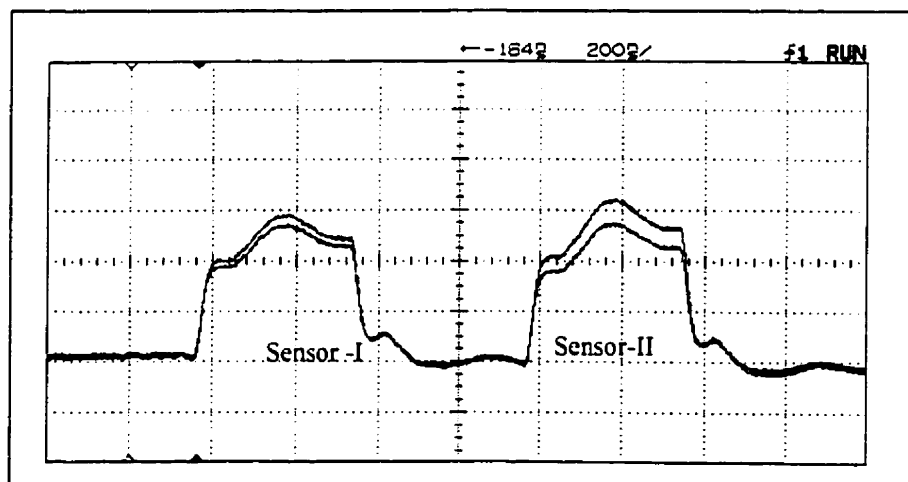


Fig. 6.1 Output Increase with 80A DC flowing through both sensors.

Sensor I: 20mV displacemente, Sensor II: 35mV displacement

For this experiment 80A DC was put through both sensors. Each sensor has 14 turns of conductor wrapped around it (e.g. $MF = 14$). Figure 6.1 depicts the difference in sensitivity of each sensor. Under the same line-current conditions and MF , Sensor-II has almost double the displacement of Sensor-I.

In order to record the linear response of the system, readings were taken in three different set-ups and the readings taken were of mV-increments per Current-step. In the first set up the same amount of current was passed through the sensors simultaneously and the line current increased in steps of 20A. In the second set-up the current was passed through only one of the sensors at a time and readings were taken. Finally two different currents were passed through the two sensors such that the sum of both currents always remained at 100A. Fig 6.2 shows the result of this experiment. From this it can be seen that the response of the sensors is linear in nature.

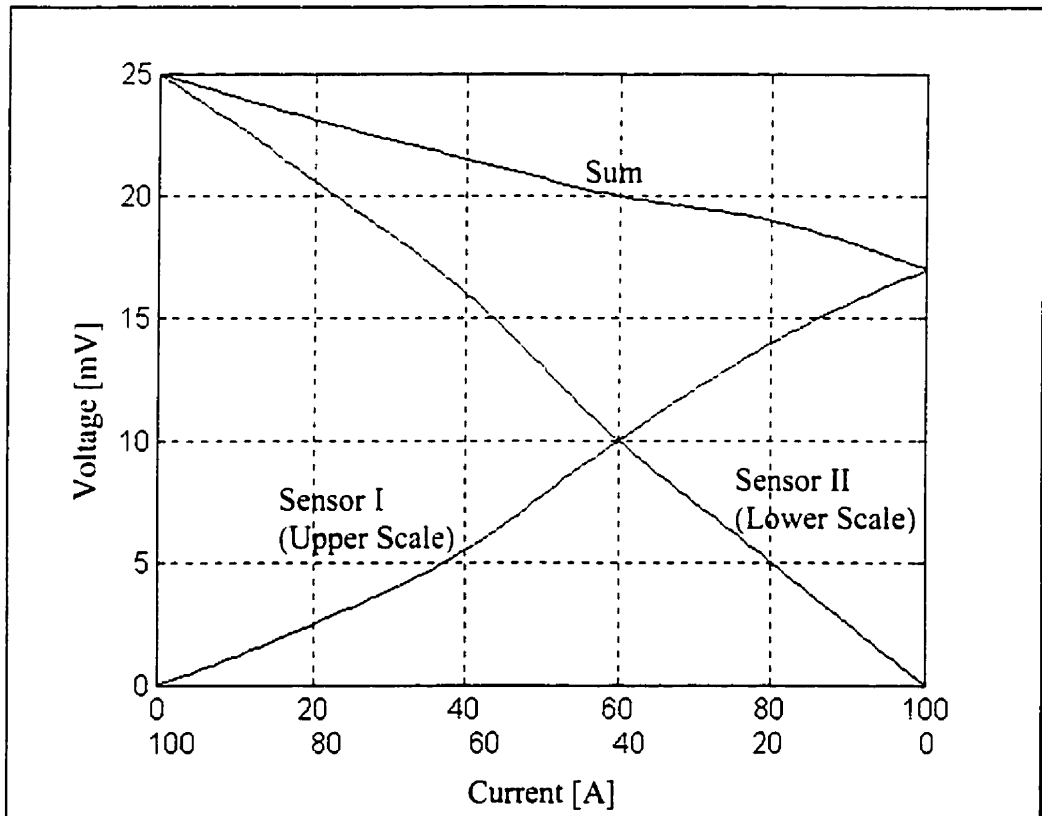


Fig. 6.2 System Response with different DC currents passing through the two sensors

It can also be seen how the FOCSNET can measure different DC currents simultaneously. The sum of the changes in the two-sensor output pulses, though linear, is not horizontal due to the fact that the sensors have different sensitivities. The response curve for each sensor has a particular slope.

The curve representing the sum of the sensor currents can be taken as a “Figure of Merit” for the system sensors in that the smaller the slope of this curve the more identical the two sensors are in terms of their response [6].

6.3 OPTICAL NETWORK AC CURRENT SENSING EXPERIMENT

The first new study done in this project is the network sensing of AC line-currents. S. Goyal’s previous work showed only the results of networked sensors to measure DC currents.

The sensing principal remains the same in that the line-current generates a Faraday Rotation in the sensing head, and that in turn is translated into an amplitude change. With DC the angle of rotation remains constant as long as the same current is constantly flowing. For AC the angle of rotation oscillates at a rate of 60Hz. The maximum amplitude of the oscillation is dictated by and proportional to the peak amplitude of the AC current flowing through the sensor.

For this experiment up to 100Arms were fed through the sensors. With the aid of a digital oscilloscope the equivalent peak-to-peak values of the currents flowing thorough the sensors were recorded.

The purpose of these experiments is to show that the sensors’ response is linear over a significant range of AC current. It is also equally important to show that the two different AC currents can be measured simultaneously.

The first step was to show that Faraday Sensors networked using a pulse or TDM technique, can detect AC current. Fig. 6.3 shows how the signal is seen by the photodetector. Shown in this figure are the 666 samples per 60Hz cycle that are modulated by the current's amplitude. For this experiment 100Arms was fed to Sensor-II.

With this it is concluded that the FOCSNET can detect AC current flowing through its sensors.

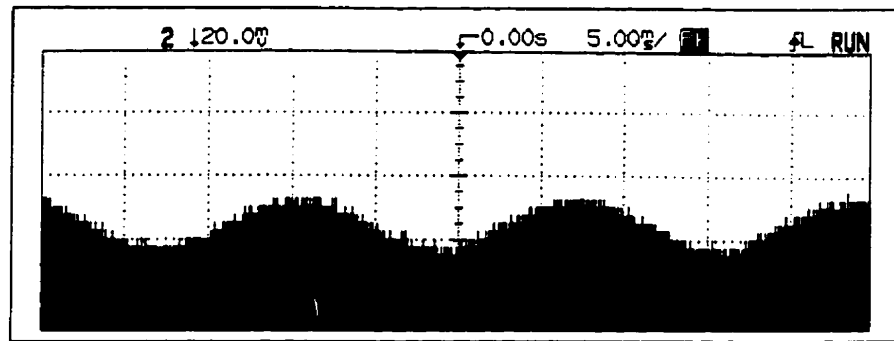


Fig. 6.3 AC Effect on Receiver output

To record the linear response of the system under AC current conditions, readings were taken in three different set-ups. The readings taken were of peak-to-peak mV-increments per current-step. In the first set up the same amount of current was passed through the sensors simultaneously and the line current increased in steps of about 20Arms. In the second set-up the current was passed through only one of the sensors at a time and readings were taken. Finally two different currents were passed through the two sensors such that the sum of both currents always remained at 100Arms. Fig 6.4 shows the result of this experiment and it can be seen that the response of the sensors' is linear in nature. It can also be seen how the FOCSNET can measure different AC currents simultaneously. Again the response curve for each sensor has a particular slope due to the sensitivity of each sensor.

The minimum detectable peak-to-peak line-current value is dependent on the noise level of the signal and it is different for each of the sensors and this is why the readings do not begin at the origin. The noise level will determine the minimum detectable AC current. The situation is different from the DC case where the measurement is the result of a differentiation and which is why the DC readings start from 0.

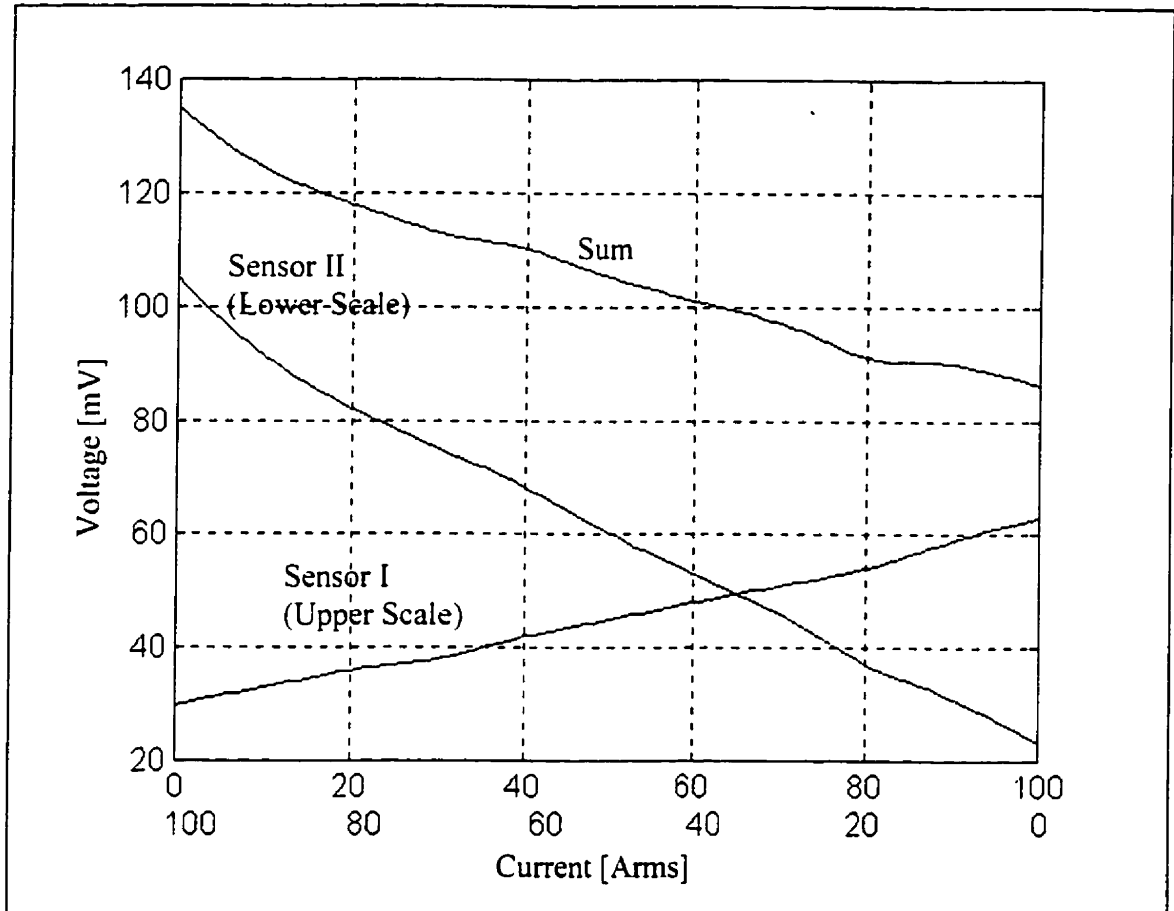


Fig. 6.4 System Response with different AC currents passing through the two sensors

6.4 LIGHT SOURCE DEPENDENCY

The FOCSNET system readings are based on the light intensity at the receiver. Any intensity changes produced by sources other than the magnetic field across the sensor will be taken as changes in the magnitude of the current being measured. The main source of

light intensity fluctuations is the Laser source, and although designed to be as stable as possible, it still has variations that could be misread as changes in the line-current.

Light intensity through the sensors is also directly proportional to the sensors' sensitivity and this means that readings from different light intensity levels will produce different amplitude changes for the same line-current.

6.4.1 Laser Characteristics

To characterize the stability of the laser its output was recorded over a five-hour period with readings taken at one-minute intervals. Fig 6.5 shows that the laser output is stable over a certain period of time but some relatively quick changes in amplitude can also be seen.

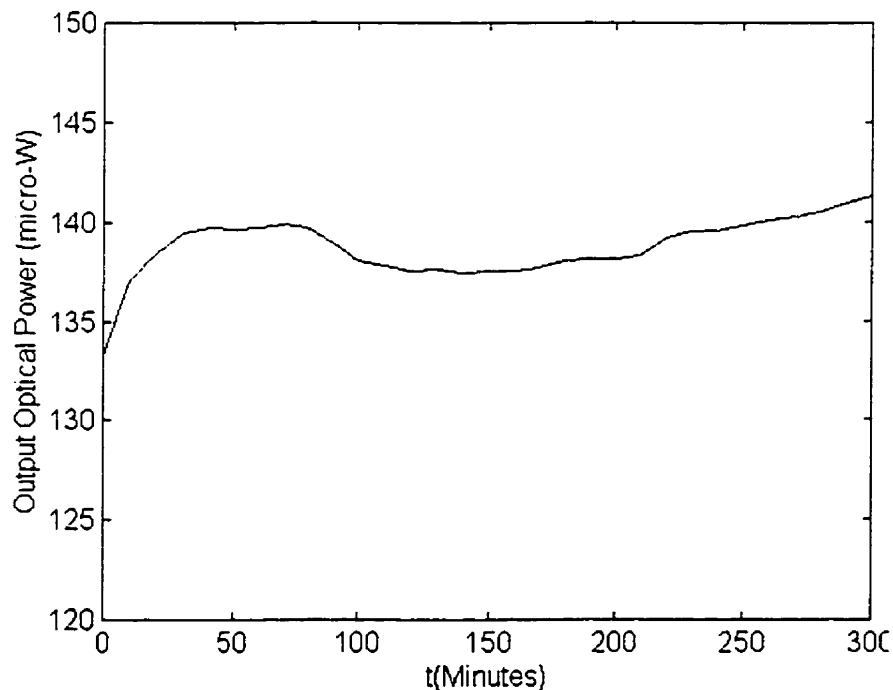


Fig. 6.5 Laser Stability Characteristics

These changes in amplitude can be misinterpreted as line-current changes and this is a reliability problem for the FOCSNET that must be eliminated.

6.4.2 Different Light Intensity Readings

A fixed line current produces different amplitude displacements depending on the light intensity level going through the sensing fiber. The experiments describe here are aimed at establishing a relationship between the light intensity through the sensing fiber and the sensors sensitivity.

The driving current that controls the Laser's output was set at different levels and for each of these levels DC and AC line current readings were taken on each sensor in steps of 20A and 20Arms respectively. Fig. 6.6 shows the results of two readings over a range of 100A DC at two different Laser intensity levels. The first sets of readings were taken with the Laser Driving current set at 61mA, which on the oscilloscope translates to a ZCL of 1.375V. The second sets of readings were taken with the Laser Driving current of 40mA which produces a ZCL of 750mV. The relationship between the Laser drive current and the Laser output is shown in Fig. 3.3.

The system has a linear response regardless of the light intensity of the laser and what is altered is the slope of the sensors' sensitivity. The results presented in Fig. 6.6, although they are for Sensor II, are consistent for both sensors and for both DC and AC currents.

From the results of these experiments it can be shown that there is a proportional relationship between the light intensity and the sensors sensitivity. Given any intensity of light the percentage change under a fixed line current is always the same. For instance Sensor II @ 14xMF under 100A DC will generate a 4% change of light intensity regardless of the original level of the Laser power. This is true within a Laser driving current range of 40-75mA. This percentage relation is particular and consistent for each sensor under DC and AC current.

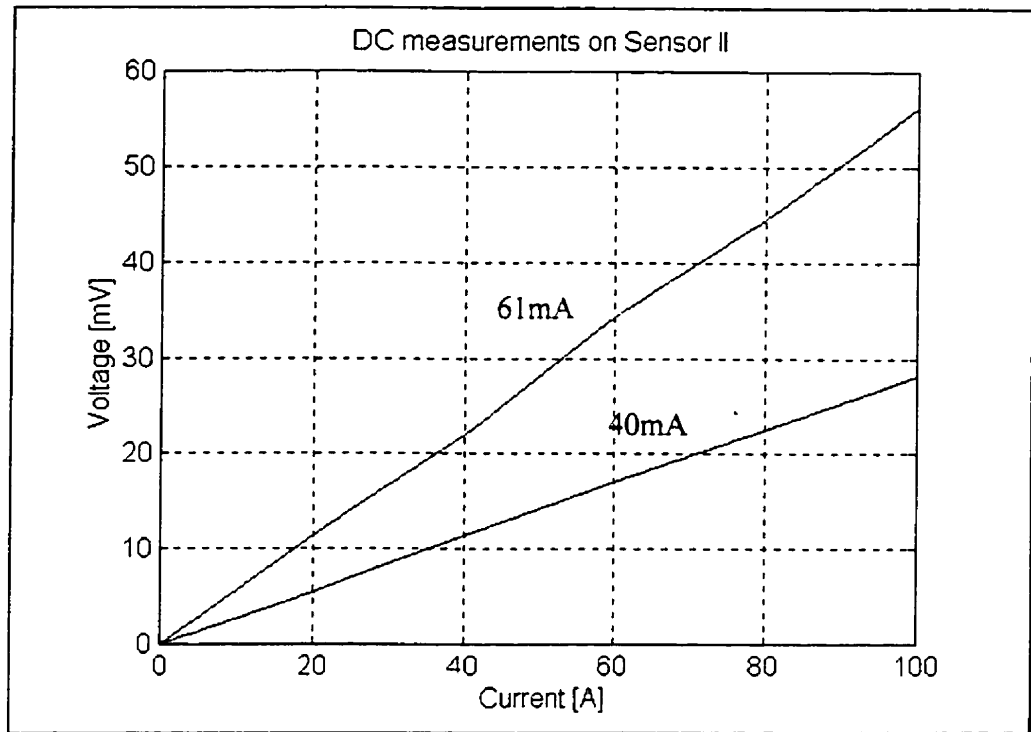


Fig. 6.6 Sensor II readings at different light intensity levels

For the experiment shown in Fig.6.6 the results are:

Line Current	Laser Driving Current	ZCL	Displacement Level	Ratio: Disp./ZCL
100A	61mA	1.375V	1.4312V	4.0%
100A	40mA	750mV	779.8mV	3.97%

Table 6.1 Percentage Light Intensity change for different Laser Power levels for SensorII

The proportionality is measured against the initial Laser power-level which, when no current is present, is known as the ZCL. Thus the proportionalities are measured against

the systems ZCL. This statement is the basis of the Ratio techniques described in the following sections. These techniques will generate measurements independent of light variations and therefore reliable current calculations.

Fig. 6.7 shows the results of the experiment shown in Fig 6.6 but this time the intensity levels are ratioed against their particular ZCL.

This figure clearly depicts the proportional relationship between light source power and the Faraday Rotation. The two experiments under different laser driving current conditions can be seen to have the same percentage change.

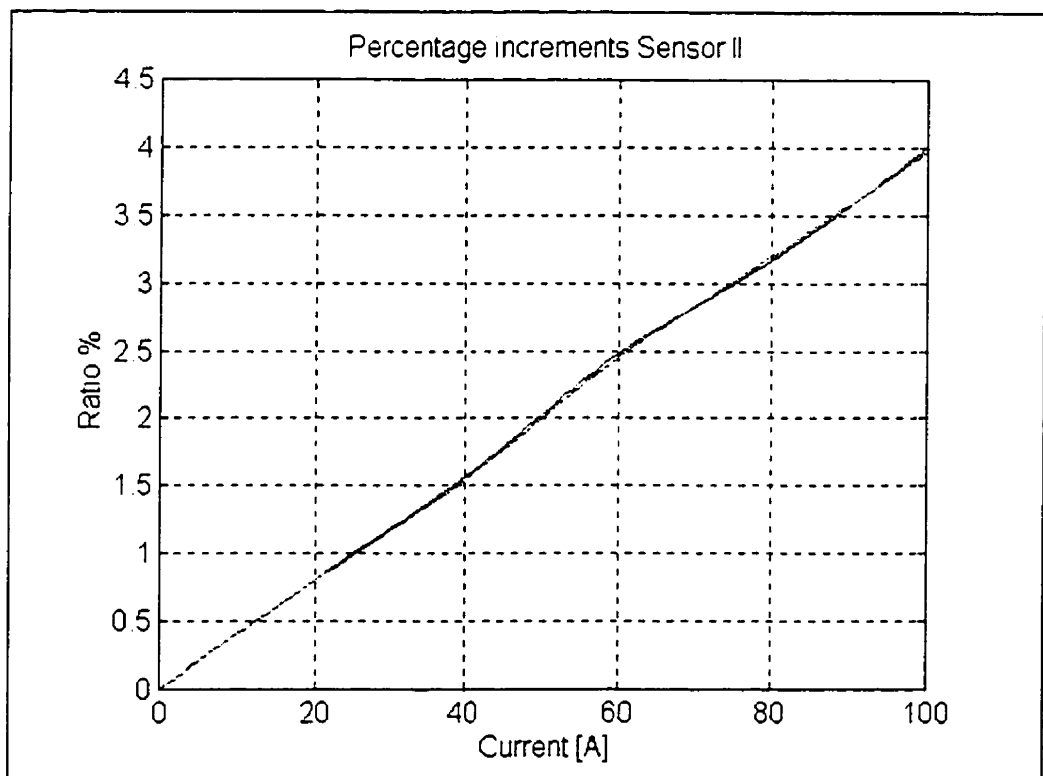


Fig. 6.7 Percentage increments of two DC current readings under different Laser driving current conditions.

6.5 RATIO TECHNIQUES THEORY

As with any measurement system the FOCSNET has to be immune to external disturbances that may influence its readings. Being based on amplitude modulation, the variation of light intensity is the main concern. Ratio techniques for both DC and AC measurement were developed in order for the FOCSNET readings to be immune to variation in light intensity through out the fiber network, and especially the ones caused by the Laser source.

The light intensity at the receiver when there is no current flowing around the sensor is denoted as the ZCL and any variations of light intensity are translated into variations of the ZCL. The ZCL is not fixed and it varies with any change in the Laser Power output. If the fiber system remains intact the ZCL varies equally in both sensors. As can be seen in Figs. 4.4 and 6.1 the pulses at the receiver, with no current flowing, have the same amplitude therefore the ZCL for both sensors is the same.

All dependencies on the ZCL must be eliminated for the current measurement to be immune to external disturbances.

6.5.1 AC Ratio

It has been shown that the FOCSNET is capable of detecting AC current flowing through the Faraday sensors. Described in this section is the theory of how that current is going to be measured and how these measurements are immune to variations of the ZCL.

When AC is flowing across a sensor the amplitude of the optical pulse oscillates at a rate of 60Hz. The instantaneous amplitude of the oscillation is proportional to the intensity of current. By detecting the minimum and maximum values of the oscillation the peak to peak value can be determined, and by direct proportionality the value of the AC current can be deduced.

The FOCSNET samples AC at a rate of 40kHz. The Digital receiver is designed to detect the maximum and minimum values of every 60Hz cycle of current flowing through the sensors. With this information the peak-to-peak value for that signal is calculated.

For AC a very simple ratio eliminates any dependency on the ZCL.

The AC current that flows through the sensor has no DC component thus the oscillation of the pulse can be basically represented as a 60Hz sine wave riding on the offset value of the ZCL as shown in the schematic of Fig. 6.8.

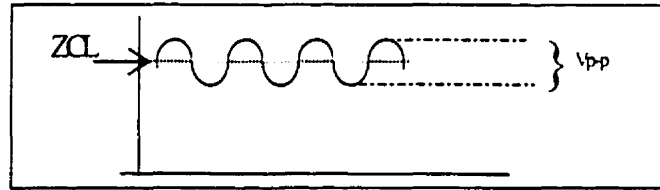


Fig.6.8 AC Oscillation with offset of ZCL

By taking a running average of all the pulses coming from this sensor in a period equivalent to one 60Hz cycle the ZCL is determined by the receiver. For any AC signal the average value is 0, for this system the average value is the ZCL. With the minimum and maximum values the peak to peak value is determined. Since all amplitude readings are proportional to the magnitude of the ZCL the following ratio can be stated,

$$ACratio = \frac{V_{pp}}{ZCL} \quad \text{Eq. 6.5.1}$$

The AC Ratio eliminates the dependence on the ZCL level and its variations and all the information needed to calculate this ratio is contained within the same pulse. This can be done with any and as many sensors as there are in the network.

6.5.2 DC Ratio

The DC Ratio calculation is more involved than the AC Ratio in the sense that not all the information needed to measure the current is contained within the pulses of the sensor in question. For the AC Ratio all that is needed is the peak to peak value and the mean value of the signal and the receiver can obtain both of these values from the pulse information of each sensor.

Changes in DC current produces a change in the ZCL, that is in general terms the DC offset level of the detected signal changes in proportion to the DC line current. In the receiver a running average has, as a result, the DC level of the signal. In the presence of no Line-current this level is the ZCL.

Because of the nature of DC current the optical pulses of the system sample what is virtually a steady state signal. Alas the advantage of the AC case where two parameters are considered is not present. The signal's amplitude is the only data that can be read under DC conditions.

The ZCL can not be extracted while a DC current is flowing through a sensor, thus the ZCL must be provided from a reference source external to that particular sensor. With the ZCL provided by a reference source then a DC Ratio can be determined in the same manner as with AC.

$$DCratio = \frac{DC_{level}}{ZCL_{ref}} \quad \text{Eq. 6.5.2}$$

As before this ratio eliminated the dependence on the ZCL and its variations. The DC Ratio can be done with any and as many sensors in the system given that a Reference ZCL is provided.

6.5.2.1 Reference ZCL

In the beginning of this section it was explained that ZCL is the same for all sensors. If this is the case then the ZCL determined for any given sensor is consistent for the ZCL of any and all sensors in the network. This ZCL value can be used to make ratio calculations for any sensor. This means that the ZCL calculated in any sensor can be used as a reference source of ZCL for another sensor measuring DC current.

It must be noted that a value of ZCL can only be obtained from a sensor that has either AC current through it or no current at all. In the presence of no current the value of the receivers running average is the ZCL. The running average calculated under AC conditions is also the ZCL. This has to be taken in consideration when we look at the different types of networks:

Type	Number of Sensors	Type of Current To Measure
A	N	AC only
B	N	DC only
C	N	AC and DC

Table 6.2 Types of Networks

In the case of Network-A, where every sensor in the system will measure AC, the sensors are independent of each other because all the information required to calculate a line current is self-contained within each sensor's pulse.

For Network-B there will be no current flowing through one of the sensors in order to obtain from it the ZCL as a reference for all the other sensors. The FOCSNET is a TDM system and varying the lengths of the fibers to each sensor generates the time intervals. The sensor with the shortest distant to the receiver must be the one used as reference, so

that the ZCL information is the first to be calculated and then used as a reference for the other sensors.

A Faraday sensor is a very expensive piece of equipment, which if bought should be used, but in the type B network arrangement one sensor is effectively wasted. To remedy this and to maximize the use of all sensors in the system, one leg of the coupler at the transmit end should go directly into the other coupler at the receiver end. The Reference ZCL can therefore be determined with the pulse information in this leg and no sensor goes to waste. It must be noted that the pulse going through the sensor-less leg has to be amplitude-matched with the ones going through the sensors and this can be accomplished with a variable attenuator.

In Network-C the ZCL is obtained from any sensor that has AC current flowing through it and no DC, thus at least one sensor must only measure AC current. For the same reasons as mentioned before, it is convenient, that the sensor with the shortest fiber length be the one with AC current only.

The receiver designed for this project can handle any of the three applications just mentioned. The receiver will always display on screen the AC current value of each sensor and the DC Current is also displayed. It is up to the user to decide which sensor to use as reference and once chosen the display on the PC screen is the ZCL and the DC current flowing through the non-reference sensor.

6.5.3 Simultaneous AC and DC

One of the most innovative developments in this study is the capability of the system to measure AC and DC current while they flow simultaneously through one sensor. The FOCSNET system is designed to measure DC and AC currents and it is capable of measuring these currents simultaneously as they flow through different sensors.

Using a combination of the ratio-techniques for AC and DC a procedure can be put forth for measuring AC and DC while these are flowing simultaneously through the same sensor. The techniques have already been combined to measure AC & DC flowing through different sensors and a slight variation allows this same measurement with only one sensor.

In this new case, where AC and DC are flowing through the same sensor, two phenomena will occur simultaneously. As seen in the schematic in Fig.6.9 the ZCL is incremented to a new DC level as a result of the DC line current and a 60Hz oscillation due to the AC is also present.

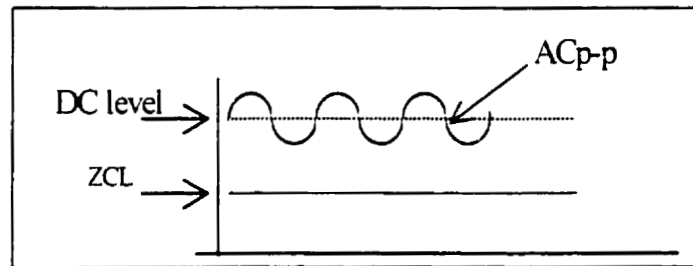


Fig. 6.9 AC and DC simultaneous response

Thus, the AC oscillation originated by the AC current flowing through the sensor will still be riding on a DC level. It will not be the ZCL but the new level to which the ZCL is effectively increased and this new level is nothing more than the result of the DC current flowing through the sensor.

It can be seen that the components of both the DC & AC currents are present and distinguishable. Any effects of variations of the Laser power have to be eliminated for both the AC and DC cases and the techniques developed for measuring AC or DC separately will be used simultaneously on the same sensor.

6.5.3.1 AC Calculation

For AC the Maximum and Minimum values of the pulses can be detected to calculate a peak-to-peak value. Again a running average will determine the DC level the AC is riding on and in this case this DC level will be different from the ZCL. When the *AC Ratio* is calculated this last fact is of little relevance. The reason being is that the peak-to-peak value of the AC produced by the photodiode is not only proportional to the intensity of AC current flowing through the sensor, but to a much smaller degree it is also proportional to the DC level it rides on at the output of the receiver. With the *AC-Ratio* any effects produced by this DC level are eliminated and in the original case this ratio eliminates the dependence on ZCL and any variations of Laser power level. In this new case it will also eliminate all effects produced by the presence of a DC current in the same sensor. The DC is taken as a variation of the light of the light intensity and is eliminated as such.

Thus the FOCSNET can measure AC current through a specific sensor regardless the presence of DC current in the same sensor.

6.5.3.1 DC Calculation

As with AC, the technique devised for DC measuring will be used when DC and AC flow through the same sensor.

As explained previously the presence of DC current will produce an increase in the effective ZCL, which will be shown as a DC level at the receiver. By taking a running average this new DC level can be determined. This is the same value obtained from the running average explained for the AC case. This new DC level is all the information needed to measure DC current. Thus, DC current can be measured whether AC current is flowing through the same sensor or not and the running average eliminates the oscillating effect of the AC current.

It must be remembered that to accurately measure DC it has to be referenced against ZLC and this can not be obtained from this sensor. The reference value of ZLC has to be provided and it is obtained from a different sensor in the system.

By simply using the techniques already established measuring AC and DC flowing through one-sensor increases the applications of each sensor in the FOCSNET. The biggest concerns are the possible effects of one current on the other, but with the procedures mentioned above the effects of one current type on the other are isolated.

This innovation can only be done in a networked system for it is the networked nature that allows this flexibility. The basis of the measuring techniques is the optical sampling of the current signal. By manipulating these samples and using concepts such as running averages and peak detection the current calculations becomes simpler. Having a network also provides the possibility of having a reliable reference source for current calculation.

6.6 EXPERIMENTAL RESULTS

This section presents the results of several line currents measurement tests done with the FOCSNET. One of the first tests performed was one to calculate the SNR of the system.

6.6.1 SNR

When neither AC or DC currents is flowing through the sensor a base noise level can be obtained. This noise is a product mainly of the electronic components in the receiver as discussed in chapter V and the base noise level is measured at 8mVpp.

This noise level sets the lower value of the operating range of the system as well as the minimum resolution. This means that any current, AC or DC, that produces an amplitude change at the receiver lower or equal to 8mVpp will not be detected.

As in any system the SNR plays a key factor and to a certain extent the higher the SNR the better the system resolution. The FOCSNET System's SNR can be increased by adding more turns of conductor around the sensor which increases the MF of the magnetic field produced by the current. In the following table a comparison of SNR is shown when turns around the sensor are doubled from 7 to 14. All these receiver measurements are made on the digital oscilloscope.

Current	Conductor Turns	Multiplying Factor	Receiver	Noise	SNR
100 Arms AC	7	7x	50mvp-p	8mvp-p	6.25
100 Arms AC	14	14x	101mvp-p	8mvp-p	12.625
100 A DC	7	7x	25mv*	4mv	6.25
100 A DC	14	14x	49mv*	4mv	12.25

*Is the difference between the level measured when 100A DC is flowing and the reference level of ZCL

Table 6.3 SNR under different MF conditions

In simple terms, the more turns of the conductor the lower the line-current that can be detected - up to a point.

6.6.1.1 AC Reading Error

Another way of increasing the SNR is to increase the Laser power and any adjustment that ensures maximum power at the receiver (e.g. reduce optical losses, polarization controller adjustments).

Shown in the following table are the effects on the SNR when the laser power is varied.

Current AC	MF	Laser Driving Current	ZCL	Receiver Output	Noise	SNR Receiver
100 Arms	14x	71.5mA	1.605v	101mvp-p	8mvp-p	12.625
100 Arms	14x	52.3mA	1.250v	80mvp-p	8mvp-p	10
100 Arms	14x	40.5mA	900mv	57mvp-p	8mvp-p	7.125

Table 6.4 SNR for AC current under different Laser power conditions

When the measurements are done using the Ratio technique the noise level will be responsible for the error in the calculations. In the AC ratio case, the error can be determined from a ratio measurement in the presence of no line-current. Here again the error is reduced if the power seen by the receiver is maximized. The AC Ratio error is simply the AC Ratio value in the presence of no current divided by the receiver base noise level. Table 6.5 shows the value for the AC Ratio Error under different Laser Power level conditions.

Current AC	Laser Power	ZCL	Ph/Amp output. (noise)	SNR _{AC} ZCL/Noise	AC Ratio Error
0 Arms	71.5mA	1.605v	8mvp-p	200.625	0.005
0 Arms	52.3mA	1.250v	8mvp-p	156.25	0.0064
0 Arms	40.5mA	900mv	8mvp-p	112.5	0.008

Table 6.5 AC Ratio Error under different Laser power conditions

An acceptable level range for the AC Ratio Error is,

$$0 < AC Ratio_{Error} < 0.008$$

Eq. 6.6.1

Within this range and a Laser driving current as low as 40mA the system has an acceptable SNR.

6.6.1.2 DC Reading Error

The SNR when reading DC can be improved if the MF factor increases and this can be seen in Table 6.3. The DC Ratio calculation error is also due to another factor. The basis of the DC Ratio is the division between two intensity levels provided by different sensors, one is the ZCL reference and the other is the level to be measured. The Reference ZCL is obtained from the first sensor in the system and the DC current calculations are taken from Sensor II. In order to calculate a DC Ratio it is necessary that all the pulses incoming from all sensors have the same ZCL level.

Even when there is no current flowing through the sensors the optical pulses are still reaching the receiver and thus a level for each is detected, this is the ZCL .

The way to equalize the ZCL for all sensors is to adjust each of the Polarization Controllers in the system. With this technique the ZCL can be matched very accurately, only incurring a small ratio error. This error, the DC Ratio error, is determined by the ratio of levels from one sensor to the next, and ideally it should equal 1. Experimentally the following readings were taken,

$$\frac{ZCL_{\{SensorII\}}}{ZCL_{\{reference_sensor\}}} = \frac{1.60501 V}{1.605995 V} = 0.9993 \quad \text{Eq. 6.6.2}$$

In this particular experiment the ZCL of the reference sensor (Sensor I) was slightly higher than that from Sensor II, this is not always the case, the ZCL of Sensor II could be the one that has the slightly higher power, and in the best case scenario both would have the exact same power

When the result of Eq. 6.6.2 is normalized ,

$$1 - 0.9993 = 0.00061 \quad \text{Eq. 6.6.3}$$

This means that in the case of zero DC current through the sensor, the DC ratio will be equal to this error of 0.00061. This error depends on the adjustment of the Polarization Controller. An acceptable range for this error is:

$$0 < DC \text{ Error} < 0.0024 \quad \text{Eq. 6.6.4}$$

An error of 0.0024 level translates to a ZCL difference between the sensors of under 4mV and 4mV is the base noise level. If the error stays within this range then the difference in levels will be negligible against the noise thus the only error in the DC calculations will be caused by the inherent noise of the receiver.

6.6.2 DC Ratio Experimental Readings

6.6.2.1 Set Up

For this experiment the sensors were wound with 14 turns of conductor each. ($MF = 14$) and current was put through Sensor II. The current ranged from 0-100A in 20A steps. The ZCL level of Sensor I was taken as reference in order to determine the DC Ratio.

6.6.2.2 Results

Up to 100A of line-current were fed through Sensor II and as expected the DC level of this sensor increased proportionally with every step increase in the line-current. When the DC current was turned off the level returned to the ZCL. The ZCL level of Sensor I remained constant throughout this experiment.

6.6.2.3 Measurements

The ZCL at Sensor II for this experiment was measured at 944mV. When the Maximum current of 100A was put through Sensor II its level jumped to a maximum of 990mV, thus a difference of 46mV. This will constitute the response of Sensor II with a 14x *MF*.

6.6.2.4 Test

A series of readings were taken in order to plot the response of the system and analyze the linearity of its behavior. Fig 6.10 shows the normalized results of this experiment. It can be seen how the response of the system using the DC ratio technique is highly linear. An example of the calculation is as follows. When the line current is set at 40 A, the level detected is 970.5mV, the ZCL is 944mV and a ratio error is +0.0106 , thus the ratio for this particular point is given by,

$$DCRatio = \frac{970.5mV}{944mV} = 1.0281 \quad \text{Eq. 6.6.5}$$

$$Normalizing = 1.0281 - 1.0106 = 0.017$$

Theoretically the response should start from the origin and the minor offset is a product of the DC ratio error.

The DC Ratio technique is designed to eliminate the effects of the Laser power source. This means that regardless of the intensity of the latter, the response of the system is consistent.

Fig. 6.11 reflects the results of two separate DC Ratio Experiments, the difference between the two being the power level of the Laser output. For these experiments the Laser Driving Current was set at 50mA and 40mA respectively. These currents generate ZCL levels at the receiver of 944mV and 920mV respectively.

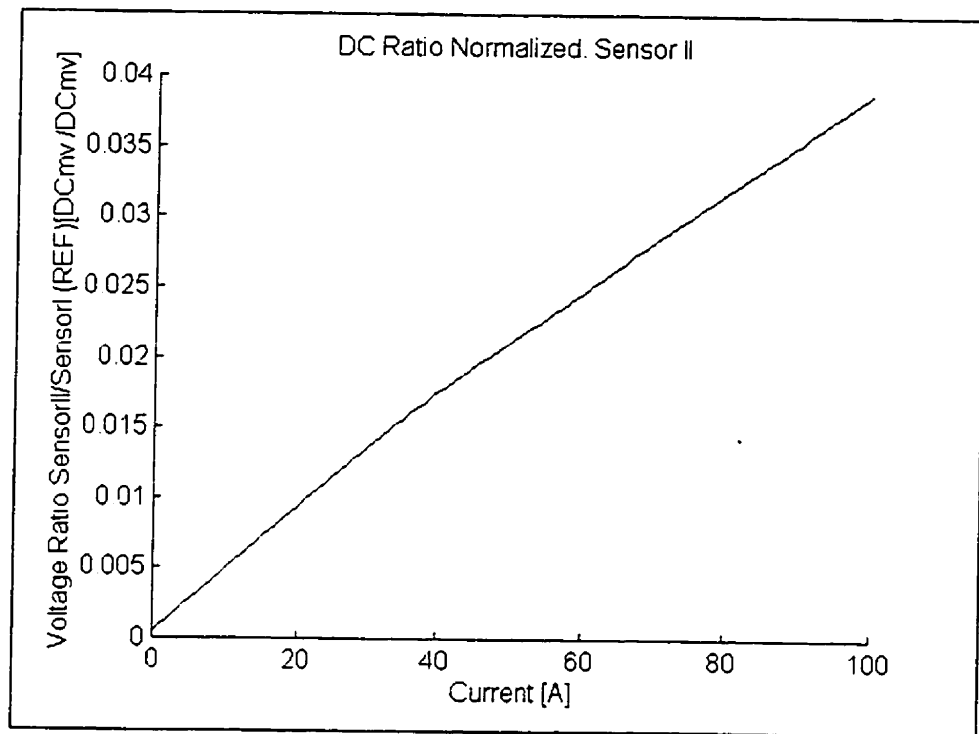
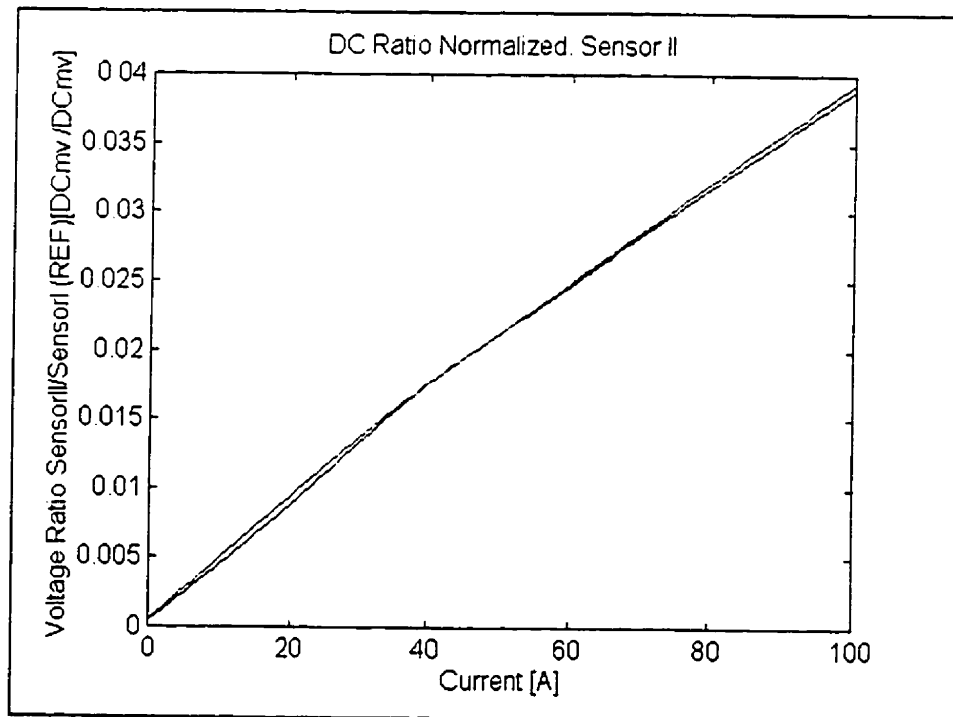


Fig.6.10 DC Ratio Experiment. Readings on Sensor II with Sensor I as Reference



*Fig.6.11 DC Ratio Experiments with Different laser drive current. Currents set at:
50mA and 40mA*

It can be concluded that the FOCSNET can measure DC current virtually regardless of the variations of the light source. The ZCL range for which this is true is 400mV - 2.5V. This range is experimental and is limited by the maximum possible laser-drive-current of 75mA.

6.6.3 AC Ratio Experimental Readings

6.6.3.1 Set Up

For this experiment the sensors were wound with 14 turns of conductor each ($MF=14$) and AC Current was put through both Sensors. The current ranged from 0-100Arms in 20Arms steps and AC Ratio measurements were taken on both sensors.

6.6.3.2 Results

Line Currents up to 100Arms were fed through each of the sensors and as expected a 60Hz oscillation was produced proportional to the magnitude of the AC line-current and with an offset level of ZCL. When the AC current was turned off the level returned to the ZCL. The degree of oscillation for each sensor under the same line-current condition was different due to the difference in sensitivities of the sensors.

6.6.3.3 Measurements

The ZCL for this experiment was measured as 1.464V. When the Maximum current of 100Arms was put through the sensor the amplitude of the oscillation was 146mVpp. This constitutes the response of Sensor II with a 14x MF . For Sensor I at this same ZCL and MF the amplitude of the oscillation was measured as 62.51mVpp.

6.6.3.4 Test

A series of readings were taken in order to plot the response of the system and analyze the linearity of its behavior. Fig 6.12 shows the AC Ratio results of this experiment on Sensor I. It can be seen how the response of the system using the AC Ratio technique is

highly linear. An example of the calculation is as follows. When the line current is set at 60 Arms, the voltage variation is 43.92mVpp and the ZCL is 1464mV thus the ratio for this particular point is given by,

$$ACratio = \frac{43.92}{1464} = 0.030$$

The AC Ratio technique is designed to eliminate the effects of the Laser power source. This means that regardless of the intensity of the latter, the response of the system is consistent.

Fig. 6.13 illustrates the results of three separate AC Ratio Experiments done on Sensor II, the difference between them being the power level of the Laser output. For these experiments the Laser Driving Current was set at 70mA, 52mA and 40mA and these produced ZCL levels at the receiver of 1.410V, 1.063V and 755mV respectively.

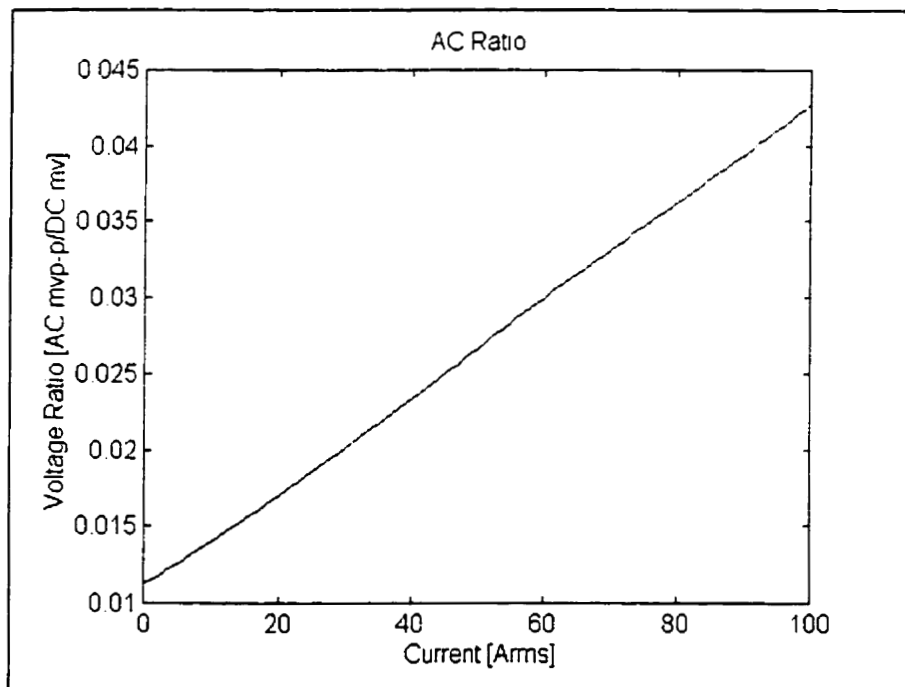
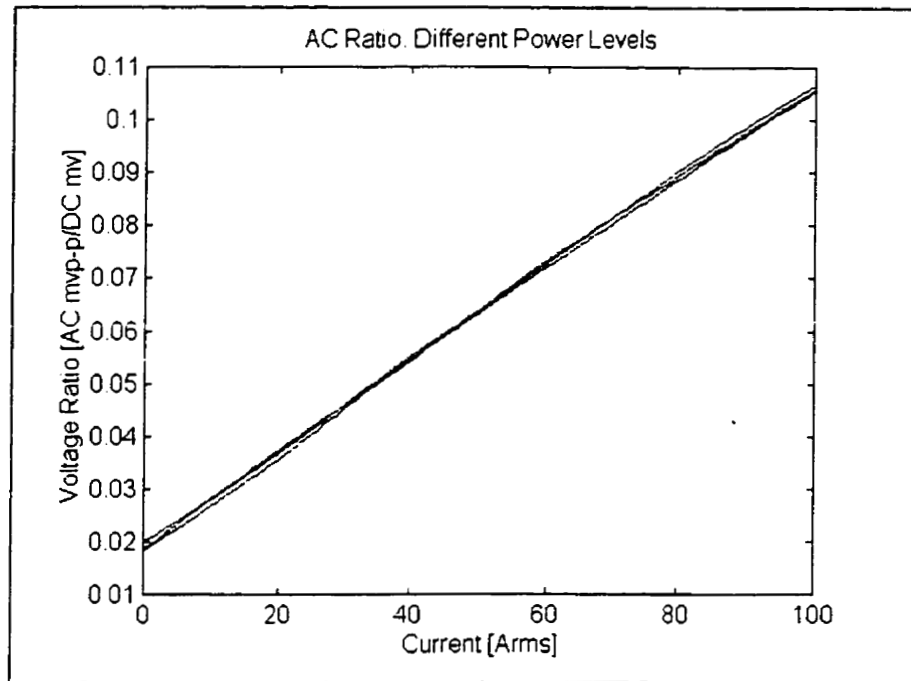


Fig. 6.12 AC Ratio on Sensor I



*Fig. 6.13 AC Ratio on Sensor II Laser Driving Current Values set at:
70mA, 52mA and 35mA*

It can be concluded that the FOCSNET can measure AC current regardless of the variations of the light source. The ZCL range for which this is true is 400mV - 2.5V. This range is experimental and is limited by the maximum possible laser-drive-current of 75mA.

Variations in the plots in Fig. 6.13 are due to the AC Ratio error and there is close to 20mA of difference between Laser Drive currents for this experiment. These conditions were generated specifically for this test, though in reality the laser will not have such big jumps in its power level, so the difference in readings will be negligible.

Using the AC Ratio an Accuracy experiment was performed where the goal was to determine the minimum detectable AC current. Due to laboratory limitations the minimum amperage steps that could be generated were 1.55Arms. Readings from 0 to

20.15Arms were taken and Fig. 6.14 shows the results. The experiment was done on Sensor II, for it has the higher sensitivity of the two in this project.

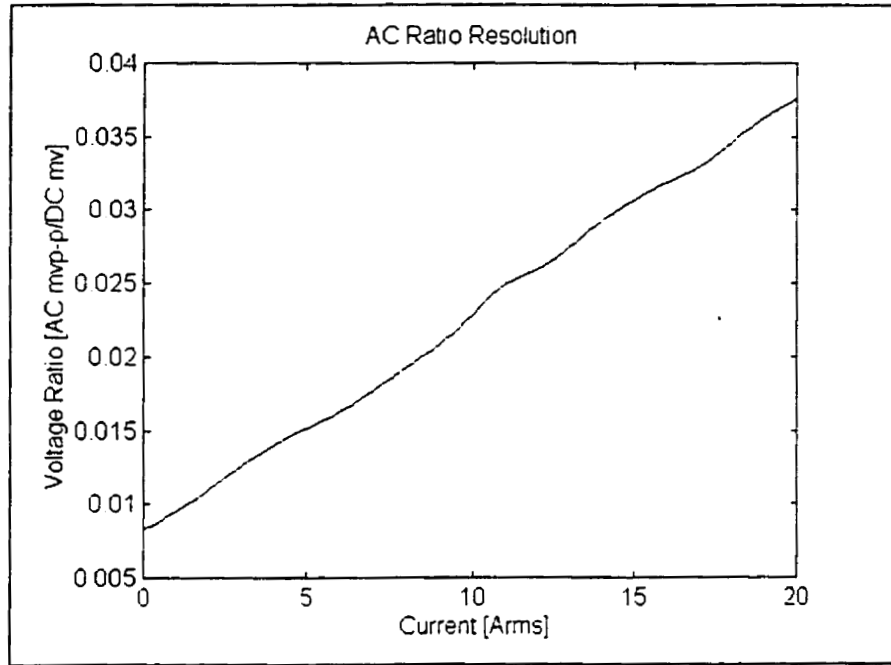


Fig. 6.14 AC Ratio Resolution. Sensor II. Steps of 1.55Arms

Although not as linear as the previous experiments the results from this graphs shows what kind of resolution the FOCSNET can achieve. The linearity is lost due to the noise of the system.

6.6.4 Simultaneous DC & AC Experimental Readings

6.6.4.1 Set Up

The set up for this experiment is a slight variation from the network set-up used to this point. The whole system remains virtually the same, the only change being the turns of current conductor around the sensor. Until now 14 turns of conductor were wrapped around the sensors, thus creating a multiplication factor of the magnetic field of approximately 14. This 14x factor has been the case in all experiments done until this stage.

In this new case, AC and DC have to flow through the same sensor, and since they both can not be fed through the same conductor due to lab constraints, then two separate conductors must be used. The two conductors must be wrapped as many times as possible around the sensor to create a MF for each of the currents. Due to the size of the hole in the sensor only 7 turns of each conductor could be fitted and this gave a $7 \times MF$ multiplication for each of the two line-currents.

6.6.4.2 Results

Line-currents of 100 Arms AC and 100A DC where fed simultaneously to the two conductors of the sensor. As expected the ZCL was increased to a new level and proportional to the DC amperage flowing through the sensor. Riding on this new level there is a 60Hz signal of amplitude proportional to that of the AC amperage flowing through the second conductor of the sensor.

When the DC current was turned off, while maintaining the AC flow, the output shows the 60Hz signal oscillating around the ZCL. When the DC flow was turned back on and the AC removed, the output this time showed a steady-state signal at a level above the ZCL, and proportional to the DC amperage.

6.6.4.3 Measurements

The ZCL value out of the receiver was measured as 1.605v. When 100A of DC current was then applied to the sensor this level jumped to a maximum of 1.630v (dif: 25mv). When 100Arms AC (no DC current) was applied the amplitude of the oscillation was 50mVpp.

6.6.4.4 Tests

A series of test were done by varying the amperage of one of the currents while the other one remained constant and then using the ratio techniques the results were graphed. The variation of current, for both DC and AC was done in steps of 20A and 20Arms

respectively and ranged from 40A- 100A. A measurement was also taken at 0A in order to have a reference point.

i. Varying AC while DC is constant.

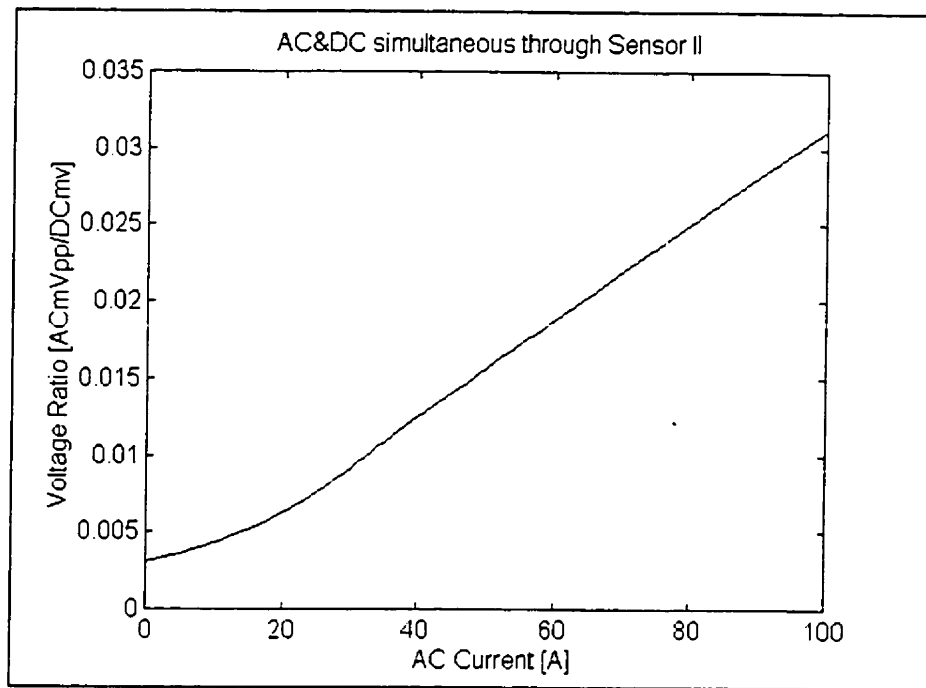
The following is a table showing how the ratios are calculated using some examples from the readings taken in this experiment. The current flowing through each conductor is as marked, but it is important to remember the 7x MF. For this experiment the DC current was set at a pre-determined value and an AC sweep was performed.

As can be seen from Table 6.6 the values of the calculated ratio of a set DC current do not change even when AC current is simultaneously flowing and varying at the same time. Figs. 6.15 and 6.16 show the results when AC current is varied and DC current was set at 100A and 0A respectively. The graphs show the values for the AC Ratio with the value of the DC current remaining constant.

DC Current [A]	AC Current [Arms]	AC Amplitude mvp-p	DC level V	AC	DC
0	0	8	1.605	0.0050	0.9994
0	60	29	1.605	0.0181	0.9993
0	100	50	1.605	0.0312	0.9994
100	0	8	1.630	0.0049	1.0149
100	60	30	1.630	0.0184	1.0149
100	100	51	1.630	0.0313	1.0149

Table 6.6 AC varying with DC constant

It is concluded that the AC measurements are highly linear regardless of the simultaneous DC current flow. The linearity is lost in the first part of the graphs since at these current levels the SNR was too low and no accurate measurements could be taken. The linearity of the response can be spread out more if the SNR is increased. For this experiment the MF was set to 7x, if this is increased the SNR improves.



DC set at 100A. AC varying 20-100Arms

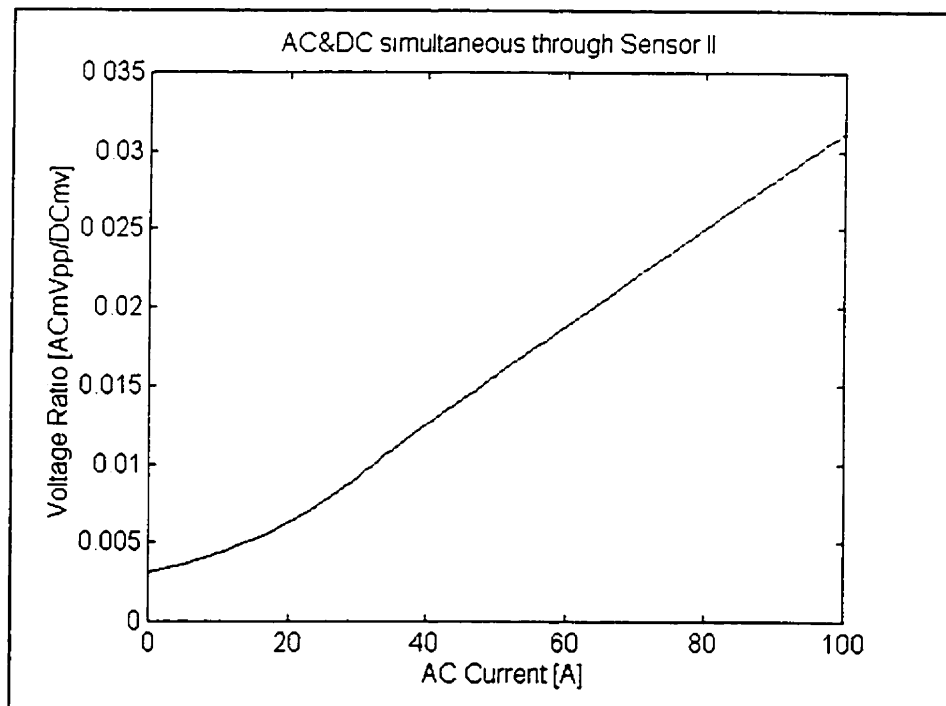


Fig.6.16 AC and DC simultaneous Through Sensor II.

DC set at 0A. AC varying 20-100Arms

In this experiment: the DC Ratio error is 0.00061 (Eq. 6.6.3). Well under the 0.0024 (Eq. 6.6.4) minimum allowable.

The ratio techniques are designed specifically to eliminate all variations other than the ones produced by the specific current to be measured. This variation which includes the variation of the Laser power, and in the case when AC is being measured the DC current may be considered as an amplitude variation external to the effects of the AC current and is eliminated as such. Fig. 6.17 shows a comparison of the results in the previous two figures and it can be seen that the graphs are almost identical. The error is due to the AC Ratio noise. This shows that the AC measuring technique works very well even when DC current is flowing simultaneous to the AC current in the sensor.

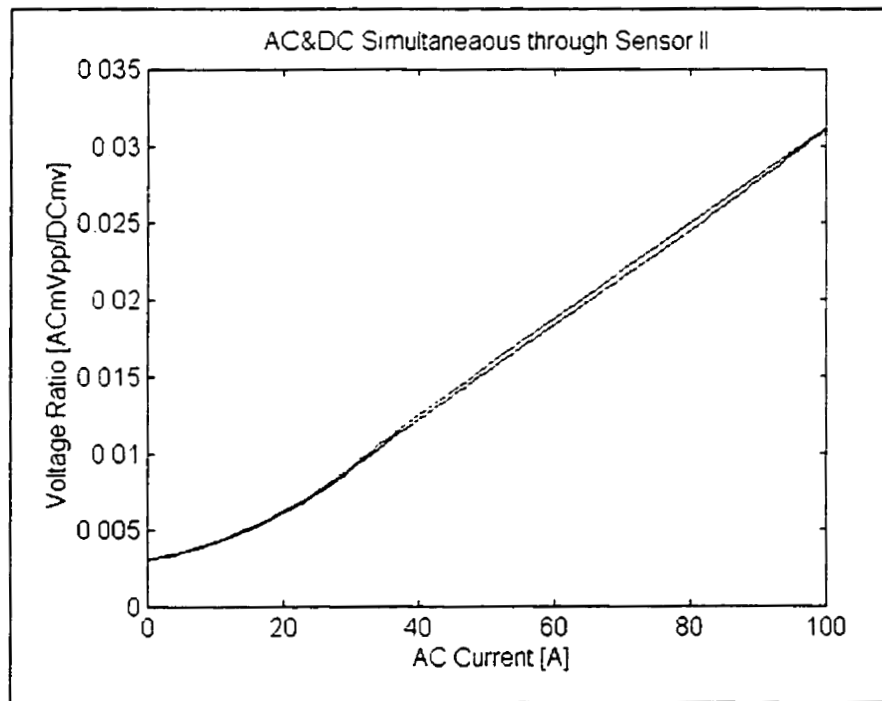


Fig.6.17 Comparison of Figs. 6.15 and 6.16

ii. Varying DC while AC constant.

Table 6.7 shows the values of the calculated ratios, this time the AC current will be set at a fixed value, and the DC current will be varied. For this experiment the AC current was set at a pre-determined value and a DC sweep was performed.

Sensor		Photodiode/Amplifier		Ratio	
DC Current [A]	AC Current [Arms]	AC Amplitude mvp-p	DC level V	AC	DC
0	0	8	1.6080	0.005	1.0025
60	0	8	1.6180	0.005	1.0087
100	0	8	1.6280	0.005	1.0150
0	100	50	1.6079	0.031	1.0024
60	100	50.3	1.6182	0.031	1.0089
100	100	50.4	1.6281	0.031	1.0150

Table 6.7 DC varying with AC constant

This time the AC ratio value remains virtually the same for a set value of AC current regardless of the DC current flowing simultaneously or its intensity. Fig 6.18 shows the normalized results of the DC ratio technique when DC amperage was applied to the sensor varying from 0-100A, while 100Arms AC was flowing simultaneously. The amplitude of the 60Hz oscillation corresponding to the AC current varied slightly from 50 - 50.4mVp-p.

The difference of 0.4mvp-p is because the oscillation amplitude depends slightly on the voltage level of the pulse and the DC current flowing through the sensor alters this level. This variation is also eliminated when the AC ratio technique is applied.

AC = 100A; DC = 0A

$$\frac{AC_{oscillation}}{DC_{level}} = \frac{50mv_{pp}}{1.605v} = 0.0310$$

Eq.6.6.7

AC = 100A; DC = 100A

$$\frac{ACoscillation}{DClevel} = \frac{50.4mv_{pp}}{1.629} = 0.0309 \quad \text{Eq.6.6.8}$$

With a fixed 100Arms AC a ratio of 0.031 is obtained for the entire DC sweep. The values for Eqs. 6.6.7 and 6.6.8 were taken from Table 6.7.

Fig. 6.18 not only shows the DC results when the AC current is set at 100Arms and DC is varying, it also shows the results when the AC current is set at 0A and DC is varying. This means the results for both these experiments are identical. The DC ratio values do not change, and even more they stay constant regardless of the AC amperage applied to the sensor. When no AC current is flowing the AC Ratio remains at 0.005 for the entire DC sweep.

6.6.5 Current Calculations

In order to determine the current flowing through the sensor an equation is required that, given the value of the ratio calculated it can compute the value of the current in Amperes. It must be remembered that the measurand is the current, thus it is always unknown.

Until now the value of the current flowing through the sensor has been known in order to analyze the behavior of the system response to current. This behavior is plotted in Figs 6.10 –6.18 where the linear nature can be seen.

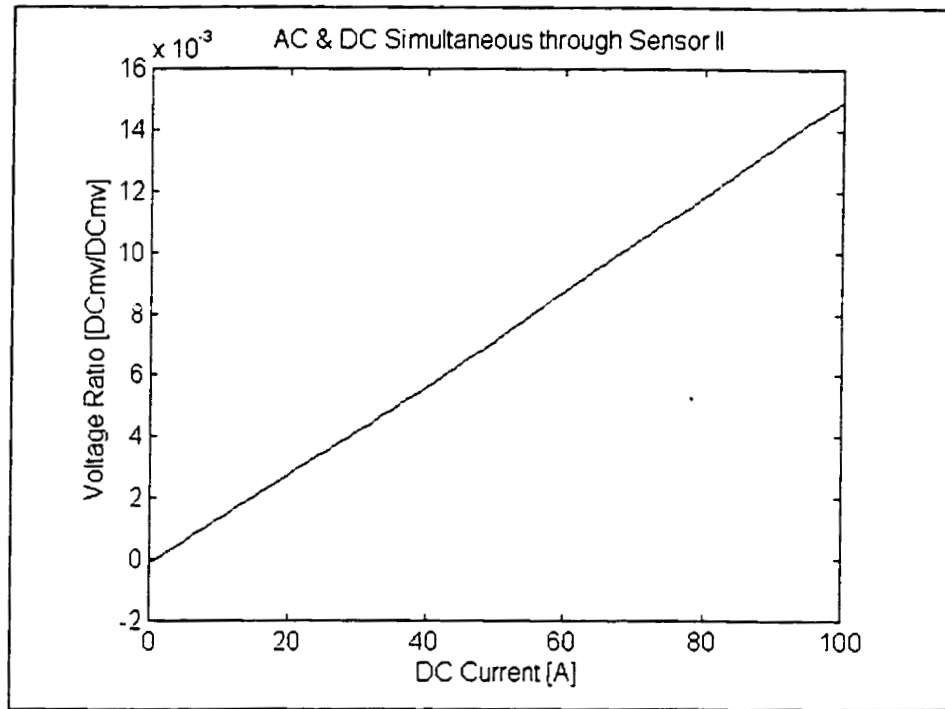


Fig.6.18 AC and DC simultaneous through Sensor II.AC set at 100Arms and DC varying 20-100A

Using the slope of the graphs is a very simple way of calculating the current and although non-of the responses are perfectly linear they can be approximated to an ideal line. Taking Fig. 6.15 and making an ideal linear approximation then the slope of the ideal line is given by:

$$m_{ideal} = \frac{y_2 - y_1}{x_2 - x_1} = \frac{ACratio [100 A] - 0}{100 A - 0 A}$$

Eq. 6.6.9

$$= \frac{0.031 - 0}{100 - 0} = 0.00031$$

From the experimental readings there are 5 points on the graph, thus 4 slopes can be obtained

<i>Points</i>	<i>Slope "m"</i>
0-40A	0.000221
40-60A	0.000310
60-80A	0.000309
80-100A	0.000309
$m_{average}$	<hr/> 0.00029

The slope between the first two points can be disregarded since the noise level prevents an accurate reading thus,

$$\therefore m_{average} = m = 0.000309 \quad \text{Eq. 6.6.10}$$

This is a valid assumption since there are enough points on the graph to compute an accurate slope value, and there is also the fact that at the lower current values the signal is buried more and more in the noise. An error rate has already been calculated and this value can be included in the current calculation when a statistically corrected equation is devised for the current calculation. This thesis will not touch on any statistical corrections for the measurements. To obtain a current value a linear equation is used of the form,

$$y = mx \quad \text{Eq. 6.6.11}$$

Where x is the Current " I " in Amps. m is the average slope of the response and y is the Ratio Calculated

$$\therefore I = \frac{\text{Ratio}}{m} \quad \text{Eq. 6.6.12}$$

Using the Ratio values from Fig.6.15,

m	Ratio	Calculated Current I [Arms]	Real Current Flowing Through sensor [Arms]	%error
0.00031	0.0122	39.35	39.56	0.52%
0.00031	0.0184	59.35	60.01	1.09%
0.00031	0.0245	79.03	79.4	0.46%
0.00031	0.0306	98.71	99	0.29%

Table 6.8 AC Current Calculations using Slope

It can be seen that the current calculated matches the real one flowing through the sensor with only a minor error and this from using a very simple formula.

The percentage error shown is given by:

$$\frac{\text{RealCurrent} - I}{\text{RealCurrent}} \times 100 \quad \text{Eq. 6.6.13}$$

For these calculations the values of the current on the 'x' axis are RMS values, that is why current calculations are given in RMS values. In order to obtain Peak Current values, the values on the graph would have to be altered by a $\sqrt{2}$ factor on the 'x' axis. This means the value of the slope m will be different. When using this new m in Eq.6.6.12 the peak value of the current would be calculated.

The Faraday rotation taking place in the sensor oscillates due to the plus and minus values of the magnetic field generated by the peak values of the current.

6.6.5.1 AC Experimental Example

For this example the 7xMF on Sensor II set up is taken into consideration. A random AC current "I" is run through the sensor produced by turning on a number of switches on the

resistor banks that draw current from the source. A value for this current will be determined using the AC Ratio technique.

For this experiment ZCL was set to 1.605V and the characteristic slope $m=0.00031$ as per Fig.6.15. The noise level is 8mVpp and the ratio error is 0.005. The output is a 60Hz sine wave riding on the dc level stated as ZCL and it has amplitude of 36.75mvp-p.

Ratio Calculation:

$$\frac{V_{pp}}{ZCL} = \frac{36.75 mV_{pp}}{1.605 V} \quad \text{Eq. 6.6.14}$$

$$Ratio = 0.0229$$

The current is obtained by using the characteristic slope m of the sensor:

$$I = \frac{Ratio}{m} = \frac{0.0229}{0.00031} \quad \text{Eq. 6.6.15}$$

$$I = 73.89 Arms$$

This last value calculated is that of the Current Flowing through the Sensor as calculated by the FOCSNET. To verify this answer we go back to the AC load banks by which the current is drawn. Using a 200A-100mV calibrated shunt as a reference. The shunt is placed in series between the power source and the resistor banks. The voltage across the shunt is measured by a precision voltmeter and it is proportional to the current flowing through the conductor by a factor of:

$$\frac{200 \text{ A}}{100 \text{ mV}} = 2 \text{ A / mv} \quad \text{Eq. 6.6.16}$$

This voltage across the shunt for this experiment is:

$$V_{shunt} = 0.03760 \text{ V} \quad \text{Eq. 6.6.17}$$

$$I_{conductor} = I = \frac{V_{shunt} * 200 \text{ A}}{100 \text{ mv}} \quad \text{Eq. 6.6.18}$$

$$I = 75.20 \text{ Arms}$$

It can therefore be concluded that the current determined calculations done by the FOCSNET system matches that of the actual measured current within a small percentage error,

$$\%error = \frac{75.20 - 73.89}{75.20} \times 100 = 1.7\% \quad \text{Eq. 6.6.19}$$

6.6.5.2 DC Experimental Example

DC current is calculated using the characteristic slope of the in the same fashion as with AC current. In this case Fig. 6.18 will be used to calculate the slope.

Ideally the slope would be,

$$m_{ideal} = \frac{y_2 - y_1}{x_2 - x_1} = \frac{DCratio_{[100 \text{ A}]} - 0}{100 \text{ A} - 0 \text{ A}} \quad \text{Eq.6.6.20}$$

$$m_{ideal} = \frac{0.015}{100} = 0.00015$$

The slopes obtained from the readings for the graph are as follows,

Points	Slope “m”
0-40A	0.000145
40-60A	0.000155
60-80A	0.000155
80-100A	0.000159
m_{average}	0.0001535

Once more using Eq.6.6.12 the ratio values from Fig. 6.18 are shown in Table 6.9,

m	Ratio	Calculated Current I [Arms]	Real Current Flowing Through sensor [Arms]	%error
0.000154	0.0058	37.79	38.6	2.11%
0.000154	0.0087	56.68	58.3	2.78%
0.000154	0.0118	76.87	77.6	0.94%
0.000154	0.015	97.72	98.9	1.19%

Table 6.9 DC Current calculations using slope

For this example a random DC current will flow through the sensor.

For this experiment ZCL was set to 1.605V and the characteristic $m=0.000153$ as per Fig.6.18. The noise level is 8mVpp and the Ratio error is 0.005. The output level for this random current is 1.6215v.

Ratio calculation:

$$\begin{aligned}\frac{DClevel}{ZCL} &= \frac{1.6215v}{1.605v} \\ Ratio &= 1.01028 \\ Normalization &= 0.01028\end{aligned}\quad \text{Eq. 6.6.21}$$

Current Calculation:

$$I = \frac{Ratio}{m} = \frac{0.01028}{0.000153} \quad \text{Eq. 6.6.22}$$

$$I = 67.18A$$

This is the value of Current Flowing though the sensor as calculated by the FOCSNET. To verify this calculation the flow of current is measured using a 200A-100mv shunt placed in the circuit as discussed before. The voltage across the Shunt in this experiment is,

$$\begin{aligned}V_{shunt} &= 0.03432 \\ I_{conductor} = I &= \frac{V_{shunt} * 200 A}{100 mv}\end{aligned}\quad \text{Eq. 6.6.23}$$

$$I = 68.64A \quad \text{Eq. 6.6.24}$$

The percentage error is:

$$\%error = \frac{68.64 - 67.18}{68.64} \times 100 = 2.1\% \quad \text{Eq. 6.6.25}$$

VII. CURRENT TRACES AND TRANSIENTS

7.1 OVERVIEW

This chapter focuses on the ability of the receiver to trace specific sections of the line current. The optical sample information stored on the receivers RAM is transmitted to the PC where a file is built and this file is traced using software with plotting capabilities.

To compare the graphs generated by the PC with what the actual line current looks like, oscilloscope traces are presented where the line-current is detected using a Hall Effect probe. The Hall effect occurs in a ribbon of metal placed under crossed electric and magnetic fields. As a result of the crossed fields, a current directed along the length of the ribbon is induced by a perpendicular potential difference [39]. The Hall effect probe enables an oscilloscope to trace current signals as opposed to voltage signals. The size of the probe head is proportional to the level of current it can handle before reaching saturation.

Since the Hall effect range of operation is proportional to the size of the metal ribbon it uses, then to measure the magnitudes of current that Faraday sensors can handle (e.g. 1000Arms) it would take a very large very and costly Hall effect device. The Hall effect probe used in this project can handle currents of up to 50Arms.

Transient conditions on line-currents are also discussed in this chapter. The experiments done are with a capacitive transient on an AC current signal. Hall effect traces are also shown to compare with the computer traces.

7.2 LINE CURRENT TRACES

In order to trace the line-current a file is generated by the computer from the optical sample information stored in the RAM. If the stream of samples stored in the RAM were

plotted as they are, the result would be a current signal trace with a lot of high frequency noise. To eliminate this noise Low Pass Filters (LPF) are designed into the receiver and computers' software. The LPF's are based on running averages of the data stored in the RAM and the graphing software does further filtering.

In this thesis the plots are generated from selected sections of the information stored in the RAM.

7.2.1 AC TRACES

The FOCSNET system is set up to sample a 60Hz AC line-current signal 666 times per cycle and the trace of a 100Arms AC signal is shown in Fig. 7.1. This particular figure is a trace of current flowing through Sensor I.

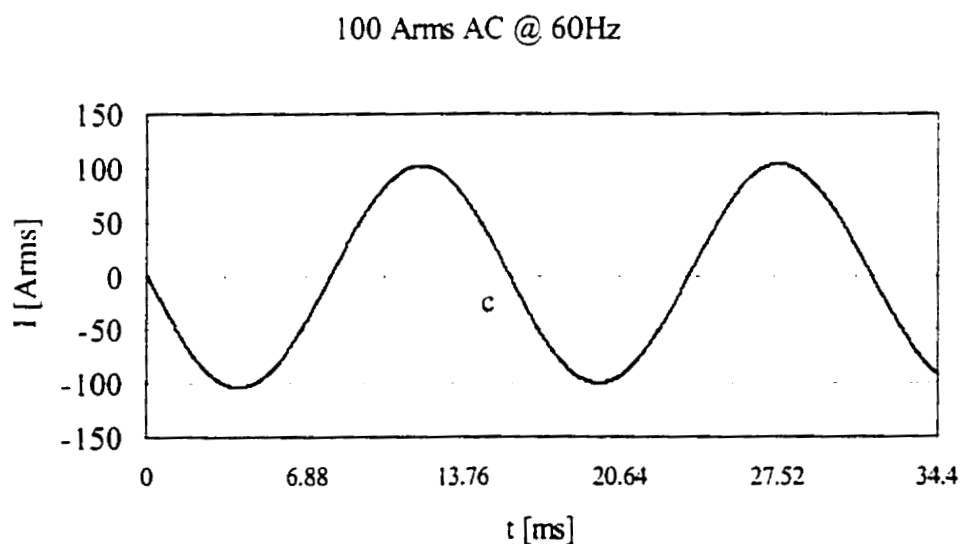
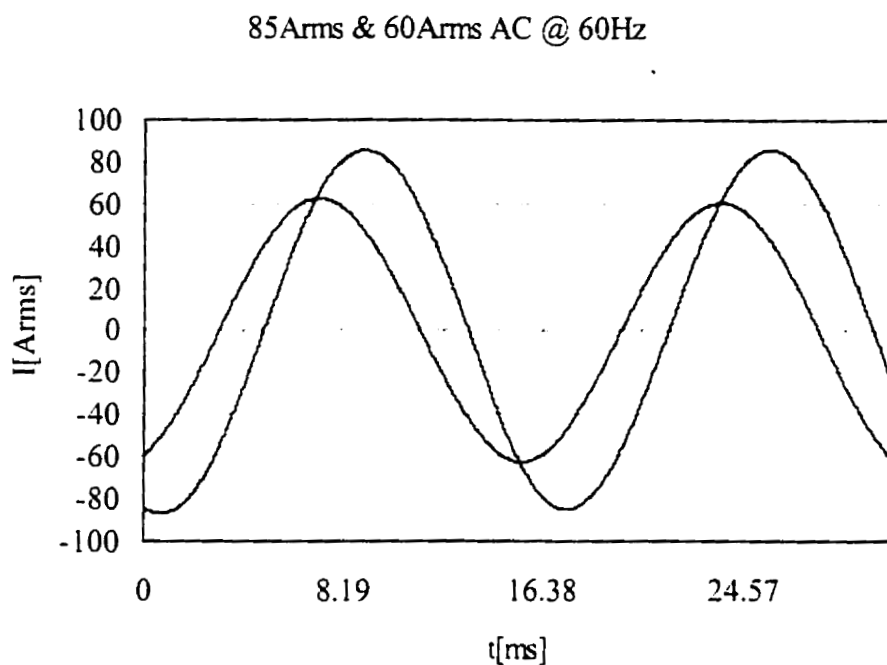


Fig. 7.1 Plot of a 100Arms AC

It can be seen that the amount of sample points per cycle along with the LPF techniques generate a reliable trace of the current flowing through the sensor.

In Fig.7.2 two traces are presented. The first one is a 60Arms signal flowing through Sensor II the second trace is an 85Arms signal through Sensor I. These two currents are flowing simultaneously through the sensors.



*Fig. 7.2 85Arms on Sensor I &
60Arms on Sensor II*

The two signals in Fig. 7.2 are not in phase since the sections of each one were chosen this way so there would be no over lap of the signals, and both could be fully appreciated.

7.2.2 DC Traces

As with the AC current the FOCSNET samples a DC signal 666 times every 16.66ms. Fig. 7.3 presents two traces for Sensor II. One trace represents the Zero Current Level

(ZCL) of the system, which is basically how the system responds when there is no current and the second trace is of 100 A DC line-current.

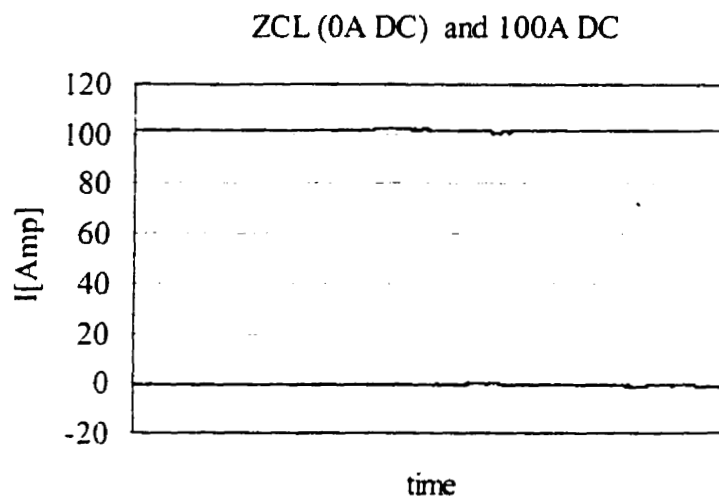


Fig. 7.3 DC Current on Sensor II

The traces on Fig 7.3 were generated from two separate experimental runs and are shown together on this figure.

7.2.3 Simultaneous AC & DC

One of the major features of the FOCSNET is its ability to measure AC and DC currents flowing through a single sensor in the system. This feature can also be plotted as seen on Fig. 7.4 which shows AC and DC currents flowing through Sensor II. For this experiment the sensor has two conductor windings, one for the DC current and the second one for the AC and this is described fully in section 6.5.5.

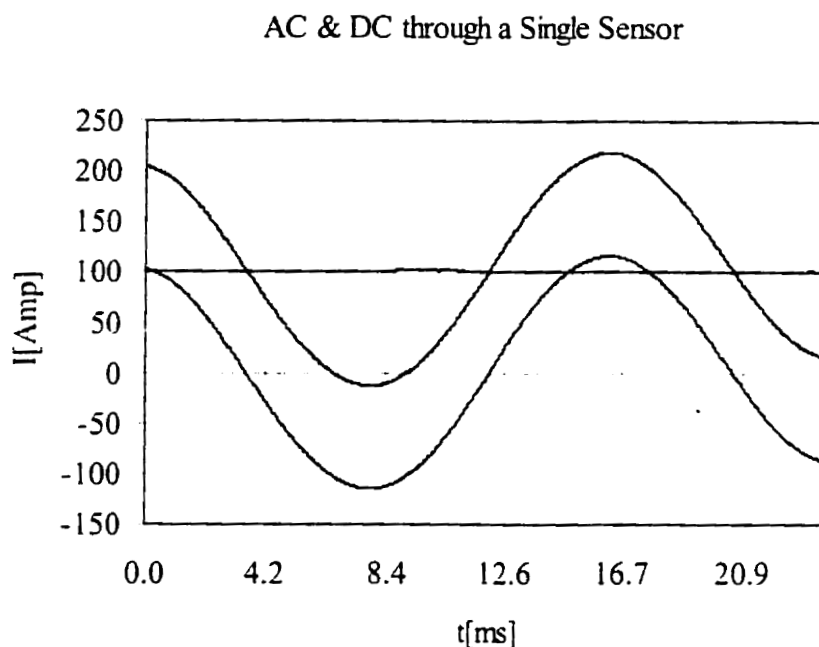


Fig. 7.4 110Ap & 100A DC (upper). 110 Ap & 0A DC (lower).

Two separate experiments are shown in Fig. 7.4. It is important to note that for this figure the values of the AC current are presented as peak values and not as RMS values. The first one shows 110Ap AC current flowing when there is no DC current present and for the second one, 100A DC was added. It can be seen that both AC traces have the same peak-to-peak amplitude regardless of the presence of DC current. In Fig 7.4 the DC current value is shown as a DC offset of the AC current. This is so both DC and AC can be plotted on the same graph.

7.3 TRANSIENTS

The time-varying line-voltages and currents resulting from the sudden application of sources, possibly due to switching, are called transients [40].

The transient experiments were done using a capacitive load on the line current since a capacitor produces a short, high level, high frequency transient spike. The equation for a capacitor is as follows [40].

$$V_C(t) = V_s - V_s e^{-\frac{t}{RC}} \quad \text{Eq. 7.3.1}$$

The second term is called the transient response, which eventually decays to negligible values. The first term is the steady-state response, which persists after the transient has decayed [40]. The current is related using the following equation.

$$I_C(t) = C \frac{dV_C(t)}{dt} \quad \text{Eq. 7.3.2}$$

The experimental results for this project were based on a capacitive load inserted into the current transmission line as shown in the following schematic.

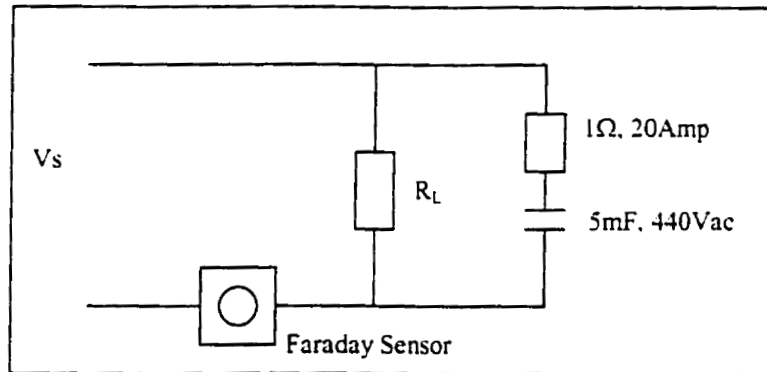
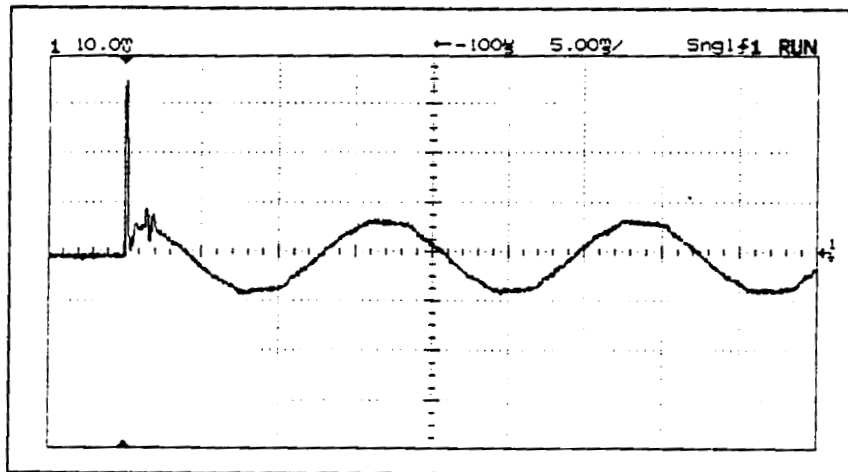


Fig. 7.5 Capacitive load schematic

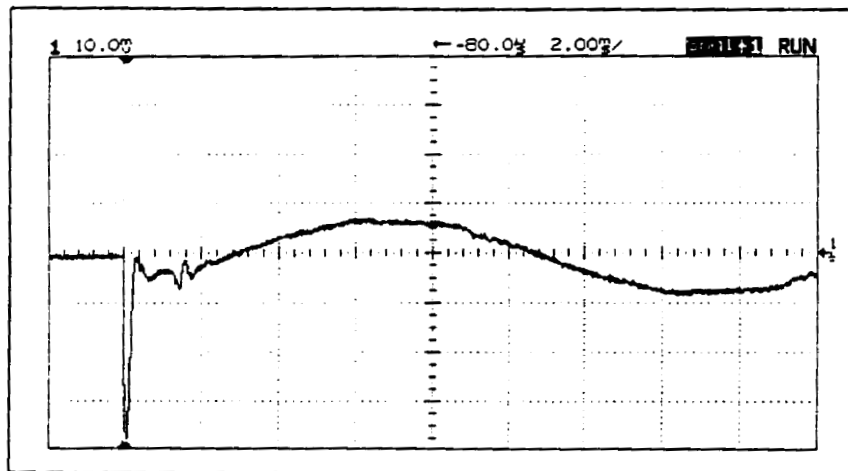
The time constant ($\tau = RC$) for this circuit is 5ms.

7.3.1 Hall Effect Traces

To record exactly what happens to the current during a transient state several tests were done using a Hall Effect probe. Figs.7.6 and 7.7 show traces resulting from these tests.



*Fig. 7.6 Hall Effect trace of a Capacitive transient on line current.
Time scale is set at 5ms/div*



*Fig.7.7 Hall Effect trace of a Capacitive transient on line current.
Time scale is set at 2ms/div*

The tests using the Hall Effect probe were done under identical conditions. The capacitive load remained constant and the current was switched on from an initial condition of 0Arms to a value of 10Arms . The following was concluded from these tests.

- Transient response is never the same from experiment to experiment, but several similarities exist. An over shoot followed by a decaying ringing characterizes a capacitive transient.
- In all instances there is a main overshoot and this “Spike” is on average 4.5 times larger than the line-current’s peak value.
- The main spike typically lasts for an average of 345 μ s.
- Secondary spikes are not necessarily present.
- The transient response exists for an average of 2.4ms and after this period of time the signal settles as a steady AC signal.

7.3.2 FOCSNET Transient Traces

The main purpose of using the Hall Effect probe was to obtain a reasonable idea of what a current waveform looked like under transient conditions. The FOCSNET is expected to perform in a similar fashion to the Hall Effect probe in terms of tracing transient conditions on line current.

The FOCSNET is a sampled system and this means that the line current is sampled by the optical pulses generated by the Laser. It has, as mentioned in previous chapters, a sample frequency of 40kHz. At this sample rate any condition on the line current smaller than 25 μ s will not be detected.

Based on the Hall Effect results the FOCSNET will have no problem in tracing the transients induced in the line current by the capacitive load. Test results show that a transient of this kind is noticeable for at least 2ms and the FOCSNET generates 80

sample points for a 2ms time period. With this amount of sampled information a reliable plot can be traced. As it was determined that the main transient spikes last for approximately $350\mu\text{s}$ thus 14-sample points will illustrate this spike. Due to laboratory equipment limitations and the spontaneous nature of current transients it was impossible to record the same event with both the Hall Effect probe and the FOCSNET simultaneously.

Figs. 7.8, 7.9 and 7.10 are traces of transients captured by the FOCSNET. These three figures show the resulting transient where the transmission line-current is suddenly switched on a with a capacitive load.

	Fig. 7.8	Fig. 7.9	Fig. 7.10
AC Signal	7 Arms	4 Arms	9 Arms
Transient Response	3.40ms	1.3ms	2ms
Main Spike Duration	$500\mu\text{s}$	$340\mu\text{s}$	$410\mu\text{s}$
Main Spike Amplitude	65 Apeak	31 Apeak	63 Apeak

Table 7.1 Figs. (7.8-7.10) Characteristics

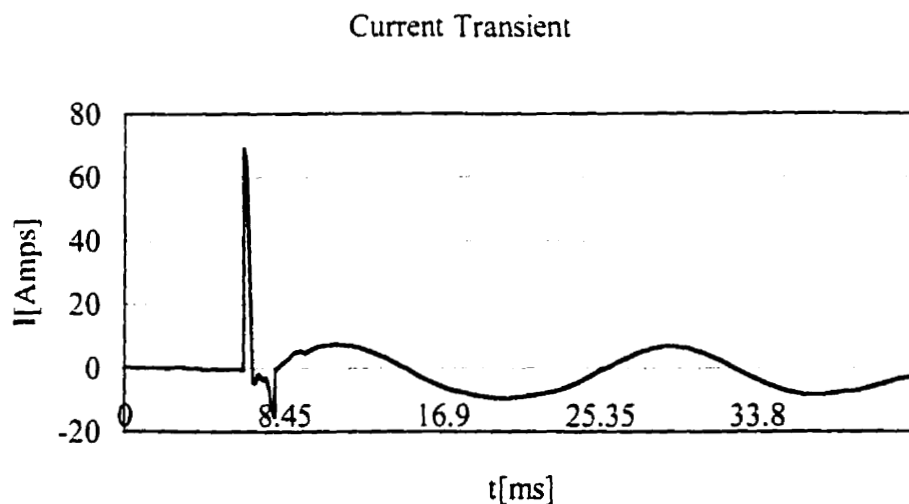


Fig 7.8 Capacitive Transient. FOCSNET Trace I

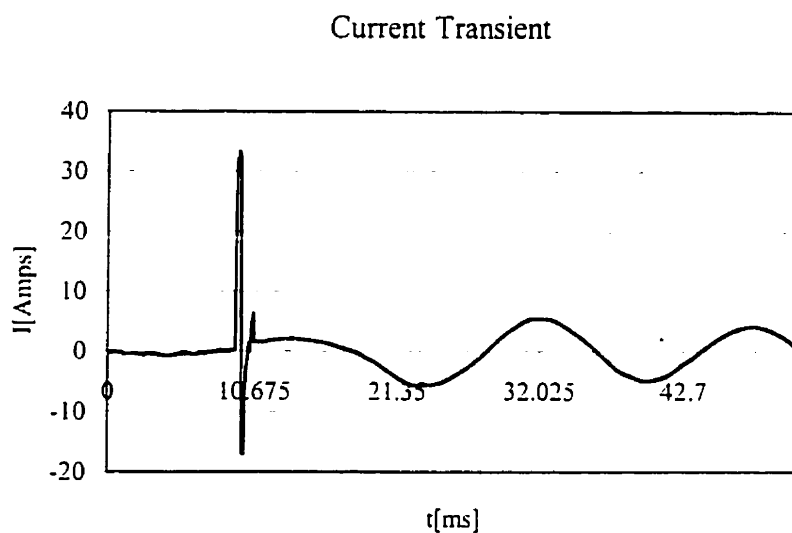


Fig. 7.9 Capacitive Transient. FOCSNET Trace II

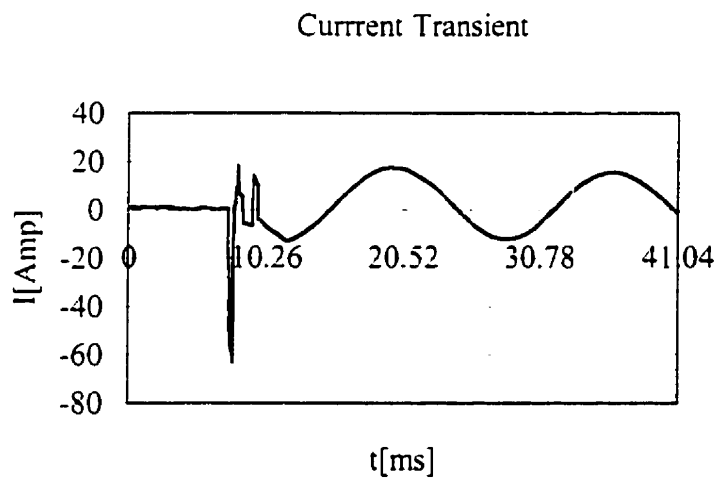


Fig 7.10. Capacitive Transient. FOCSNET Trace III

VIII. CONCLUSIONS AND FUTURE WORK

In this work a proof of concept time division multiplexing based fiber optic current sensor network has been implemented and several of its applications have been studied and tested. The receiver designed for this project is capable of measuring AC and DC currents. Techniques put forth in this thesis allow the receiver to measure currents accurately, eliminating external disturbances produced mainly by light source intensity variations. The system developed is also capable of tracing specific segments of the measured line-current and it can also successfully capture transient events on the current.

The polarization properties of light and the principles of the optical current sensor based on the Faraday magneto-optic effect are analyzed theoretically. The operation of the fiber optic current sensor and a network of such devices having a single transmitter-detector scheme are discussed in detail.

The optical components and their interconnections that make up the TDM based Star topology of the network are detailed. Being an all-fiber system without intermediate amplification makes it a passive network. The components that make it up are: Laser, single mode star couplers, single mode fiber, polarization controllers, polarized fiber and annealed sensing fiber coil.

The receiver's design and implementation which consists of many different inter-linked subsystems is described. The photodetector/amplifier converts the optical signal to an electric signal and then amplifies it and feeds it to a differential amplifier so that only the part of the signal containing the change in intensity is amplified and digitized by the ADC.

The FPGA is the brain of the receiver, along with the DSP, processes the signal and based on the ratio techniques developed, it sends to the PC information relating to the DC and AC levels of each sensor. The C++ software loaded on the PC allows this

information to be translated into a current reading. Since the PC is capable of tracing specific sections of the line-current then this allows the possibility of tracing transient conditions on the line-current.

Finally, the experiments on current sensing were successfully conducted. First S. Goyal's DC experiments were repeated and his conclusions on the linearity of the system were proven. In this thesis it is shown that AC current can be detected by the networked system and that the response of the system under AC conditions is also linear.

One of the main issues touched upon is the dependency that line current measurements have on light source variations. To eliminate this dependency two ratio techniques are put forth and subsequently, by means of experimental tests, are proven to be a reliable approach to measure current. It is concluded that the FOCSNET can measure AC and DC currents accurately and virtually regardless of variations in the light source intensity

One of the most innovative developments in this study is the capability of the system to measure AC and DC current while they flow simultaneously through the one sensor. Ratio techniques apply here as well for accurate measuring

The final tests done on the system show the ability of the FOCSNET to trace segments of the line current being measured, and not only this but it has the capability to capture transient states on the line current and plot them.

As a proof of concept the tests done on the FOCSNET exceeded all expectations.

Future work will involve improving the ability of the light source to transmit much narrower pulses with a minimum of distortion since for large networks the difference in distance to any two sensors may be only a few meters.

A number of changes can be made in the FPGA, DSP and C++ software. The present system is designed for only two sensors but it can be scaled easily. The system is designed for the proof of concept of this thesis thus several more applications can be built in for more reliable measuring, such as statistical error compensation.

There is a possibility for the receiver not to include both the FPGA and DSP but only one of them. This would involve very skilled digital programming of either component.

Work must be done in order for the system to be able to plot real time traces of the line current flowing through the sensors. This would involve implementing a graphic interface within the C++ software.

The capabilities of the FOCSNET are such that it may be used for metering, as a protection system due to its ability to capture transient spikes, or to simply study the long term behavior of the line current signal.

REFERENCES

- [1] J. Song, P.G. McLaren, D.J. Thomson and R.L. Middleton, "A Prototype Clamp-on Magneto-optical Current Transducer for Power System Metering and Relaying", *IEEE Transactions on Power Delivery*, vol. 10, No. 4, October 1995, pp. 1764-1770.
- [2] Jun Song, "development of Magneto-Optical Current transducers for Power Systems", Ph.D Theses, University of Manitoba, January 1996
- [3] T.W. MacDougall, D.R. Lutz and R.A. Wandmacher, "Development of a fiber optic current sensor for power systems", *IEEE Transactions on Power Delivery*, vol. PWRD-7, No. 2, April 1992, pp. 848-852.
- [4] P-G. Zhang, "Faraday Effect Optical Current Sensor", M.Sc., University of Calgary, Alberta , Canada, August 1993.
- [5] P-G. Zhang and D. Irvine-Halliday, "Faraday Effect Optical Current Sensor", IEEE, CCECE 96, Calgary, Canada, pp. 871-875.
- [6] S. Goyal et al, "Fiber Optic Current Sensor Network ", IREE Journal, 1999
- [7] T.Fujimoto, M. Shimizu and H Nakagawa, " Development of an Optical Current Transformat for Adjustable Speed Pumped storage Systems", *IEEE Transactions on Power Delivery*, vol.12, No. 1, January 1997, pp. 45-50.
- [8] T.W. Cease and P. Johnson, " A Magneto-Optic current Transducer", *IEEE Transactions on Power Delivery*, vol. PWRD-5, No. 2, April 1990, pp.548-555.
- [9] J.W. Dawson, T.W. MacDougall and E. Hernandez, "Verdet Constant Limited Temperature Response of a Fiber-Optic Current Sensor", *IEEE Photonics Technology Letters*, vol. 7, No. 12, December 1995, pp. 1468-1470.
- [10] T. Yoshino, "Optical Fiber Sensors for Electric Industry", *Fiber Optic Sensors II*, SPIE. 1987, pp.258-265.
- [11] P.Menke and Th. Bosselmann, " Magneto-Optical AC-Current Sensing with an Annealed Fiber Coil and Intrinsic Temperature Compensation", *Proc. SPIE*, vol. 2292, 1994, pp.26-33.

- [12] J.R. Boyle, et al, "The Tennessee Valley Authority's Experience and Action Plans with Freestanding oil-filled current Transformers", IEEE transactions on Power Delivery, vol.PWRD-3, No. 4, October 1988, pp.1769-1775.
- [13] S. Goyal, "Fiber Optic Current Sensor Network", Master's Thesis, The University of Calgary, September 1997.
- [14] B. Culshaw and J.P. Dakin, *Fiber Optic Sensors, Volume II, Systems and Applications*, Artech House, London and Norwood, 1988.
- [15] A.R. Nelson and D.H. McMahon, "Passive Multiplexing Techniques for Fiber Optic Sensor Systems", *Proc. IFOC*, March 1981, pp. 27-30.
- [16] B.Culshaw, "Fiber Optic Sensor Networks" *Proc. SPIE*, vol. 1511, 1991, pp. 168-175.
- [17] J.L Brooks, et al, "Coherence Multiplexing of Fiber-Optic Interferometric Sensors", *Journal of Lightwave Technology*, vol 3, No.5, October 1985, pp.1062-1071.
- [18] M. Faraday, "Experimental Researches in Electricity", *Philosophical Transactions of 1846-1852*, Bernard Quaritch, 1855, pp. 1-26. Reprint found in "Polarized Light", *Benchmark Papers in Optics*, vol. 1, Dowden, Hutchinson and Ross, Inc., 1975, pp. 104-123.
- [19] C.Yeh, "Handbook of Fiber Optics", Academic press inc., 1988
- [20] D. Clarke and J.F. Grainger, *Polarized Light and Optical Measurement*, Pergamon Press, 1971.
- [21] R.C. Jones, "A New Calculus for the Treatment of Optical Systems", *J. Opt. Soc. Am.*, vol. 31, July 1941, pp. 488-493. Reprint found in "Polarized Light", *Benchmark papers in Optics*, vol.1, Dowden, Hutchinson and Ross, Inc.,1975, pp.187-192.
- [22] W.A. Shurcliff and S.S. Ballard, *Polarized Light*, D. Van Nostrand Company, Inc., 1964.
- [23] A.M. Smith "Polarization and Magneto-Optic Properties of Single Mode Optical Fiber Optic", *Applied Optics*, vol. 17, No.1 , January 1978, pp.32-56.
- [24] S.C. Rashleigh, "Origens of Polarization Effects in Single Mode Fibers", *Journal of Lightwave Technologies*, vol.1, No.2, 1983, pp.312-331.
- [25] J.M. Senior, "Optical Fiber Communications", 2nd Edition, Prentice Hall Inc., 1992.

- [26] Oz Optics Ltd., *Polarization Maintaining Fiber Optic Components*, 1995.
- [27] J. Noda, K. Okamoto and Y. Sasaki, "Polarization-Maintaining Fibers and their Applications", *Journal of Lightwave Technology*, vol. 4, No. 8, August 1986, pp. 1071-1089.
- [28] M.R. Khan, "Measurement of Beat Length in High Birefringent Fibers Using Faraday's Magneto-Optic Effect", M.Sc. Thesis, University of Calgary, June 1996.
- [29] J.R. Simpson, R.H. Stolen, F.M. Sears, W. Pleibel, J.B. MacChesney and R.E. Howard, "A single-polarization fiber", *Journal of Lightwave Technology*, vol. 1, No. 2, 1983, pp. 370-373.
- [30] M.J. Messerly, J.R. Onstott and R.C. Mikkelsen, "Broad-band single polarization optical fiber", *Journal of Lightwave Technology*, vol. 9, No. 7, July 1991, pp. 817-820.
- [31] R.I. Laming and D.N. Payne, "Electric Current Sensors Employing Spun Highly Birefringent Optical Fibers", *Journal of Lightwave Technology*, vol. 7, No. 12, December 1989, pp. 2084-2094.
- [32] A.H. Rose, Z.B. Ren and G.W. Day, "Twisting and Annealing Optical Fiber for Current Sensors", *Journal of Lightwave Technology*, vol. 14, No. 11, November 1996, pp. 2492-2497.
- [33] D. Tang, A.H. Rose, G.W. Day and S.M. Etzel, "Annealing of Linear Birefringence in Single Mode Fiber Coils: Applications to Optical Fiber Current Sensors", *Journal of Lightwave Technology*, vol. 9, No. 8, August 1991, pp. 1031-1037.
- [34] S. Zhang, "Flexible Controller Maintains Fiber Optic Polarization", *Photonics Spectra*, April 1998
- [35] T.W. MacDougall, J.W. Dawson and E. Hernandez, "State of the Art Fiber Optic Current Sensor", *OFS*, 1996.
- [36] Hewlett Packard "HFBR-24X6 Low-Cost 125 MHz Receiver", HP Technical Specifications, 1997
- [37] "The Programmable Logic Data Book", Xilinx 1998
- [38] H. Killen, "Modern Electronic Communication Techniques", Macmillan Publishing 1995, pp. 288-289

- [39] K.R. Forrester, "The Quantum Hall Effect", M.Sc. Thesis, university of Calgary, May 1989
- [40] A.R. Hambley, "Electrical Engineering Principals and Applications", Prentice Hall, 1997, pp. 160-200
- [41] H. Schwarz and M. Hudasch, "Optical current transformers-successful first field test in a 380 kV system", *ABB Review*, March 1994, pp. 12-18.
- [42] A.J. Rogers, "Principles for optical-fibre applications in electricity supply", *Journal of Optical Sensors*, vol. 1, January 1986, pp. 5-25.
- [43] C.P. Yakymyshyn, M.A. Brubaker, P.M. Johnston and C. Reinbold, "Manufacturing challenges of optical current and voltage sensors for utility applications", (*Invited Paper*) *SPIE Proceedings, Pittsburgh*, October 1997.
- [44] Y.N. Ning, Z.P. Wang, A.W. Palmer, K.T.V. Grattan and D.A. Jackson, "Recent progress in optical current sensing techniques", *Review of Scientific Instruments*, vol. 66, No. 5, May 1995, pp. 3097-3111.
- [45] A.H. Rose, Z.B. Ren and G.W. Day, "Twisting and Annealing Optical Fiber for Current Sensors", *Journal of Lightwave Technology*, vol. 14, No. 11, November 1996, pp. 2492-2497.
- [46] J. Mlodzianowski, D. Uttamchandani and B. Culshaw, "A Simple Frequency Domain Multiplexing System for Optical Point Sensors", *Journal of Lightwave Technology*, vol. 5, No. 7, July 1987, pp. 1002-1007.
- [47] B. Culshaw, "Fibre optic sensor networks", *Proc. SPIE*, vol. 1511, 1991, pp. 168-175.
- [48] Internal Laser Design Document, *TRLabs*, Edmonton, Alberta, Canada, 1996.
- [49] P. Menke and T. Bosselmann, "Temperature Compensation in Magneto optic AC Current Sensor Using and Intelligent AC-DC Signal Evaluation" *Journal of Lightwave Technology*, vol.13 No 7, July 1995